FLOWNEX ANALYSIS OF HIGH TEMPERATURE TEST REACTOR THERMO-HYDRAULIC BENCHMARKS

Frank Norman Emslie
B.Eng (Mechanical)

Thesis submitted in partial fulfilment of the requirements for the degree
Magister Ingeneriae
in the
School of Mechanical and Materials Engineering.
Faculty of Engineering
at the
North-West University

Supervisor: Professor Gideon Greyvenstein

Potchefstroom

South Africa

2005

ABSTRACT

The High Temperature engineering Test Reactor (HTTR) is an experimental High Temperature Gas-cooled Reactor (HTGR) built by the Japanese Atomic Energy Research Institute (JAERI) to facilitate tests of HTGR technology. One of these test activities involves the validation and verification of thermo-hydraulic codes used in the design of similar HTGR plants. This report details the benchmarking of the Flownex simulation package as used by PBMR (Pty.) Ltd., a South African company developing another type of HTGR known as the Pebble Bed Modular Reactor. The benchmark is of a loss-of-off-site-power event that was tested at the HTTR facility. The event involves a cut of the electric power supply to the circulators, a reactor SCRAM and the activation of the Auxiliary Cooling system to remove decay heat.

The need for verification of thermodynamic software is very important in modern nuclear power plant designs, as so much depends on the results produced. Any errors in these results can have serious economic and safety consequences.

This report firstly discusses the background of the study, elaborating on the need for the work and the benefit that can be derived from it. Thereafter the process of software verification and validation (V&V) is discussed so that the need for V&V may be clearly understood. Various modelling and simulation methods are then compared, to provide an idea of the work already done in this field. Following this more detail is given on the HTTR test plant and how it is modelled in Flownex. This model is then used for both steady-state and transient simulations, the results of which are then compared with test data.

With some exceptions, the study shows that the simulation results are very close to the measured data. Differences are of such a magnitude that they may be attributed to instrumentation inaccuracies.

The study contributes to the field in that the methodology of analysing thermo-hydraulic systems is further broadened. The conclusions drawn from this study are aimed at the simulation design engineer, to help him or her understand similar problems and to find solutions faster.

OPSOMMING

Die *High Temperature engineering Test Reactor* (HTTR) is 'n eksperimentele hoëtemperatuur-gasverkoelde kernreaktor of HTGR. Dit is gebou deur die Japannese kernnywerheid JAERI (Japanese Atomic Energy Research Institute) om toetse te doen op HTGR-tegnologie. Een van hierdie aktiwiteite behels die validasie en verifikasie van termo-hidrouliese rekenaarkodes wat gebruik is in die ontwerp van ander HTGR-aanlegte. Hierdie verslag detailleer die yking van die *Flownex*-stelselkode soos gebruik op die ontwerp van die Korrelbedkernreaktor of PBMR (Pebble Bed Modular Reactor), wat deur Suid-Afrika ontwikkel word. Die yking het betrekking op 'n skielike verlies in die verkoelingstelsel van die HTTR. Die gebeurtenis word veroorsaak deur die verlies in elektriese krag na die heliumwaaiers in die stelsel. Die gevolg is dat die reaktor se kernreaksie onmiddellik gestaak word deur beheerstawe in te druk. Hierna word die noodverkoelingstelsel geaktiveer om die oorbodige hitte weg te neem.

Die vereiste vir verifikasie van ontwerpprogrammatuur is baie belangrik in die moderne kernbedryf, omdat soveel belangrike keuses gemaak word op grond van die inligting wat van die programmatuur verkry word. Enige foute in die resultate kan groot ekonomiese en veiligheidsnagevolge hê.

Die verslag bespreek eerstens die agtergrond van die studie en die noodsaaklikheid van die werk wat gedoen is. Daarna word die proses van programmatuurverifikasie bespreek, om daardeur die behoefte van verifikasie uit te lug. Verskeie modelleringstegnieke word vergelyk om die leser 'n idee te gee van die werk wat al reeds gedoen is. Vanaf hierdie basis word die HTTR gemodelleer in Flownex en verskeie toetse gesimuleer.

Van die belangrike analiseresultate het gewys dat die simulasieresultate baie goed ooreenstem met die toetsdata. Die grootte van verskille is so klein dat dit aan instrumentasie-onakkuraatheid toegeskryf kan word.

Die studie maak 'n bydra tot die veld van ingenieurswese in die sin dat dit die metodiek van modellering van termo-hidrouliese stelsels verbreed. Die gevolgtrekkings van die studie is op die simulasie-ingenieur gemik, sodat hy/sy 'n beter begrip kan vorm van soortgelyke probleme in die veld en sodat probleme vinniger opgelos kan word.

ACKNOWLEDGEMENTS

This thesis is the end result of many months of work. At some points it seemed like an unreachable goal, but at other times the motivation was there to see me through to the end. This achievement could not have been reached with out my faith in the Lord or without the help and motivation of my supervisor, Prof. Gideon Greyvenstein. I would thus like to express my heartfelt gratitude for his assistance in this work.

Furthermore, this work could not have been completed without the resources of the North-West University (Potchefstroom campus), JAERI and PBMR.

I would also like to thank my family, friends and wife, Chantelle for their support through this time.

Thank you all very much.

CONTENTS

LIST OF FIGURES

TABLES

NOMENCLATURE

A	= area
CV	= Control volume
c	= specific heat
D	= hydraulic diameter
f	= friction factor
h	= convection coefficient
i	= node number in x-direction
j	= node number in y-direction
k	= conduction coefficient
M	= Mach number
m	= mass
N	= Rotational Speed
p	= Pressure
Q	= Net heat added to system
R	= Gas constant
T	= Temperature
t	= time
T	= static temperature
T_0	= total temperature
$T_{i,j}$	= temperature at node i, j
T^{k-1}	= temperature at previous time step
V	= Velocity
x	= length in the direction of the flow
ρ	= Density
η	= Efficiency
Δx	= distance between nodes in x-direction
Δy	= distance between nodes in y-direction
γ	= the ratio of the specific heats

ABBREVIATIONS

ACACIA	=	AdvanCed Atomic Cogenerator for Industrial Applications
ACM	=	Aspen Custom Modeller
ACS	=	Auxiliary Cooling System
AEA	=	Atomic Energy Association
AGC	=	Auxiliary Gas Circulator
AHX	=	Auxilliary Heat Exchanger
AVR	=	German pebble bed reactor
CAD	=	Computer Aided Design
CAE	=	Computer Aided Engineering
CFD	=	Computational Fluid Dynamics
CHT	=	Conductive Heat Transfer
CRP	=	Coordinated Research Programme
FEA	=	Finite Element Analysis
GT-MHR	=	Gas Turbine Modular Helium Reactor
GUI	=	Graphical User Interface
HPC	=	High-Pressure Compressor
HPT	=	High-Pressure Turbine
HTGR	=	High-Temperature Gas Reactor
HTR	=	High-Temperature Reactor
HTTR	=	High-Temperature engineering Test Reactor
IAEA	=	International Atomic Energy Association
IHX	=	Intermediate Heat Exchanger
INEEL	=	Idaho National Engineering & Environmental Laboratory
JAERI	=	Japan Atomic Energy Research Institute
LPC	=	Low-Pressure Compressor
LPT	=	Low-Pressure Turbine
LWR	=	Light Water Reactor
MCS	=	Main Cooling System
PBMR	=	Pebble Bed Modular Reactor
PGC	=	Primary Gas Circulator
PPWC	=	Primary Pressurised Water Cooler
PRA	=	Probabilistic Risk Analysis
PT	=	Power Turbine
PWR	=	Pressurised Water Reactor

R&D	=	Research and Development
RPV	=	Reactor Pressure Vessel
SGC	=	Secondary Gas Circulator
SVVP	=	Software Verification and Validation Plan
SUD	=	Software Under Development
V&V	=	Verification & Validation
VCS	=	Vessel Cooling System
SCRAM	=	Shut-down of the reactor
SPWC	=	Secondary Pressurised Water Cooler

1. INTRODUCTION

1.1. Introduction

With the global demand for electricity increasing every year it has become evident that alternative sources of energy are becoming more and more important. One such source is nuclear power, which (even though the public views it with some contention) seems to be the most sustainable successor to fossil fuels. Nuclear power is also beneficial in that environmental pollution is limited.

Although nuclear energy will play a major role in future world energy supply, current nuclear power generation suffers a few drawbacks. Firstly, the cost of building and operating nuclear plants is still a determining factor. This is mainly due to the cost of the safety systems used and the high requirements for quality of the plant. Much less emphasis is placed on safety at coal-fired plants and they are therefore much more economical. As can be concluded, the cost is directly related to safety, and unfortunately safety requirements are, to an extent, non-negotiable. This is due to the obvious danger of radiation. Secondly, public sentiment towards nuclear energy is negative due to a lack of education and to previous incidents such as Chernobyl. The public needs to be educated in the benefits of nuclear power and the quality of the safety measures implemented to protect it. The last major drawback of nuclear energy is the disposal of nuclear waste. This is a very contentious issue, as nobody wants to have the waste stored in his or her proverbial backyard, even though authorities have made substantial efforts to ensure the safety of waste disposal facilities.

These drawbacks have forced attention to shift to High Temperature Reactors or HTRs, where gases such as helium, and not water, is used as the cooling medium. The main advantage of HTRs is in the reactor design, which results in a strong negative temperature coefficient. This allows the fuel to decrease in reactivity as the temperature increases above a certain value. Therefore, in the case of a classic accident where the cooling to the reactor is cut off, the HTR fuel will decrease its reactivity as the fuel temperature goes up. This is opposed to conventional power plants where a core meltdown could occur if safety systems malfunction along with the loss of coolant.

Because of this advantage many different countries have done a lot of research and development of HTR technologies over the last few decades. Japan built a test reactor known as the High-Temperature engineering Test Reactor or HTTR in the 1990s, while China has also built a test reactor named the HTR-10, which uses fuel spheres instead of fuel blocks as used in the HTTR. Other countries have HTR development programmes in place, with South Africa leading in the development of the Pebble Bed Modular Reactor (PBMR). When complete, the PBMR will be the world's first commercial HTR power plant. The HTTR uses block fuel designs in the reactor, while the HTR-10 and PBMR use dynamic cores through which fuel balls are continuously circulated. This ensures that the plant never has to be shut down to refuel, as with the block fuel reactors. In the power conversion unit the PBMR uses two turbo-compressor units and a power turbine. This is configured in a three-shaft lay-out.

The design of HTR nuclear power plants relies heavily on simulation and analysis. These analyses include structural, nuclear physics and thermo-hydraulic analyses. The advantage of having thermo-hydraulic software available is that the plant may be optimised for maximum efficiency, with minimal experimental work. This is invaluable in the long term, as the cost of electricity production is minimised. Such software also helps predict the repercussions of accidents and fault conditions in the plant in safety analyses.

It is this last requirement that makes it important for software to be thoroughly verified and validated. This thesis deals with the verification and validation of one such code, Flownex, as used in the design of the Pebble Bed Modular Reactor (PBMR). The HTTR loss-of-off-site power transient event is used as a test case.

1.2. Background

The concept of high temperature reactors was first introduced in the 1950s when the British AEA built the Dragon HTR. The principle used in the HTR is to use high temperature gas, like helium, as a coolant in a graphite moderated reactor. Following Dragon, the Germans designed and built the AVR plant. This plant clearly showed the potential of HTRs as highly efficient and emission-free power sources. At the time though, the availability of helium as a coolant and the challenges involved in helium turbo-machinery and valve design prevented HTRs from entering the main stream of electricity production. Light Water Reactors (LWRs) were favoured in the nuclear industry due to the more conventional technology at the time. Along with technological obstacles came social disfavour of nuclear plants after the Three Mile Island and Chernobyl accidents.

Technological advances have been made over the last two decades as far as high efficiency gas turbo-machinery, valve systems and heat exchangers are concerned. These advancements have thus made it possible to revert to the original HTR designs so as to realise their high efficiency and safety. The international community has taken the initiative and launched research programs to further develop HTR technology under the watchful eye of the IAEA. Consequently research reactors such as the Japanese HTTR and Chinese HTR-10 have been built and operated. Until recently the USA was developing the GT-MHR power plant, while South Africa is in the process of developing the PBMR.

1.2.1. Overview of the HTTR

The HTTR or High Temperature engineering Test Reactor was built by JAERI during the 1990s and its primary function is to test the concept of HTRs. The system is comprised of a graphite-moderated prismatic block reactor, a primary cooling circuit, a secondary cooling circuit and an auxiliary cooling circuit. Helium is used as the working fluid. During normal operation the helium is heated in the reactor and is then circulated via concentric pipes to two parallel heat exchangers. The first is the Primary Pressurised Water Cooler (PPWC), which is a shell-and-tube water-cooled heat exchanger. The second is the Intermediate Heat Exchanger (IHX), which is a spirally wound shell-and-tube type. Its function is to transfer heat to the secondary helium circuit. Both heat exchangers' exits are connected to helium circulators providing the mass flow rate needed in the circuit.

In the secondary helium circuit a helium circulator is used to circulate flow between the IHX and the Secondary Pressurised Water Cooler (SPWC), the latter being of similar but smaller design to the PPWC. Both water coolers' watersides are part of the water circuits that exchange heat with the atmosphere via water-to-air heat exchangers. The cycle lay-out will be explained in detail in Chapter 3.

During an accident condition such as the loss-of-off-site electrical power, the Auxiliary cooling circuit is used. This circuit uses two gas circulators to force a low mass flow rate of helium between the reactor and the Auxiliary Heat Exchanger (AHX). The AHX is a water cooler of similar but smaller design to the PPWC. The function of this system is to remove decay heat from the reactor core after a reactor shutdown or SCRAM has been initiated.

The HTTR attained its first criticality in November 1998, with the start-up core physics tests being successfully completed in January 1999. Following that, rise-to-power tests were conducted starting in September 1999. As part of the ongoing testing of the operational events in the plant, it was necessary to test the cooling of the reactor core in the case of accidents. As such, loss-of-off-site power tests were planned for the operation points of 15MW and 30MW.

1.2.2. IAEA Coordinated Research Project on evaluation of HTGR performance

The International Atomic Energy Agency (IAEA) facilitates collaborative efforts among its member states in the interest of promoting technological advances in nuclear power. Such initiatives are organised into Coordinated Research Projects or CRPs that take approximately five years to complete. The CRP on the evaluation of HTGR performance is specifically focused on thermo-hydraulic and reactor physics behaviour of HTRs and specifically benchmarking design software against research reactor test data. This thesis discusses the benchmarking of a thermo-hydraulic software package against the measured performance of the HTTR during a loss-of-power transient event as prescribed by the IAEA CRP on evaluation of HTGR performance.

1.3. Problem statement

The problem at hand is to simulate the thermal and fluid dynamic behaviour of a power system, in this case the HTTR research reactor. This system is a series of closed loop helium circuits that interact thermally and then release heat to the environment through water cooling systems. In any flow system, whether it contains a liquid or a gas, the effect of pressure losses is of primary concern, as this determines the powers of prime movers in the circuit such as pumps, blowers or compressors. With gases such as helium, the variation of density with temperature strongly affects these pressure losses and as such both conservation of energy and momentum need to be solved for. Of equal importance is the accurate modelling of heat addition and removal devices such as the reactor and heat exchangers.

As with most engineering problems, the onus is on the analyst to use sound judgment when representing physical components with mathematical models. This is especially important where unique and unusual components are to be modelled but the simulation model used was developed for a totally different configuration. In such cases there are two choices – either to have the software developer create a model for the unique component or to make do with standard models and use engineering judgment to alter inputs so as to best represent the component. The former choice is usually difficult to realise, due to the costs involved.

This thesis discusses the method used to model the physical HTTR plant in a thermo-hydraulic code so as to do transient analyses. Assumptions used are described and motivated in the text so as to make it possible for any independent analyst to model the HTTR and get the same simulation results.

1.4. Objectives

The objective of this study is to develop a Flownex model of the HTTR and to compare the model results with measurements taken on the actual plant. The model will then be used to simulate both transient and steady-state operation at different power levels. This study will form an important step in the validation of Flownex.

1.5. Layout of thesis

Following this introductory section is a literature survey. The survey discusses verification and validation requirements and techniques used in software development, and modelling approaches used in similar problems. Lastly it gives a brief history of the HTTR that is modelled in this study.

Chapter 3 gives an overview of the HTTR system so that the reader may become acquainted with the complexities of the system. Flownex , the software package used in the simulations, is discussed in Chapter 4, while Chapter 5 presents the modelling process, assumptions and strategies used in modelling the HTTR in Flownex. Steady-state and transient results are given in Chapters 6 and 7 respectively.

The findings of the study are summarised in Chapter 8, where conclusions are drawn and recommendations for future work are made. The appendices contain the detailed Flownex results for the analyses which were done.

2. BACKGROUND STUDY

2.1. Introduction

In this chapter the study is placed in context. Firstly, the importance of Validation and Verification (V&V) is discussed along with the process involved. This is to give the reader a broad understanding of why there is a need for benchmarked solutions of HTR plants. Following this is a broad discussion of system codes used in general thermo-hydraulic problems. More emphasis is placed on codes used in conventional and nuclear power plant design. Some codes are elaborated on with respect to their modelling methodologies and appropriateness for the problem at hand. In closure the survey on V&V and the various system codes are placed in context with the current study in a discussion of where the HTTR test reactor fits in.

2.2. The importance of testing and V&V in software development

Over the last fifty years the need for adequate testing of the thermo-hydraulics codes used in the design of nuclear power plants has become a necessity. Initially only the very limiting accident and enveloping conditions were analysed, while overall system performance analyses did not get sufficient attention due to limitations in test and analysis tools. Today though, the need to create an adequate integrated test and analysis programme is of primary importance. This shift in focus is due to several factors.

One of these is that legal regulations demand that performance of every safety feature and the interdependency of these features be demonstrated by analysis, test programmes, practical experience or a combination thereof. Enough data needs to be available to assess the analytical tools over a suitable range of steady-state conditions, transient events and accident conditions. Such requirements can only be satisfied with a comprehensive interactive test programme at system level.

Next, large system computer codes are used to predict the performance of complex systems during normal operation, transients and accident scenarios. These codes are useful as it is not always economical or practical to build scaled prototypes just for testing. Very often the recovery procedures after certain transients can only be formulated with the use of these codes. Of importance here is the accuracy of the results and how to prevent the inaccuracies from exceeding the safety tolerances.

Lastly, system codes need to be benchmarked against tests. Levy (1999) discusses these tests and categorises them under separate effects tests, component performance tests, integral system tests and prototype operational tests. These different tests focus on developing the fundamental component models and then checking the overall performance of complex systems.

Separate effects tests deal with the basic phenomena involved in gas or liquid systems. Examples of these include measurement of variables such as pressure drops and heat transfer in basic systems, the effects of sudden closure of valves on downstream components. These tests are used to develop empirical correlations or to verify existing models.

Component performance tests are used in correlating the behaviour of various components and machines. They are performed on either reduced or full-scale models of the relevant

component. Examples include pumps, fans, valves, heat exchangers, etc. These tests result in empirical correlations or to verify existing theory and models relevant to the specific component.

Integral system tests refer to tests that simulate the overall behaviour of a system. These are usually done for transient and steady-state conditions expected in the final system. They are usually restricted to sub-systems that are practical to construct or to reduced scale models of the final system. These are the final check of the simulation code before it is employed in analysing the complete system.

Once the prototype system has been constructed it is subjected to various start-up and transient tests to confirm the accuracy of the computer codes used in its development. These tests offer the best type of validation of computer codes, as they are full-scale and do not compromise any dynamic behaviour in the system.

For a system code to be accepted by licensing authorities it needs a Software Verification and Validation Plan (SVVP) as developed based on the IEEE Standard 1059. Such a plan would detail the various tests as discussed above in a detailed programme assigning requirements for the various tests. The first two forms of tests are usually well utilised by code developers during the formative stages of the code development. The basic modelling of flow phenomena are tested with separate effects tests and then the various component models available in the code are each thoroughly checked with test components. This code is then utilised in system development where systems of components are built up and analysed. By analysing the overall system, all the relevant phenomena are identified and the effect of interactions between phenomena and components can be observed. Integral system tests can be performed to check the accuracy of simulation results and quantify the uncertainties involved. From there, additional tests can be identified for further verification or the process can move to the prototype test phase.

It is thus evident that a good integrated test plan must be in place in the development of simulation software, focusing both on component level tests and on testing of integrated systems.

2.3. The Verification and Validation Process

A simulation model is used to represent an actual system, whether it exists now or in the future. Simulation is indispensable where experimentation is unfeasible or expensive. If the model cannot provide valid representations of the actual system, any conclusions derived from the results may be incorrect and may result in poor decisions being made. That is why validation should be performed on all simulation models, regardless of whether the corresponding real-world system currently exists in some form, or whether it will be built in the future.

The aim of a validation has been fulfilled when the model can be used to make engineering decisions about the system it simulates. The ease of validating a model is inversely proportional to the complexity of the system and whether it exists or is still in the design phase.

The verification and validation process for a system code is regulated by international and national licensing authorities. These authorities require the developer's validation process to focus on the following main elements:

- dominant physical processes,
- derivation of equations,
- numerical methods,
- empirical correlations,
- comparison with relevant data:
    - comparison with experimental data,
    - comparison with actual plant data and
    - comparison with analytical solutions;
- independent verification and validation,
- biased calculations and
- best estimate calculations.

2.3.1. Physical processes

The main physical processes that occur in the system should be identified. These processes will always occur when the model is applied. It is important that these processes are accurately modelled and that the limits of the model in terms of the processes are thoroughly understood and adhered to.

2.3.2. Derivation of the equations

The physical processes are represented by mathematical models consisting of differential equations derived by applying conservation laws such as the conservation of mass, momentum and energy. The derivation of these equations needs to be validated for correctness and any simplifying assumptions are to be challenged until suitable arguments can be formulated.

2.3.3. Numerical methods

The first step in the derivation of a numerical method is the discretization of the differential equations. These are then solved with a suitable solution algorithm. A part of the validation is to ensure that the numerical method used is justified and that the accuracy of its results is within suitable limits. Any numerical problems that can occur using the method are to be documented with an explanation of why such problems will not negate the validity of the method's calculations. Conservation laws should be satisfied by the particular numerical method.

2.3.4. Empirical correlations

Most system codes also employ empirical correlations to represent some components or phenomena such as convective heat transfer. For example, instead of using the governing equations of turbo-machine theory it is much easier to use characteristic curves for a particular machine and let the code interpolate the required pressure ratios and efficiencies from the curve for a specified mass flow. Similarly correlations may be used to represent component behaviour. The claimed accuracy and the range of validity of the correlation need to be validated.

2.3.5. Comparison of results with data

After validating the models, numerical methods and correlations used by the code, the results of the code calculations need to be verified. As discussed earlier, the need for an integrated test plan comes into play here. The code will firstly undergo separate effects tests, component performance tests, integral system tests and prototype operational tests. Simply stated, these are a series of experiments beginning with simple representations and leading to situations that are more complex, representing conditions that are expected in the actual operation of the plant. The experiments should be conducted either at a scale close to that of the actual plant, or at a scale that allows easy interpretation of the results in relation to the actual plant size. For all experimental results obtained, the quality status as well as the traceability of these experiments will have to be demonstrated.

Furthermore, existing plants can be a very good source of information against which to compare the results of the simulation. Tests carried out in the full-sized plant during commissioning or start-up procedures, as well as operational transients or accidents, can be a useful source of data and should be included in the validation submission, whenever possible. Care should be taken, though, as most commercial plants are not as well instrumented as specially designed plants and experiments, and measurements taken from them may be too coarse to quantify accuracy of the simulation. They will, however, indicate if the simulation predicts the correct trend. It is for this reason that the HTTR is used as a validation benchmark to verify the trends as calculated with Flownex.

Finally, the code may also be validated against well-defined analytical solutions. Analytical solutions only serve to verify that the formulae used in the models were programmed in the correct way. They do not check the appropriateness of the model for the particular problem; here empirical data is much more valuable as the code is verified against what actually happens in practice.

2.3.6. Conservatism of models

During modelling a particular process the engineer may build a conservative model where uncertainties are present. Such biased models need to be documented and it must be shown in the validation process how conservative they are. On the other hand, whenever unbiased or best-estimate calculations are made, the validation process should look into the combined uncertainty limits from all the individual models within the system.

2.4. System computer codes

Now that the importance of verification and validation of analysis codes has been discussed, the focus will shift towards what exactly system computer codes are and how they work. As the name implies, these codes deal with the entire system's thermo-hydraulic behaviour during various scenarios. Not only must these systems accurately model sub-systems and components but also the interaction of these components during normal operation and transient events.

The difficulty of dealing with such large integrated systems is that accuracy must sometimes be compromised to get results timeously. Unlike Computational Fluid Dynamics (CFD) codes, system codes employ overall characteristics of some components instead of attempting to calculate a detailed distribution of velocity and temperature within a component. These simplified flow models are termed homogenous models. System code results are thus much

faster but not as accurate and detailed as CFD codes. The results obtained are, however, of high enough accuracy to do adequate system design and simulation.

System codes evolved from thermal-fluid modelling. Thermal-fluid modelling is a generalised methodology for calculating system-wide distributions of flow rates and temperatures in a network representation of water or gas reticulation systems.

Thermal-fluid systems may be considered as networks of flow paths through components such as pipes, valves, filters, fans, bends, compressors, turbines, combustion chambers, heat exchangers and power sources. The characteristics of these components in terms of their flow/pressure drop relationship and/or thermal behaviour may be obtained from handbooks, vendor specifications, or by experiment. Their use in the thermal-fluid approach provides a fast and accurate prediction of the flow distribution and the resulting thermal performance of the system.

An enhanced design cycle that incorporates thermal-fluid simulations in the early design stage, is shown in Figure 2.1. By using thermal-fluid analysis the conceptual design of a flow system is significantly reduced. Once the concepts are established more detailed flow and structural analyses can be performed with CFD and FEA codes respectively. Use of CFD analysis is impractical for examination of a large number of design alternatives in the early design stage. This is because it is time-intensive in terms of model setup, computation, and interpretation of the large amount of data. Thus, a quick and simple analysis procedure that allows evaluation of the flow performance of various design options in a scientific manner is necessary for conceptual system design.

The proposed design cycle significantly shortens the time required for arriving at the final design and improves the quality of the product by enabling the design engineer to explore more design options. Thus, the use of a thermal-fluid codes improves the productivity in the thermal design process and results in an optimum design cycle.

Apart from being used in optimising system level designs, thermal-fluid analysis is very effective in testing the sensitivity of systems to changes in sub-system performance. Some codes also allow transient analyses to be done so as to investigate the effect of parameter changes on dynamic behaviour.

One-dimensional network modelling has some limitations, which the user should be aware of during design. The method cannot calculate temperature or pressure distributions at component level but rather uses averaged control volume temperatures and pressures. These codes rely on the flow resistance inputs and as such incorrect input parameters will result in incorrect results. Furthermore, any system that consists of large volumes and flow paths cannot be modelled in great detail. Such systems require two or three dimensional flow and thermal analyses to predict the flow properties to the required level of detail.

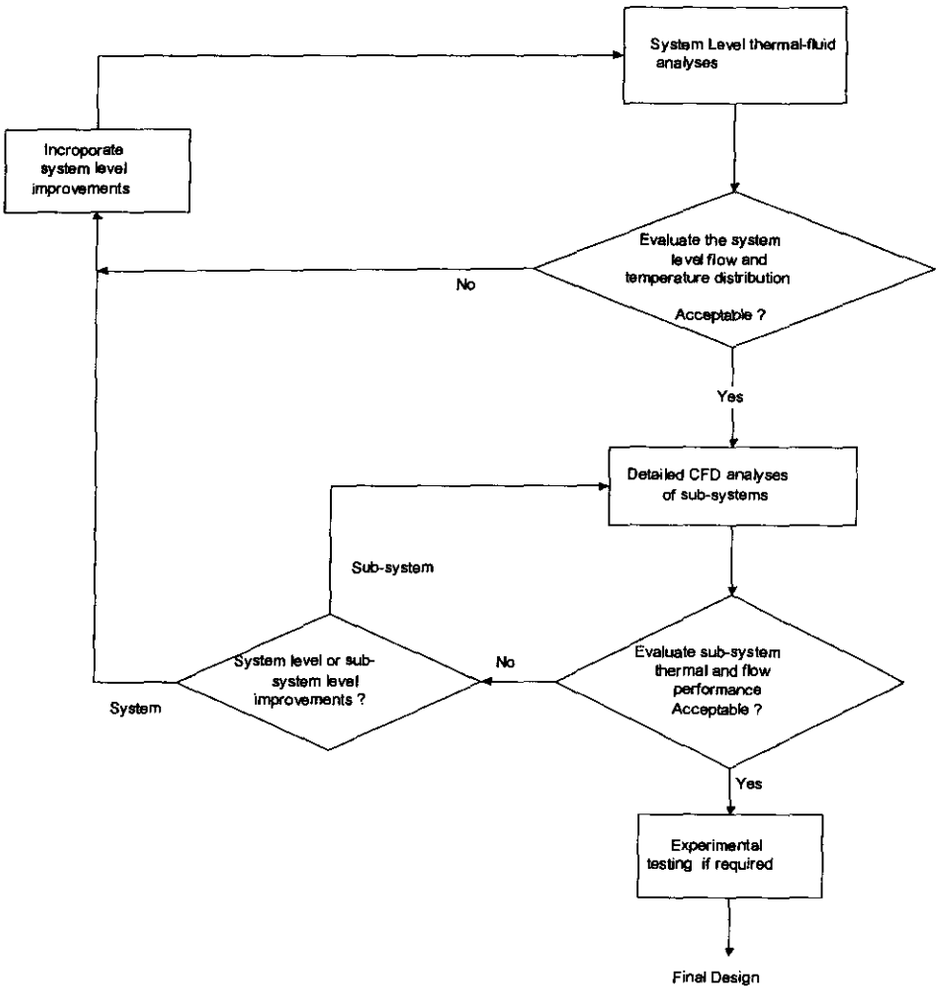

Figure 2.1 : Flow chart showing the design process using thermal-fluid analyses.

2.5. Commercial system codes

A number of system analysis codes are commercially available. Each of these codes have their advantages and disadvantages; where one lacks ability in a specific area, there are various other codes that can be used with more success. This section discusses a few commercial system codes and elaborates on some of their advantages and disadvantages.

2.5.1. SINDA/Fluint

SINDA/FLUINT is a finite-difference, lumped parameter (circuit or network analogy) tool for heat transfer design analysis (SINDA) and fluid flow analysis (Fluint) in complex systems. It is widely used in the aerospace, electronics, petrochemical, biomedical, and automotive industries. The analyst chooses the features required and can decide what levels of accuracy and approximation are appropriate. Customised features are also available to the analyst.

The code solves radiation, convection and conduction heat transfer, steady-state and transient flows while time and temperature dependent fluid properties are solved. One of the key capabilities of this programme is its ability to provide high-level design decision support. These capabilities include:

- goal seeking: find design inputs as a function of the desired model response,

- optimisation of multiple design variables using arbitrarily complicated constraints ,
- automated model correlation to test data,
- reliability engineering to quantify the design reliability and
- synthesis of a design that meets reliability requirements up front, intelligently balancing cost against risk.

The user has control over the solution techniques, sequences, accuracies and outputs. Restart and parametric analyses can be performed. Furthermore, SINDA/Fluint has advanced two-phase flow capabilities including boiling, flashing and cavitation models; equilibrium and non-equilibrium phases and capillary models.

All these advanced features, mainly focused on the process industry, negatively impact the solution time.

2.5.2. Flowmaster

Flowmaster is one of the more widely used thermal-fluid analysis codes with several applications in the power generation, process, marine, aerospace and oil industries. From research into the applications it was found that Flowmaster is mainly used in liquid pipelines, as very few gas applications were found. However, the code is capable of analysing both gas, liquid and mixed flows. Furthermore, the code's transient capabilities are widely used. It also has very good interfacing linkups with other programs used in the CAE process, like Simulink (control), CAD packages and three-dimensional flow analyses using CFD packages.

2.5.3. Aspen Custom Modeler

Aspen Custom Modeler (ACM) is a systems analysis code mainly used in the chemical industry. It utilises data blocks that represent components in a system. These are then linked with streams that represent pipe linkages. The main feature that makes ACM versatile is that every component block may be customised for the process it represents. The analyst can input the process equations into the block in a C programming environment. The code allows one to also adjust the flow resistance characteristics of the stream links between blocks. Furthermore, the code forms part of a suite of programs that include a database of fluid properties of 5000 pure and 5000 binary mixtures, a steady-state solver as well as a dynamic solver.

2.5.4. RELAP 5

Relap 5 is a thermo-hydraulic code that has been developed at the Idaho National Engineering and Environmental Laboratory (INEEL) primarily for Light Water Reactor (LWR) simulations. The code is especially suited for transient events such as small and large pipe breaks and the resulting loss of forced cooling. It uses a semi-implicit solution algorithm to enhance the solution accuracy without using smaller cell sizes. Although Relap was developed to analyse two-phase flows it can be used for single-phase flows as well. It is also used in Probabilistic Risk Analyses (PRA) studies to verify probabilities of accident scenarios.

The code includes many generic models which one can use to simulate general thermo-hydraulic systems. The models include pumps, valves, pipes, heat releasing or absorbing structures, reactor point kinetics, electric heaters, jet pumps, turbines, separators,

accumulators, and control system logic elements. RELAP5 represents the aggregate accumulation of experience in modelling reactor core behaviour during accidents, two-phase flow processes, and LWR systems. The code development has benefited from extensive application and validation against a large number of experimental programmes.

2.5.5. MacroFlow

MacroFlow is a thermal-fluid solver that utilises a visual representation of the network under consideration. MacroFlow enables accurate prediction of the system-level thermo-hydraulic behaviour in a variety of engineering applications. The component library in MacroFlow is both comprehensive and flexible to enable network analysis of a large variety of engineering systems. Furthermore, a comprehensive database of fluids allows analysis of gas and liquid systems. The heat transfer capability is comprehensive so that the temperature distribution throughout the system can be predicted for a variety of thermal boundary conditions.

The code allows the solution of steady-state and transient problems for compressible and incompressible fluids. Heat is transferred to the surroundings by convection and radiation. Mass and energy sources can be used on boundaries. Components included in the program are pipes, ducts, fans, pumps, intakes, diffusers, valves and tanks. The code does not have heat exchanger models, but customisable resistance components are available.

Solution control parameters, such as relaxation factors, convergence criteria and matrix-inversion procedure, can all be specified through dialogues or pull-down menus.

2.5.6. Flownex

Flownex is a system code that has been developed in South Africa since the late 1980s. Initially it was used in the modelling of simple gas and liquid networks and air conditioning systems. Major developments in the code took place with its use in the modelling of the PBMR, resulting in a well-rounded package. Applications include HTR nuclear power plants, conventional power plants, gas turbine systems (aviation and power generation), gas and liquid pipe networks, heat exchangers, ventilation systems, gas networks, combustion chambers and various other applications. The code is capable of solving both steady-state and transient thermo-hydraulic problems. These include both slow and fast (millisecond timescale) transients; the latter enables the tracking of sonic pressure waves in the fluid (Greyvenstein et al, 2002). Furthermore, the code supports compressible and incompressible fluids and mixtures, and all fluid properties can be calculated based on process conditions. The code has interfaces with control software like Simulink and SCADA programs such as UNAC. A further feature is conductive heat transfer elements that can be used to solve conjugate heat transfer.

2.6. Modelling approaches for power plant design

The choice of system code often depends on the problem to be analysed, as some programs are better suited to particular problems than others. Next, one needs to consider the modelling approach to be used in the problem. It is easy to over-discretise the system by having too many resistance elements and, vice versa, it is just as easy to underestimate the complexity of the scenario and thus the results will be inaccurate. In the survey some papers were found detailing the modelling approaches used in modelling scenarios. These are discussed below.

2.6.1. *Design of a heat recovery system of a mining truck using the MacroFlow system code*

This study involved the design of an innovative heat recovery system used in a mining truck. The large mining trucks use a very high-capacity engine for fulfilling the large power requirement at the mining site. It is therefore desirable to recover the waste heat from the large amount of hot exhaust generated by the engine. The heat recovery mechanism involves directing the flow through the beams supporting the dump platform. The objective of the design was to minimise the backpressure at the engine exhaust while recovering as much heat as possible.

The flow system involved a number of hollow beams of various cross-sections joined to each other, creating a complex system for the flow to travel from the engine exhaust to the atmosphere. MacroFlow was used to represent the flow system as a network of ducts, bends, orifices (formed at the joint of two beams), and tee and cross-junctions. Most parts of the system were standard and correlations for pressure loss and heat transfer were readily available. Where correlations were not available a CFD code was used to determine the performance characteristics.

The analysis predicted the flow rates and pressure drops in all parts of the system and backpressure at the engine exhaust. This enabled identification of the parts of the system in which the pressure drops are large and localised. Modifications, such as rounding of the bends and incorporation of ducts to provide parallel paths, were incorporated and their effect on the heat recovery and backpressure was analysed. After several interactive modifications, an optimum design of the flow/structural system was determined. The final design was validated on a prototype and then deployed in practice. Note that a conventional design method would have involved an iterative testing on a prototype – a procedure that would be very expensive and time consuming, given the scale of the physical system involved. Using a system code such as MacroFlow significantly shortened the design cycle and enabled determination of an effective design at substantially reduced cost.

2.6.2. *Comparison of RELAP and ACM in the modelling of a HTR gas turbine plant*

The modelling of thermal systems like HTRs requires careful considerations of the individual components in the circuit. Various codes have been written to simulate power cycles. Verkerk and Kikstra (2003) compared the modelling strategies and results of the RELAP and Aspen Custom Modeller (ACM) codes. The comparison was done on a model of the conceptual design of the Dutch AdvanCed Atomic Cogenerator for Industrial Applications (ACACIA).

The plant has a 40 MW thermal power and an electrical output of 13.6 MW. The cycle is a direct, helium-cooled Brayton cycle, which significantly reduces costs and prevents the water ingress risks that are present using an indirect steam cycle. The cycle consists of a HTR pebble bed reactor, a high-temperature turbine, recuperator, pre-cooler and compressor. The turbine and compressor are linked by a single shaft and are then linked to the generator as shown in Figure 2.2.

The nuclear reactor does not have an active fuelling system in which spent fuel is removed and fresh fuel is added during operation. Instead fresh fuel is only added as the lower fuel spheres become spent, thereby raising the pebble-bed over time. High-pressure helium is heated in the pebble bed and then flows into a turbine that drives a shaft with a compressor

and electric generator as loads. Before compression takes place again, the gas is cooled in a recuperator and a water cooler.

The recuperator transfers heat from the low pressure stream leaving the turbine to the high pressure stream leaving the compressor, thereby greatly improving the cycle efficiency. All the excess heat is lost in the cooler that generates steam in a secondary loop. This is used for process or industrial purposes, which is not covered in the study. Once cooled, the gas is compressed in the radial compressor and reheated in the recuperator before entering the reactor. The control of power output is done by adjusting the mass flow through the cycle. This is done by injecting or removing helium from the cycle and storing it in helium tanks. A bypass control valve is used to remove power from the turbine in the event of electrical load rejection.

The article presents a comparison between two codes used to model the ACACIA cycle. The widely used RELAP5/MOD3.2 is used for the first model. The main advantage of this is that this code is well validated as a nuclear code, while the drawback is that it was primarily developed for steam cycles. Furthermore, due to its age the input methods are very time consuming and intricate; a condition which promotes errors creeping into the model. The second model is built on ACM, which has the advantage of very efficient solver algorithms and easy adaptation of the code to the specific modelling needs.

Using ACM, the compressor is modelled using the Euler equation for isentropic and total enthalpy rise per stage. Slippage losses, clearance losses and backflow losses are accounted for. The enthalpies are then non-dimensionalised by division by the impellor velocity squared and then used to draw up a set of curves for pressure ratio versus flow coefficient. These curves are used for the system calculations. The same curves are used in RELAP, where a user routine was created to convert this data into usable data for the code. As the same curve was used for both codes, large differences in results are not expected.

As with the compressor, analytical expressions are used to characterise the turbine behaviour. The total and isentropic enthalpy drops are calculated using an explicit version of the Euler equation and then non-dimensionalised. Losses such as blade profile losses and tip losses are also accounted for. In RELAP the code's steam turbine model is used, which is based on a lumped-parameter approach which is more simplistic than the ACM model. The results of pressure ratio versus isentropic efficiency and mass flow rate were compared. For pressure ratios less than 1.75, the difference in efficiencies is very large, with RELAP not at all suited for these conditions, while the ACM model is better equipped to describe this region. However, for pressure ratios greater than 1.75 the discrepancy between the two models is never more than 2 percent.

The two heat exchangers in the system are modelled as many small heat transfer nodes. This discretised method is suited for numerical calculations but lacks accuracy if there are not enough subdivisions. Both ACM and RELAP use correction factors to correct the outlet temperature errors based on empirical data for the actual heat exchanger.

When modelling the reactor, ACM is superior to RELAP in that it uses a two-dimensional discretisation and it combines internal heat production, convective and conductive heat transfer for radial and circumferential directions. RELAP only solves heat transfer radially while combined convection and conduction in the mesh is not solvable. Both models account for pressure drop due to friction in the pebble bed. In both models the point kinetics approach

is used to model the neutronic behaviour of the core. The point kinetics model is discussed later in this document as it is also used in the Flownex model.

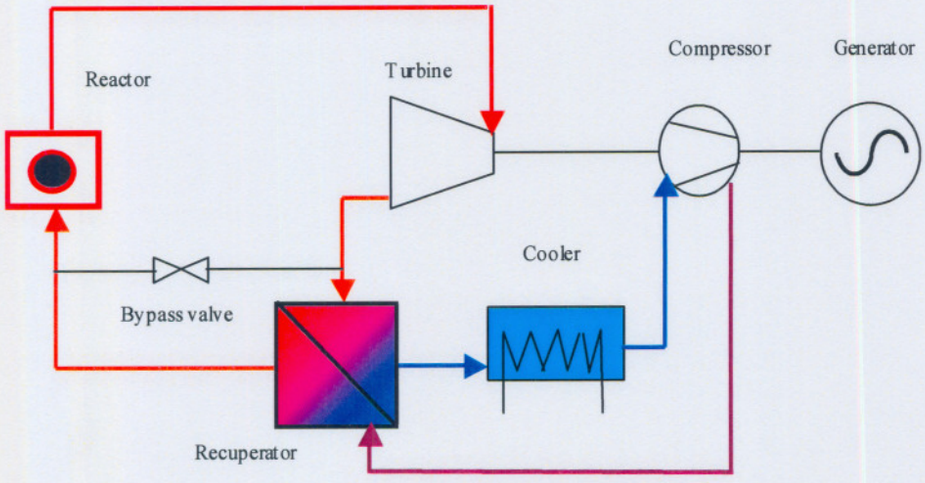

Figure 2.2 : Schematic representation of ACACIA plant's Brayton cycle.

Now that all the component models have been compared, the overall system results are compared. With the reactor outlet temperature fixed at 800°C, various steady-state points were compared to investigate the effect of shaft speed on generator power. ACM predicts highest power at slightly higher shaft speed than what RELAP predicts. This difference is attributed to the differences in turbine models, as the compressor models are essentially the same.

A short-term transient called *load rejection* is also modelled. In this case the generator load is stepped down to zero, instantaneously forcing the shaft to overspeed. This has a downstream effect that compares very well between the two codes. Once again the only real difference is in the mass flow and shaft speed at which the system reaches steady-state. This is due to the differences in turbine models, with the ACM version being favoured.

A second transient is also discussed, which occurs over a much longer time period. In this case a switch to part-load operation is analysed. Helium is extracted from the system until the inventory is at 50 percent. The effect of xenon build-up in the reactor is monitored, as it strongly affects the heat produced in the core. The comparison reveals that the difference between the two recuperator models results in some discrepancy. The discrepancy is however not very significant.

In conclusion the two models compare very well, except for the already mentioned differences in turbine and recuperator models. This is a good example of where a particular system code has been benchmarked against another well established and validated system code utilising both separate and integral effects tests.

2.6.3. Modelling of the PBMR with Flownex

The Pebble-Bed Modular Reactor (PBMR) system uses a recuperative Brayton cycle with helium as the working fluid to convert the nuclear energy into electrical power. A schematic layout of the system is shown in Figure 2.3. The system uses hot, high-pressure helium (9Mpa, 900°C) to drive a high-pressure turbine and then a low-pressure turbine. These are

mechanically linked to a high-pressure compressor and a low-pressure compressor respectively. The gas is then expanded in a power turbine (5.2 MPa to 2.9 MPa, 680 °C inlet temperature) that drives the electric generator. This hot gas then exchanges heat with high pressure return gas to the reactor in a recuperator before being cooled in a pre-cooler (2.9 MPa, 33°C pre-cooler outlet condition). The cooler gas is then compressed and cooled in the low-pressure compressor and intercooler respectively. The high-pressure compressor further compresses the gas to 9MPa before returning it to the reactor via the recuperator. The reactor produces 400MW of thermal energy that is converted to approximately 165 MW of electrical power in the generator.

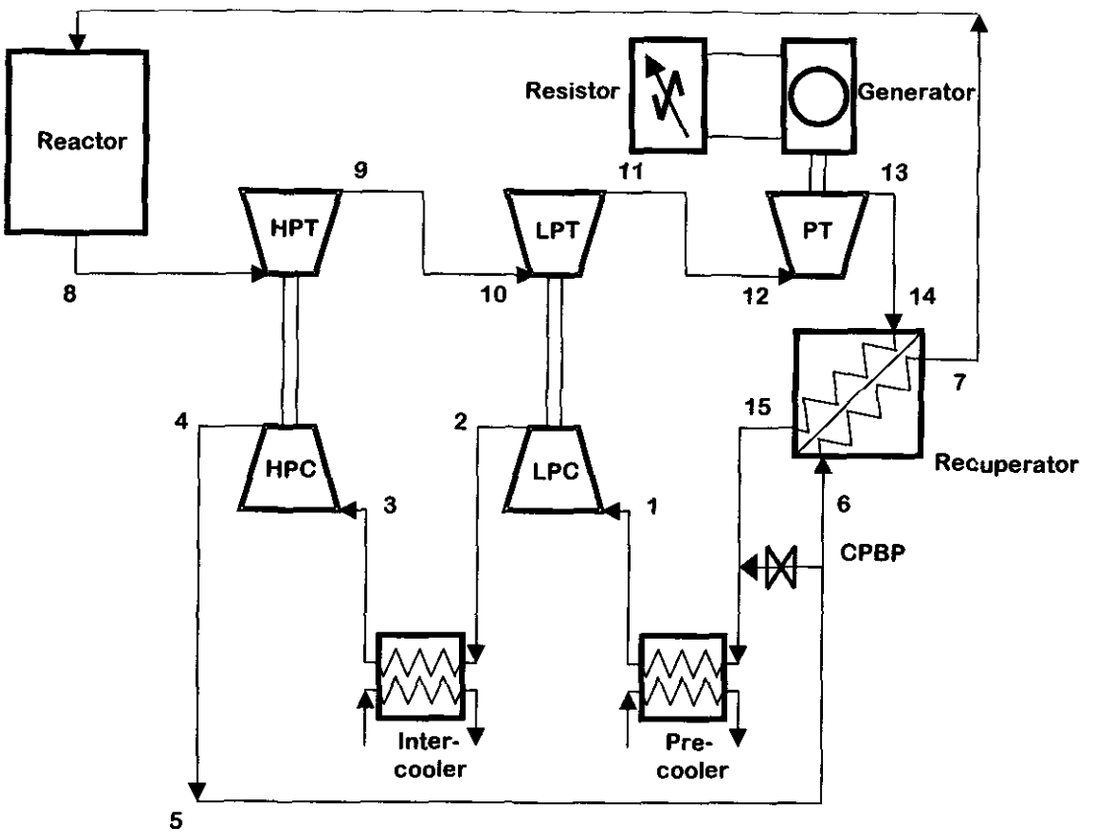

Figure 2.3 : Schematic layout of the PBMR main power system.

Figure 2.4 shows a temperature-entropy diagram of the cycle. The various stages of the cycle are labelled numerically in Figure 2.3 with their corresponding temperatures and entropies shown in Figure 2.4.

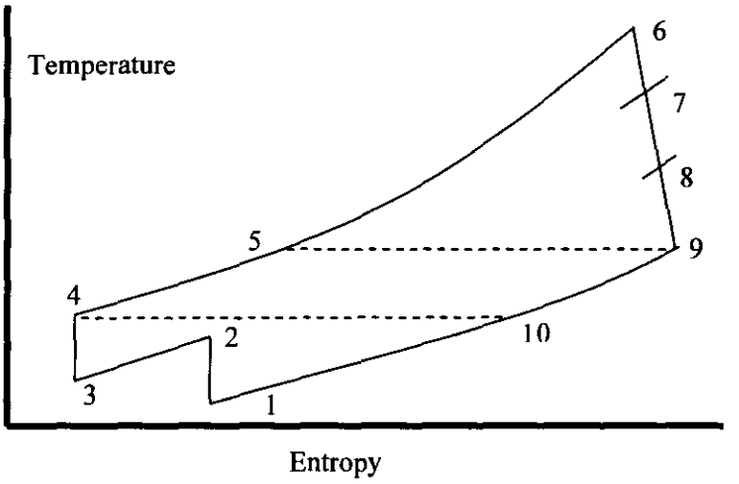

Figure 2.4 : T-s diagram of the PBMR main power system.

This cycle has been modelled in Flownex so as to observe steady-state conditions and to investigate the transient effects of any changes in these conditions. The engineers at PBMR then use the data for further design iterations of the various components and sub-systems. A high level version of the model is shown in Figure 2.5. In the figure the circles represent flow elements while the squares represent nodes (junction points)

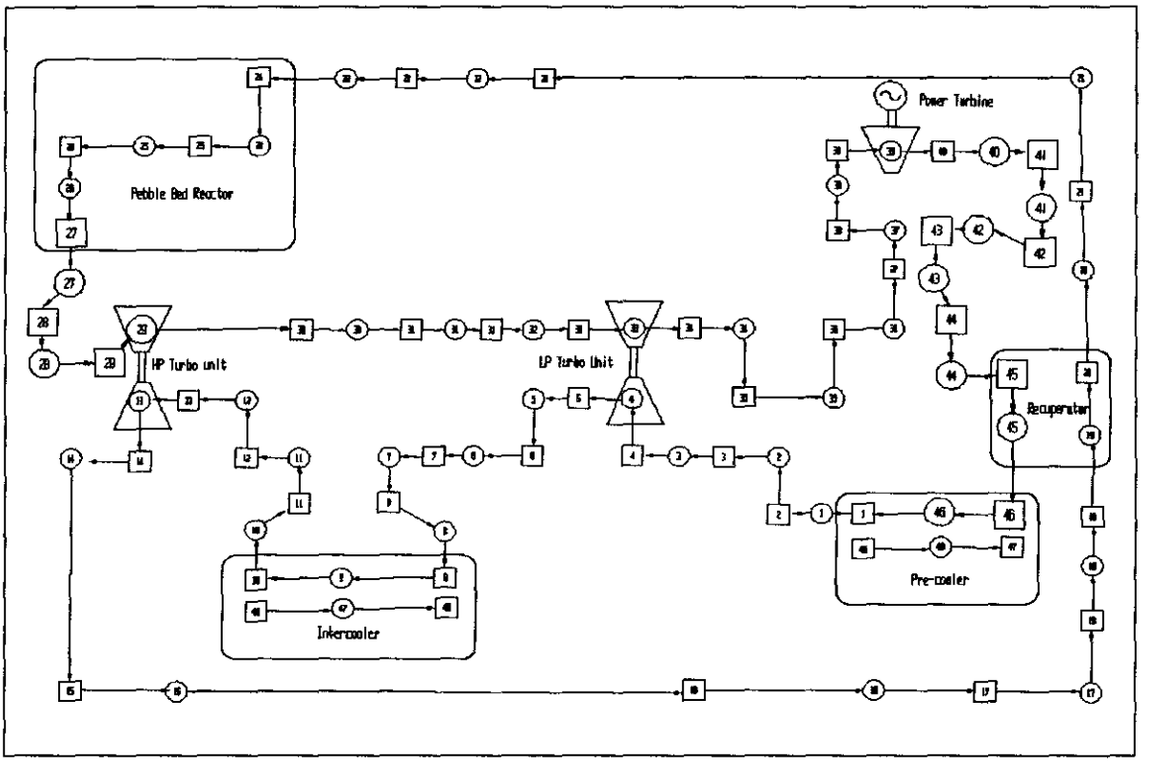

Figure 2.5 : Flownex model of PBMR.

The ducts and pipes in the system are modelled with the Darcy-Weisbach equation to account for pressure drop; special valve models model all valves or use restrictors with discharge coefficients. The larger components are discussed next. More detail on the modelling techniques of Flownex can be found in the Flownex user manual (Coetzee et al, 2002).

2.6.3.1. Recuperator

The recuperator is used to recover heat from the outlet of the power turbine and transfer it to the high-pressure gas entering the reactor. This greatly increases the efficiency of the whole plant. High efficiency recuperators are usually very complex structures. Designers have to find a compromise between the pressure drop and the heat transfer area of the recuperator. To obtain such large heat exchange areas with minimal flow length the designers normally opt for plate fin designs. Much emphasis is placed on the flow length and the flow channel shape as both of these influence pressure drop and whether the flow is turbulent or laminar, which in turn has an effect on the heat transfer coefficient. The thermal inertia of all the plate fins is also important as it influences the heat exchange during transients. This is one of many aspects considered during the modelling of the recuperator. In Flownex there is a specially developed element for the recuperator that accommodates such all these requirements. This element is discussed in more detail in Chapter 4.

2.6.3.2. Compact gas/liquid heat exchangers

The pre-cooler and intercooler are known as compact heat exchangers due to the very large heat transfer surface area to volume ratio that they have. Flownex uses a model called a *compact gas/liquid heat exchanger model* to represent such components. The model applies to all heat exchangers that have a single gas pass and multiple liquid passes.

In the PBMR the pre-cooler and intercooler are identical but have different operating conditions. They are designed in an axi-symmetric shape with the gas flowing from the outer circumference inward through two sets of u-tubes. The cooled gas then passes from the centre of the heat exchanger up to the compressor situated directly above the cooler. On the gas side there are fins to enhance heat transfer while in the tubes the walls are smooth. Figure 2.6 shows a schematic of this type of heat exchanger indicating important parameters required in the model.

The Flownex model is designed to accommodate any fin geometry on the gas side. To do this the model requires the user to input data describing the pressure drop and heat transfer characteristics of the gas side. In the industry this is most commonly done by providing the friction factor and the Colburn factor as function of the Reynolds number. The Colburn factor is a non-dimensional number defined as $StPr^{2/3}$ where St is the Standton number and Pr is the Prandtl number (Incropera, 1996:308). A common source for many such heat exchanger geometries and a surface is Kays and London (1984). On the water side the same equations apply as those used in the pipe model.

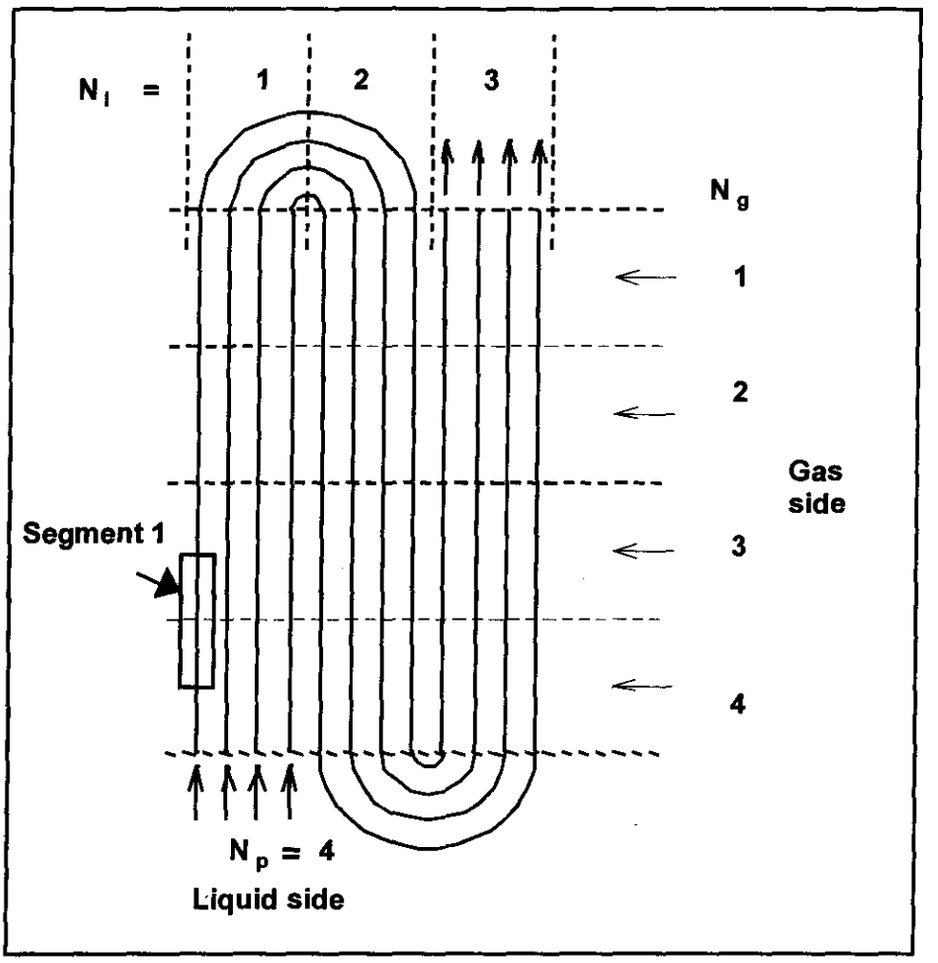

Figure 2.6 : Schematic representation of compact gas/liquid heat exchanger model.

In the modelling process the heat exchanger is discretised into smaller segments, like the one shown in the previous figure. These segments are referred to as computational cells and can be described schematically in the form shown in Figure 2.7. The cell consists of two streams, one hot and one cold linked by a metal element that represents the tube wall. In the figure the smaller circles denote convective heat transfer links while the smaller squares denote temperatures nodes in the metal separating the hot and cold streams.

To model a particular heat exchanger layout these computational cells can be arranged in the appropriate topology. For example a typical counterflow arrangement is shown in Figure 2.8.

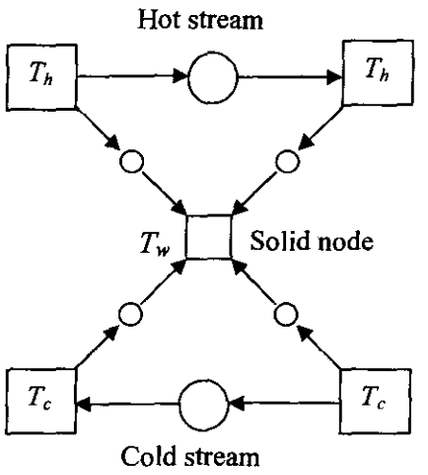

Figure 2.7 : Heat exchange computational cell.

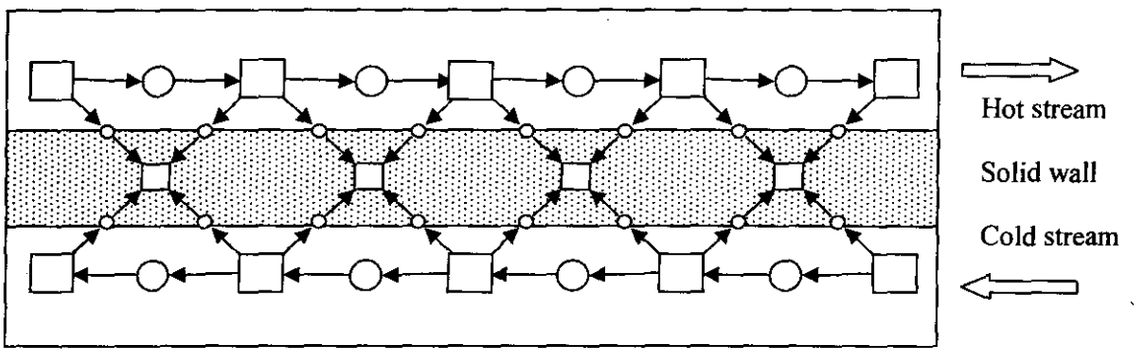

Figure 2.8 : Network representation of the computational cell used in counter-flow configuration.

Figure 2.9 shows the discretisation of a typical cross-flow arrangement. As in the previous figure larger circles and squares denote flow elements and nodes respectively, while smaller circles and squares denote convective heat transfer links and metal temperatures respectively.

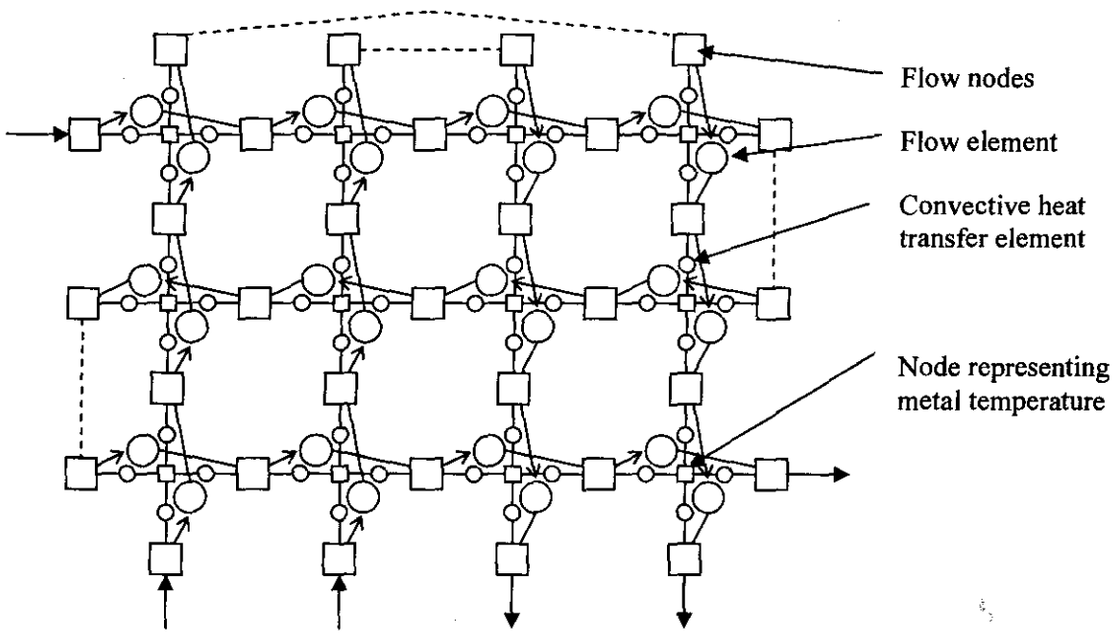

Figure 2.9 : Discretisation of a cross-flow heat exchanger.

A more detailed description of the various heat exchange models is given in Chapter 4.

2.6.3.3. Turbo-machines

The Flownex model for turbo-machinery is very flexible. Any number of compressor and/or turbines may be placed on a single shaft and multiple machines may be simulated in a system during a simulation. Power losses caused by mechanical and generator-related events are also accounted for in the model. Furthermore the shaft speed can be set constant by the user or allowed to vary as the simulation finds a working point for the input speed and mass flow. The model uses characteristic curves (see Figure 2.10 and Figure 2.11 for examples), from which it uses inputs such as shaft speed or mass flow to interpolate the pressure ratio and efficiency of the unit. In contrast to the difficulty experienced by other techniques, the solver can solve on positive slopes of a constant $N\sqrt{T_0}$ curve.

The only limitations of the current model are that the performance tables used in the simulation are Reynolds number independent and that predictions in the surge regime are unsatisfactory. Reynolds number effects are, however, not very significant and may be neglected for the time being.

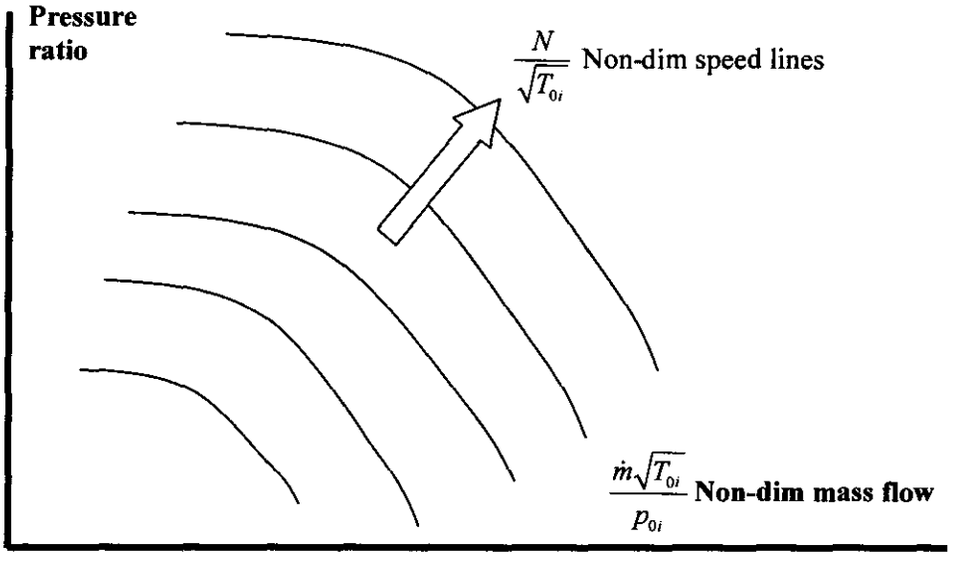

Figure 2.10 : Pressure ratio versus non-dimensional mass flow for a compressor.

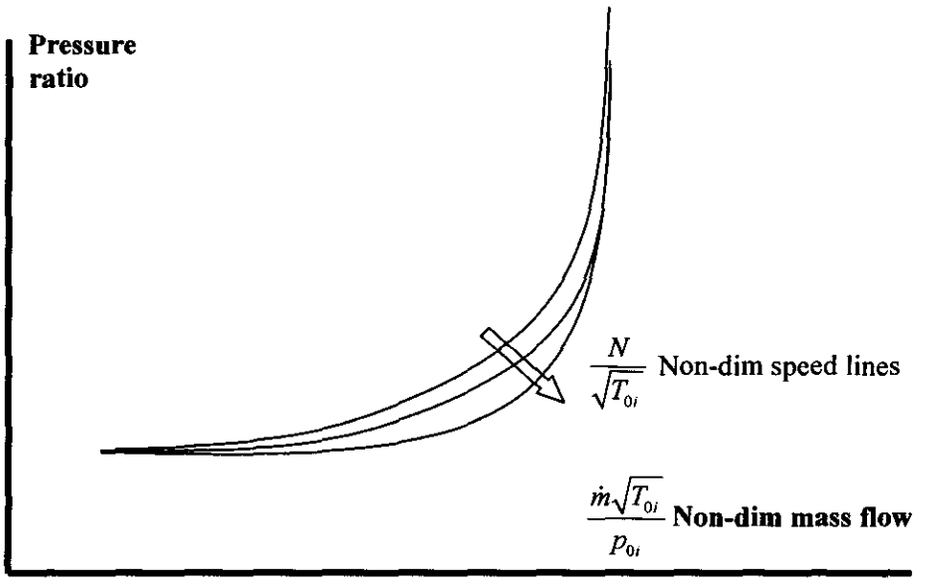

Figure 2.11 : Pressure ratio versus non-dimensional mass flow for a turbine.

The compressor model is discussed in more detail in Chapter 4 as it is used to model the HTTR's ciculators.

2.6.3.4. PBMR reactor model

The PBMR's heat source is the pebble bed reactor containing fuel spheres. This pebble bed reactor is modelled by discretising it into a number of control volumes using a two-dimensional axially symmetrical coordinate system. In each control volume a representative fuel sphere is discretized in the radial direction into a number of one dimensional control volumes. The average reactivity, temperature and heat transfers are calculated for a fuel sphere control volume layer and these values are used to generate a power profile in the core as a function of core height. The neutronic behaviour is calculated using a point kinetics model (Duderstadt et al., 1942:235).

This model has been successfully used to obtain process data to be used in further refinement of the mechanical design of the plant. Important results are obtained for transient events such as the start-up of the plant. An example of transient results is shown in Figure 2.12 which shows the recuperator in- and outlet temperatures during start-up. Such results are very important in calculating fatigue life of components, especially since the proposed operating life of the plant is as long as 35 years.

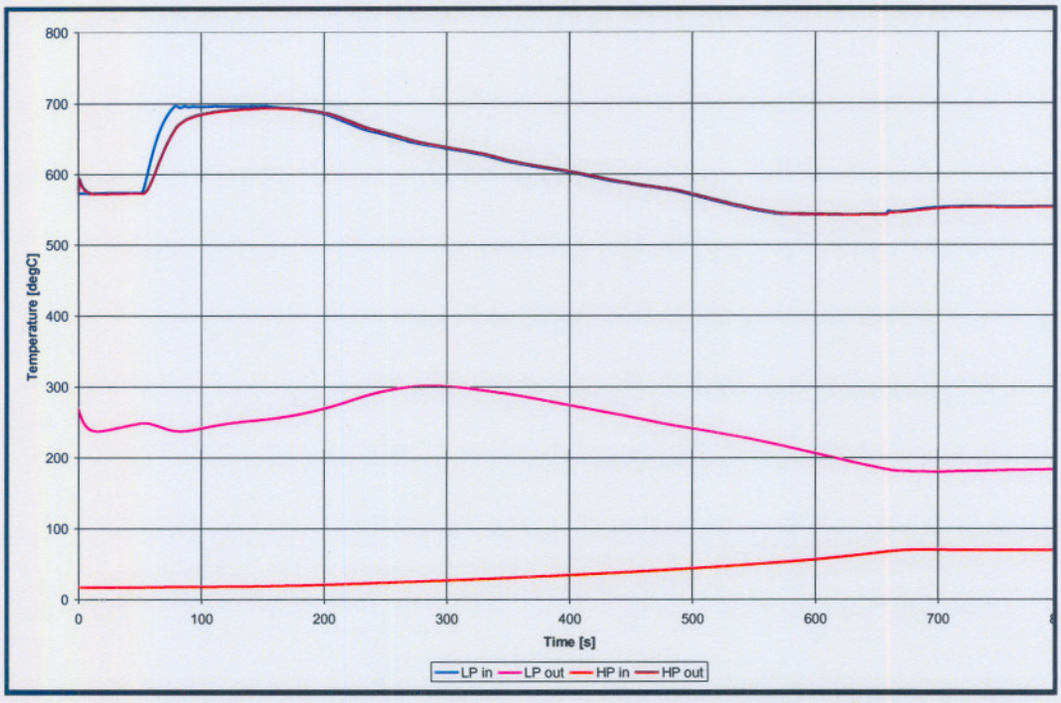

Figure 2.12 : Typical start-up temperatures in the recuperator based on Flownex model.

2.6.3.5. Conclusion

The Flownex model of the PBMR has been developed over the last five years, with each design iteration adding more detail to the model as the physical design has evolved. The model is very beneficial to engineers in terms of the steady-state and dynamic results it has produced. For example, the start-up transient yields excessively high temperatures in the turbines and recuperator at low mass flows. This gives a very steep concentrated temperature gradient in the recuperator heat exchange matrix (see Figure 2.13). Such high thermal gradients cause very high stresses in the base material, which negatively impacts operating life. In the past, when system codes were not available, it would have been very difficult to identify such high stresses without building test rigs and prototypes – a much more costly operation than using a computer program.

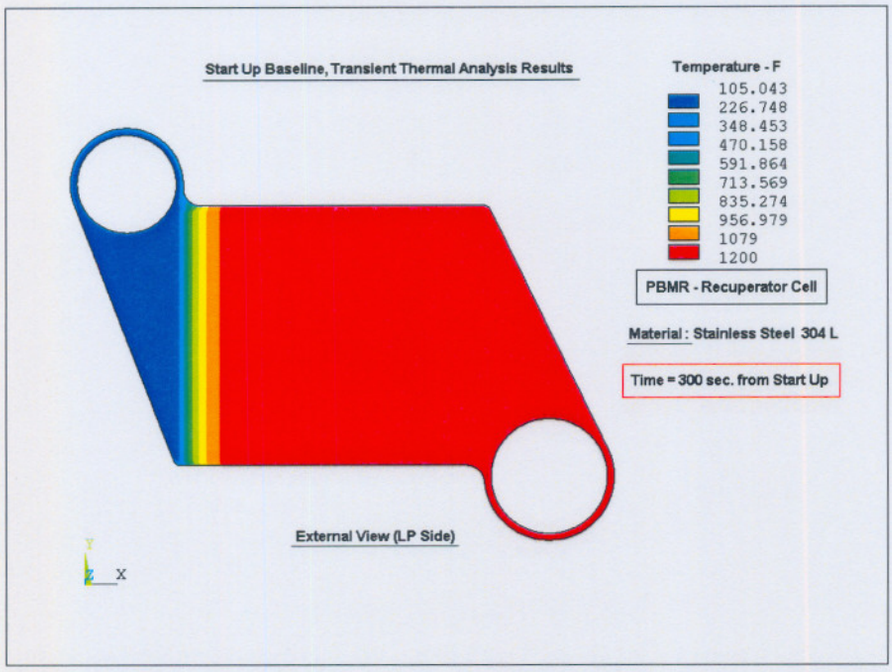

Figure 2.13 : Thermal footprint of the PBMR recuperator's heat exchange area during a Start-up.

2.7. Where the HTTR fits in

Now that the verification and validation process, commercial codes and case studies have been discussed, it is necessary to put the current study into perspective. In response to the increasing international interest being shown in HTR technology over the last decade, the International Atomic Energy Association or IAEA has organised Co-ordinated Research Programmes (CRP). Each of these CRPs is typically 3 to 5 years in duration and involves up to 15 member states. The participants provide most of the resources to host, organise and perform work necessary for the CRP.

In 1997 the IAEA initiated the CRP on Evaluation of HTGR Performance scheduled for completion in 2004. The CRP has the following scope of research:

- modular HTGR reactor physics benchmark analysis;
- modular HTGR thermo-hydraulic transient benchmark analysis and
- demonstration of modular HTGR safety characteristics.

For the CRP, benchmark problems were identified for comparison of code results to experimental results. The experimental data was obtained from HTR-10 (China), HTTR (Japan) and PBMR's ASTRA experiments, all of which are test reactors and associated facilities. The countries involved in the CRP include: China, Japan, USA, Germany, Netherlands, France, Russia, South Africa and Indonesia.

The primary function of this CRP was to specify experimental benchmark problems and to exchange data between participants for comparison. In each case the participant supplying the benchmark was responsible for providing the details of the facility and provides sufficient technical data for the other participants to use in analyses. The Japanese Atomic Energy Research Institute (JAERI) prepared the benchmark documentation for the HTTR test reactor (Takeda et al., 2000). This document provides benchmark information for the thermo-

hydraulic benchmarks based on the HTTR results. Two problems were identified: a vessel cooling benchmark, where the passive heat removal system in the reactor cavity is analysed, and a loss-of-off-site power problem, where the transition from normal operation to auxiliary cooling is analysed. The latter benchmark is dealt with in this thesis.

In the next section a more detailed description of the HTTR is given, along with the requirements of the benchmark. This is followed by a detailed overview of the system code to be used for the benchmark, namely Flownex. From then on the text investigates the models used and the results obtained from the study.

3. OVERVIEW OF THE HTTR

3.1. Introduction

The High-Temperature engineering Test Reactor (HTTR) is a HTR test reactor built at the Oarai Research facility in Japan. This chapter discusses the HTTR's history and purposes and also the technical aspects of the plant. These are all in anticipation of the work to follow in Chapters 5 to 7, where the HTTR cooling system is simulated using the system code Flownex.

3.2. Background

The Japan Atomic Energy Research Institute (JAERI) has performed research and development (R&D) of HTGR technology since 1969. This R&D work has focused on both electricity generation and process heat applications. In 1987 the institute issued a long-term programme into the development and utilisation of nuclear energy, recommending that the country proceed with the development of advanced nuclear technologies both in their conventional plants and in HTGRs. This resulted in the HTTR being proposed as a test reactor for HTGR technology to be built as soon as possible. JAERI received a permit for installation from the Japanese government in 1990 with construction starting in March 1991 and the first criticality planned for 1998. Figure 3.1 shows a cutaway view of the reactor and its enclosure.

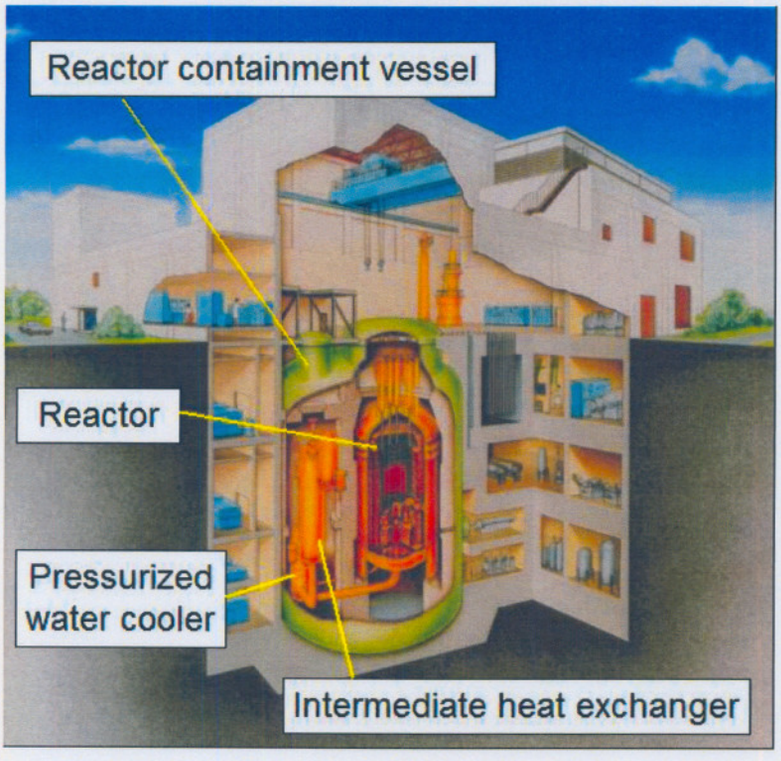

Figure 3.1 : Cut-away view of the HTTR and its building.

The HTTR was commissioned with the following objectives in mind (Saito et al., 1994): firstly to establish the basic HTGR technologies in a test facility; then to demonstrate the HTGR's safety operations and inherent safety characteristics. Further objectives are to demonstrate the heat utilisation of a nuclear process, for the irradiation of materials in the core and, in general, to serve as a test bench for R&D work in HTGR technology.

The plant consists of a reactor building, spent fuel storage building, a machinery building and various other smaller buildings. The reactor building is approximately 48m by 50m in footprint, with the HTTR being housed underground and with support systems housed in the levels above ground. Figure 3.2 and Figure 3.3 show views of the HTTR site and reactor building respectively.

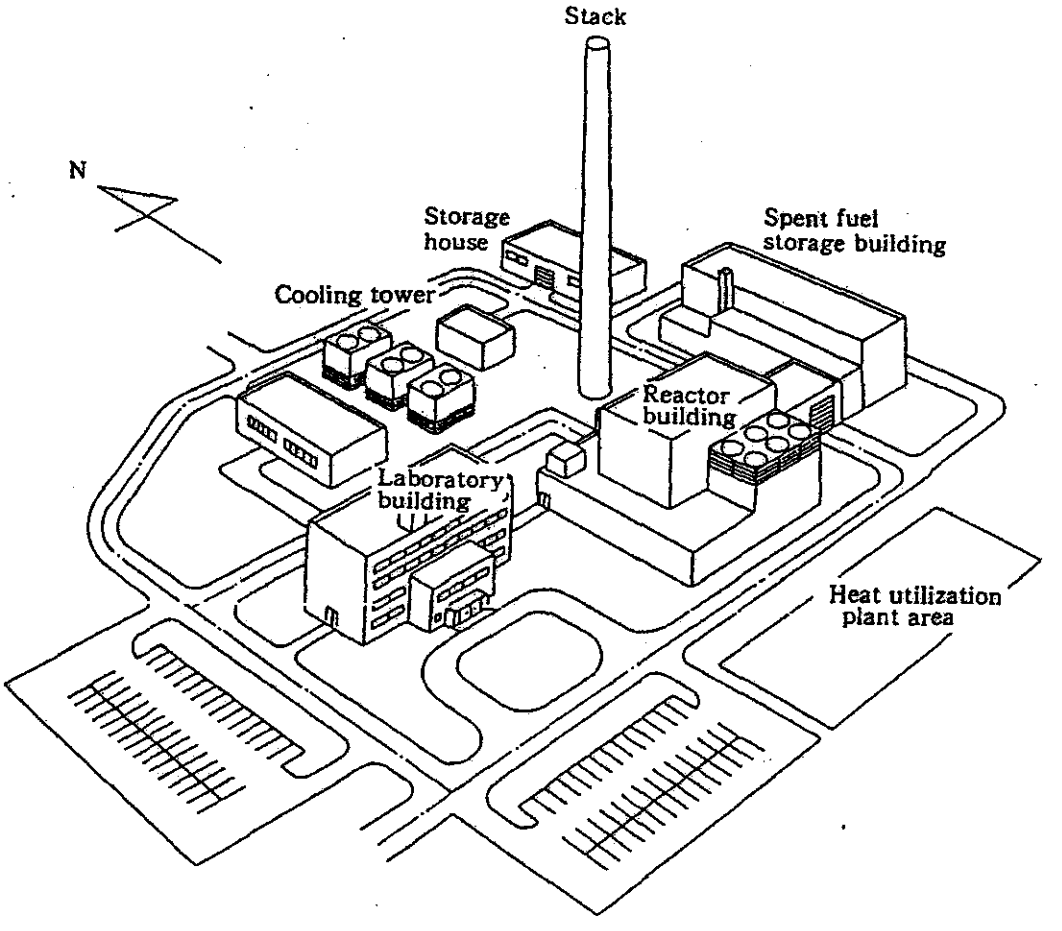

Figure 3.2 : Site plan of the HTTR plant.

The HTTR attained its first criticality in November 1998, with the start-up core physics tests successfully being completed in January 1999. Following that, rise-to-power tests were conducted starting in September 1999. As part of the ongoing testing of the operational occurrences in the plant, it was necessary to test the cooling of the reactor core in the case of accidents. As such, loss-of-off-site power tests were planned for the power levels of 15MW and 30MW.

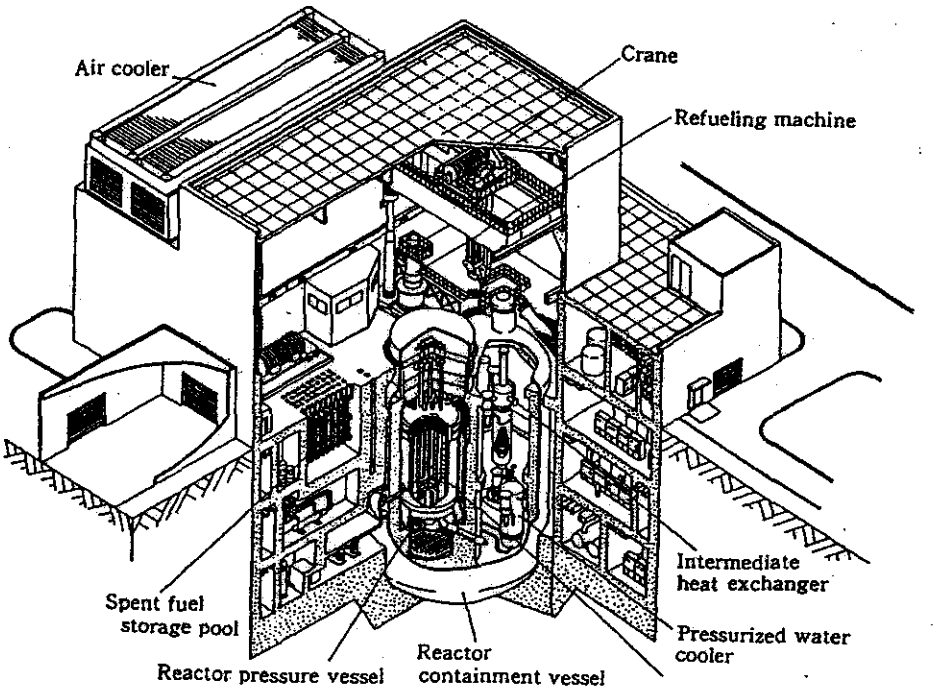

Figure 3.3 : Reactor building of the HTTR.

3.3. System overview

Figure 3.4 shows a schematic representation of the HTTR showing the reactor and the different cooling systems used to process the heat generated. Unlike the PBMR, the HTTR uses block fuel and not fuel spheres in its reactor. This implies that the fuel cannot be dynamically loaded and unloaded, as is the case with PBMR, but rather the fuel is loaded once and remains in the reactor until spent. The fuel is compressed into hollow cylindrical elements that are then placed in a metal sleeve to form a fuel rod. These fuel rods are placed into borings in the graphite reflector of the core. Helium flows through a gap between the fuel rod and the boring, where it is heated by the fuel rod. The reason for using block fuel is that it is easier to perform irradiation tests on various materials (Saito et al., 1994) and the complexity of a fuel handling system required by fuel spheres is also negated. More detail is given on the reactor design in Chapter 5.

The heat generated in the reactor needs to be removed. For this function various cooling systems are employed. Firstly, there is a Main Cooling System (MCS)comprised of a Primary Pressurised Water Cooler (PPWC), helium circulators or fans and an Intermediate Heat Exchanger (IHX) where heat is transferred to a secondary helium cooling circuit. The secondary circuit consists of another helium circulator and a Secondary Pressurised Water Cooler (SPWC).

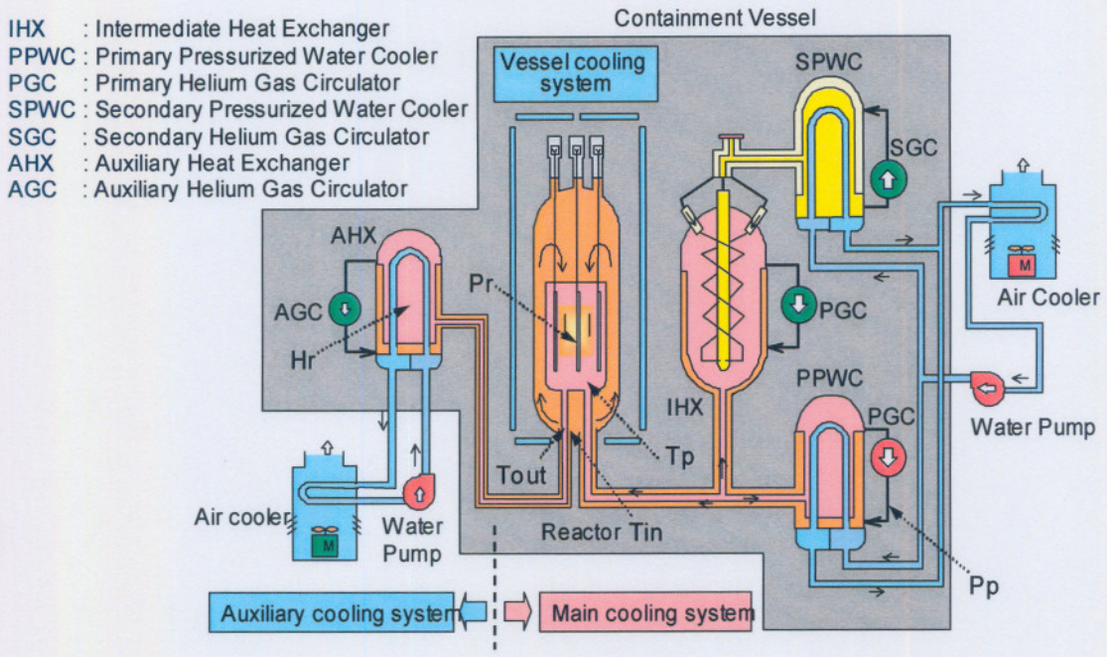

Figure 3.4 : Schematic diagram of the HTTR cycle.

Both water coolers reject heat to a water circuit that is cooled with air coolers. In the event of a problem in the main cooling system, such as a loss of power to the circulators, an Auxiliary Cooling System (ACS) is employed to perform the cooling function. This system comprises of an Auxiliary Heat Exchanger, similar to the PPWC and SPWC and a circulator. A back-up electricity generator supplies the power needed in this circuit.

During normal operation the helium is heated in the reactor and is then circulated via concentric ducts to the IHX and the PPWC, which are connected in parallel. The PPWC is a shell-and-tube water-cooled exchanger while the IHX is a spirally wound shell-and-tube type helium-to-helium heat exchanger. Valves in the circuit allow the HTTR either to be operated using only the PPWC as cooler or both the PPWC and the secondary circuit (called *parallel cooling*).

The Vessel Cooling System, or VCS, is a passive heat-removal system that cools the reactor walls during normal operation. In the event of either the main or auxiliary cooling systems malfunctioning, the VCS will remove the decay heat generated in the core. The VCS is a safety system and is redundant in that it has two independent sets of cooling systems. The VCS is not discussed further, as it falls beyond the scope of this thesis.

In the next chapter the thermo-fluid analysis code Flownex is discussed. The information given in this chapter can then be used along with the Flownex models discussed to develop a system model for the HTTR as described in Chapter 5.

4. OVERVIEW OF FLOWNEX

4.1. Introduction

Flownex is a pipe-network based thermo-hydraulic system code. This chapter discusses the background of the code and then looks in more detail at the working of the code and the underlying theory on which it is based. This theory discusses the discretisation methods, solution algorithm and component-specific models. The purpose of this chapter is to introduce the reader to the capabilities of Flownex, in particular its sub-models.

4.2. General overview

Flownex predicts the flow, pressure and temperature distribution in large unstructured thermal-fluid networks and is mainly used as an engineering tool in analysis and optimisation of thermal-fluid systems such as power plants. It accommodates various component models, ranging from general pipe and duct models, turbo-machinery, and heat exchangers through to special elements like high-temperature reactors such as the PBMR and HTTR. Another useful element in Flownex is the Conductive Heat Transfer (CHT) element that allows one to model heat transfer paths in solid structures linked to flow paths. The program's graphical user interface (GUI) is easy to understand, while catering for different user competencies.

Some of the flow components supported by the program include pipes, ducts with area change, restrictors, valves, pumps, fans, compressors, turbines, shell-and-tube heat exchangers, complex heat exchangers, recuperators and various other components. Control problems may be analysed using the PID controller element or using interfaces with programs such as Simulink and UNAC.

4.3. Network approach

Flownex uses a network approach in which flow components such as pipes, turbo-machines, heat exchangers and other thermo-hydraulic components are modelled as flow "elements" interconnected at "nodes". Elements have pressure drop and heat transfer correlations that are unique to the specific component being modelled. Apart from serving as junction points in between elements, nodes can also be used to model large volumes and manifolds. The velocity in such volumes is too small to contribute to flow resistance but is nevertheless important when analysing transient flows. This becomes apparent during transients where they serve to dampen fast changes in flow parameters such as pressure and temperature disturbances.

This method can also be explained as a one-dimensional control volume code that uses the same governing equations as in Computational Fluid Dynamics (CFD), but is simplified in that it does not solve fluid properties in three dimensions but rather uses volume averaged properties. This implies that flow velocity, pressure and fluid properties are equal throughout the cross-sectional flow area of a duct and vary only in the flow direction. This improves solution speed by orders of magnitude with a negligible effect on accuracy. This is especially advantageous when doing transient analyses where conventional CFD analyses are extremely time consuming and economically unfeasible.

The program is coded in such a way that sub-networks can be accommodated in component elements. An example of this is the heat exchanger models that can be sub-divided into

smaller heat exchanger elements to more accurately model the thermal results. Figure 4.1 shows an example of a node-element network. The elements are denoted by circles, while nodes are denoted by squares.

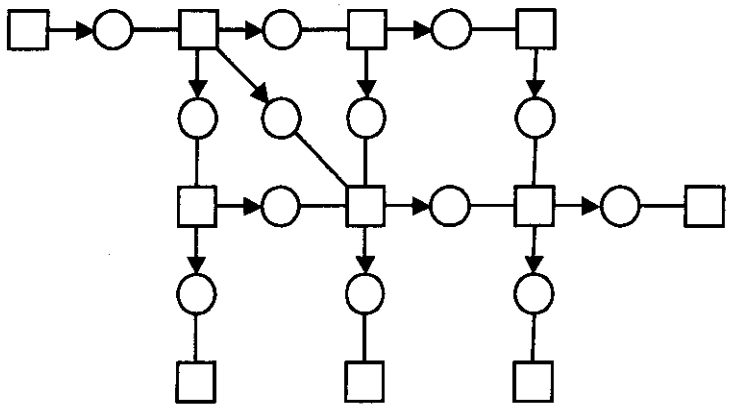

Figure 4.1 : Example of a Flownex thermo-hydraulic network (circles – elements, squares – nodes).

4.4. Solution algorithm

The equations that govern the pressure, flow and temperature distribution in a thermal-fluid network are the mass, momentum and energy conservation equations. These equations are described mathematically in the form of partial differential equations. To solve these equations a numerical technique is employed whereby the network is first discretised in a number of control volumes or nodes, whereupon the spatial derivative terms in the partial differential equations are integrated over the nodes to yield a set of ordinary differential equations. Thereafter an appropriate time integration scheme is used to yield a set of coupled algebraic equations that are solved simultaneously by means of an apt numerical method. A requirement for the solution is that there be an equal number of equations, as there are unknown variables, which calls for appropriate initial and boundary conditions to be available for the solution. A detailed description of the solution algorithm is given by Greyvenstein and Laurie (1994).

The development of methods used to solve one-dimensional flows has undergone much research. Botha (2002) gives a thorough overview of the methods used to solve steady-state and time dependent problems in pipe networks. In general, two types of solution algorithms are used, namely explicit methods and implicit methods. In explicit methods such as the Method of Characteristics (MOC) (Wylie & Streeter, 1993) and the Lax-Wendroff methods, the flow variables at a certain time step are expressed in terms of variables at only the previous time step, which makes it relatively easy to solve.

With implicit methods, such as the SIMPLE method (Patankar & Spalding, 1970), the flow variables at a certain time step are expressed in terms of variables at both the current and the previous time step. This requires the use of matrix techniques to solve the set of simultaneous equations. Although explicit methods are generally faster per time step than implicit methods, they are limited by the so-called Δx-Δt relationship that requires the time step Δt to be smaller than $\Delta x/c$, where c is the sonic velocity. This implies that solution times are restricted by the shortest pipe run in the network. This is a major disadvantage in cases of slow transients or steady-state solutions where many time steps are required. On the other hand, implicit codes are unconditionally stable and time step limitations do not affect their

stability. Even though implicit methods require complex coding, their advantage in numerical stability make them favourable for use in system codes.

An implicit solution method called the IPCM (Implicit Pressure Correction Method) is used in Flownex and is described by Greyvenstein (2001). In this method the flow path is divided into meshes, as shown in Figure 4.2. The mesh consists of a control volume known as a node (i) connected to a number of flow branches, referred to as elements. Node i is connected through elements e_{ij} to neighbouring nodes n_{ij}, with $j = 1,2,\ldots,J$. J is the number of branches associated with node i. In this way the entire flow network is subdivided into node meshes that are characterised mathematically by connectivity matrices.

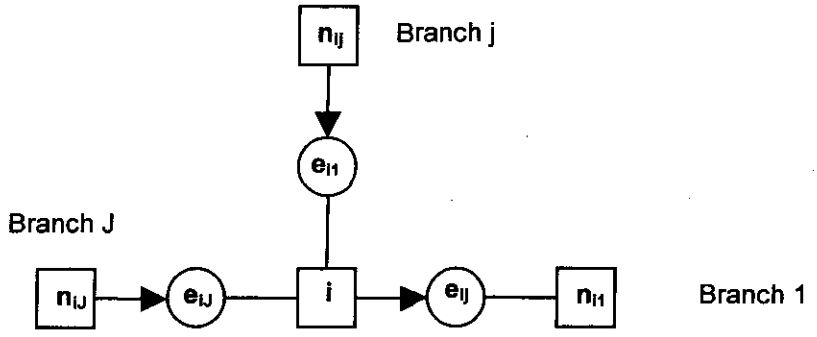

Figure 4.2 : Network of j branches joined to a node.

Greyvenstein (2001) describes the underlying principles used in the solution algorithm. The paper elaborates on the solution algorithm and its application in time-dependent problems. Such a discussion is beyond the scope of this document. However, a short discussion on the solution algorithm is appropriate.

For compressible flows (subsonic flow with variable density) the pressure and densities are guessed before the coupled continuity and momentum conservation equations are solved. These solutions yield updated pressures, mass flows and densities in the network. During this solution the temperatures are assumed to be constant. In some networks, though, the temperature may vary from element to element and as such an energy balance is performed after a fixed amount of pressure/flow rate iterations. Then the process is repeated until convergence is reached. Any time-dependent (transient) analysis can then commence.

The code user has an influence on the solution process by adjusting convergence criteria and initial conditions. An advantage of this method is that mixed boundary conditions (either pressure or flow rate) can be used in the network. The implicit nature of the algorithm is advantageous in that it is stable, regardless of time step or length of increments.

4.5. Verification and validation plan used in Flownex development

Flownex is categorised as software under development, or SUD. Furthermore, Flownex is also a first of a kind product, in that it is used as a system code for HTGR design work and a diverse number of V&V activities are required to qualify the code. This point is emphasised, as there is thus a limit on the amount of available codes against which Flownex can be benchmarked.

M-Tech Industrial, the code developer, performs the V&V process. Verification of the code is part of the overall software engineering process. This includes verification of the theory used in the development of relevant models. Validation is done by comparing the code results

with benchmarked data obtained from similar codes, experimental results and analytical solutions.

In a simplified form, the Flownex development may be described as follows: Firstly, a user requirement specification is supplied by a developer and its clients. This process is followed by a theory manual encapsulating all the theory needed to develop the models to be used in the code. Here the tasks split, with the code development running in parallel with the validation process. In the code development process a software requirement specification is developed which provides input to the software detail design. The software is then implemented and is followed by acceptance testing. These acceptance tests are benchmarked against existing or empirical data provided in the validation process. If the code results are found to be in line with the validation requirements, the code is released for use by the client.

An example of one of the benchmarks done in validating the code is shown in Figure 4.3. The example is a test involving compressible gas flow through a long pipe (Greyvenstein et al., 2002). At time zero, a valve is suddenly closed at the end of the pipe. The inertia of the fluid causes auto-compression at the end of the pipe, which in turn results in a pressure wave travelling back through the pipe. Flownex data is benchmarked against data obtained using the Lax-Wendroff method, an explicit code. The data shown is the pressure wave travelling through the pipe.

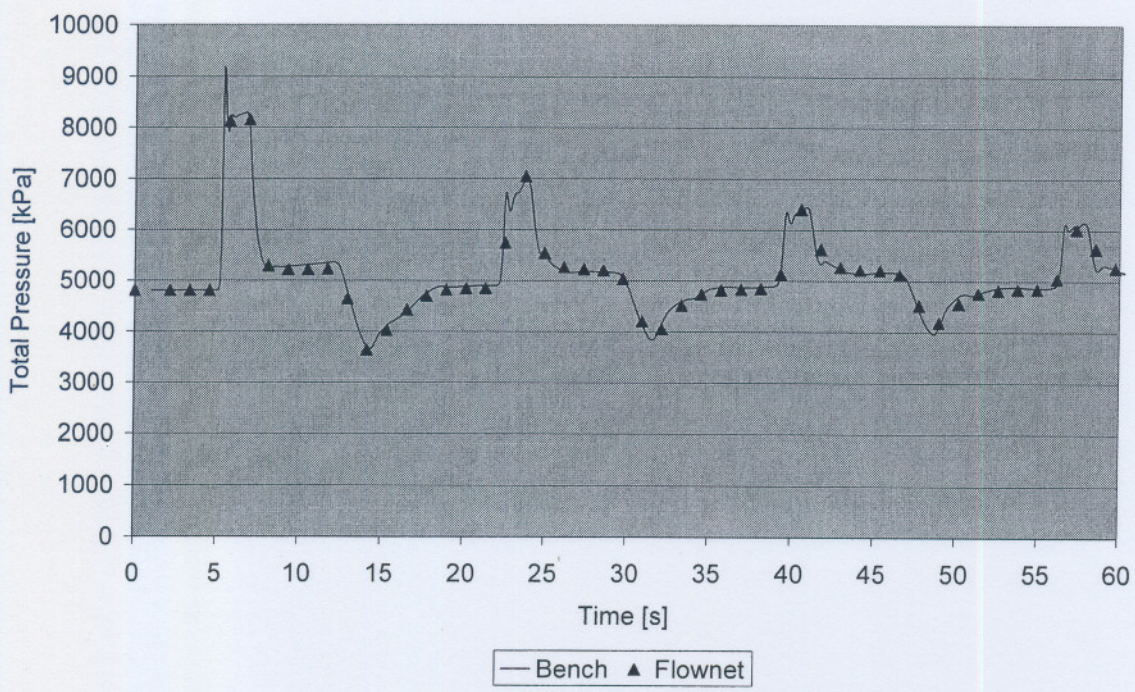

Figure 4.3 : Total pressure versus time for the sudden closure of a valve at the end of the pipe.

In the work of Botha (2003) and Olivier (2003) the basic methods and benchmarks are discussed in much more detail.

4.6. Flownex components

Flownex has a very comprehensive suite of component models that the user can choose from. This suite has evolved with the program as new applications were modelled and special components were needed. These components range from pipes and ducts, orifices and valves, turbo-machinery and pumps through to heat exchangers. As mentioned before, a number of

special elements are also available, such as nuclear reactors; controllers and conductive heat transfer elements. A discussion of each individual element in Flownex would be exhaustive, and thus only the elements used in the HTTR model will be discussed here.

4.6.1. Pipe and duct elements

In Flownex ducts may be modelled using one of two methods: either a Darcy-Weisbach or a Hazen-Williams pressure drop model. The latter is mainly used in civil engineering and is not discussed further. Furthermore, both pipes of constant and differing inlet and outlet cross-sectional areas may be modelled. Both compressible and incompressible fluids can be simulated in Flownex with the compressible model being described below.

The total pressure drop is calculated (Saad,1985) using

$$\Delta p_0 = \left(\frac{fL}{D} + \sum K_S + \frac{\Delta T_0}{T_0} \right) \frac{p_0 \gamma M^2}{2} \tag{4.1}$$

where f = friction factor,

L = pipe length [m],

D = pipe diameter/ hydraulic diameter [m],

T_0 = total temperature [K],

p_0 = total pressure [Pa],

γ = ratio of specific heats of the gas,

ΣK_s = sum of secondary losses and

M = Mach number.

A term for the pressure drop through sharp edged orifices also included in the model is not shown, as it is not used in the present study. A correlation based on the Moody diagram is used to calculate the friction factor (Shames, 1992:366):

$$f = \frac{0.25}{\left[\log\left\{(e/3.7D) + 5.74/\mathrm{Re}^{0.9}\right\}\right]^2} \tag{4.2}$$

This correlation is valid for $5000 < Re < 1 \times 10^6$. Flow below $Re = 2300$ uses the formula:

$$f = \frac{64}{\mathrm{Re}} \tag{4.3}$$

In between these ranges a linear interpolation is used. An important aspect of the pressure drop correlation is the secondary loss factors (ΣK_S). These factors account for the effects of geometry changes in the pipe section, such as bends, t-junctions, contractions and expansions. Such geometric changes often result in the fluid boundary layer separating from the duct wall, which in turn results in additional losses. Various sources were consulted for loss factors, including Miller and Idelchik (1989).

In the case of pipes that have different inlet and outlet flow areas, the pressure loss may be based on either the higher velocity of the two or on the average velocity. This option is often

used to model complex geometries like turbine diffusers where complex 3-D shapes strongly affect the pressure drop. Usually these geometries are characterised by experiment or CFD to determine a loss factor based on the inlet or outlet velocity (whichever is higher). This is then used in the Flownex pipe model to represent the component.

Further flexibility in the pipe model includes its ability to be sub-divided into smaller increments. This is useful in fast transients when pressure or thermal waves need to be monitored. The effects of heat losses through the length of the pipe can also be accounted for in the code. The pipe model has various other capabilities, but these fall beyond the scope of this document.

This pipe model is used in the next chapter to model the concentric gas ducts found throughout the HTTR main and auxiliary cooling systems.

4.6.2. Shell-and-tube heat exchanger

The heat exchanger models employed in Flownex include a few simple heat exchanger elements that are described by means of NTU-effectiveness models. The accuracy of these models are limited to steady-state use, as the thermal capacitance of the heat exchanger is not catered for and thus the thermal inertia will not come into play in a transient. In reality such thermal inertias greatly influence the fluid parameters and should be accounted for to get realistic results. A further draw back of the lumped heat exchange model is that one cannot get any usable results inside the heat exchanger. These limitations lead the developers to include detailed heat exchanger models that can accurately simulate heat exchange to high resolution in steady-state and transient conditions. These models include compact heat exchanger models, shell-and-tube heat exchangers, recuperators (gas-to-gas) and evaporator models.

A sectional view of a typical shell-and-tube heat exchanger is shown in Figure 4.4. The shell-and-tube heat exchanger refers to multiple primary side tube passes passing through a pressure vessel that contains baffles, used to direct the secondary flow in a cross-flow configuration across the tube passes. The secondary fluid is usually inside the tubes, while the primary side is on the outside of the tubes in a pressure vessel containment called a "shell". The shell-side fluid is guided over the tube-bank one or more times by means of baffles. The tubes can also have one or more passes and are connected to a manifold at either end of the shell where the tube fluid is gathered.

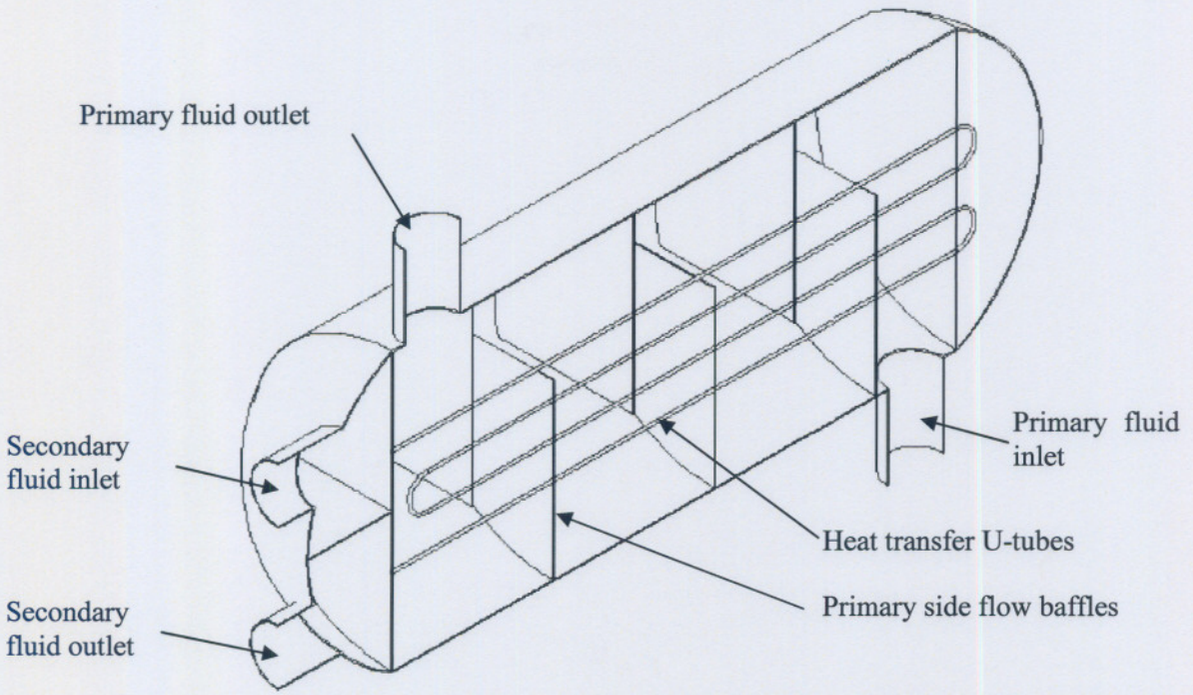

Figure 4.4 : Cross-section through a typical shell-and-tube heat exchanger.

In Flownex the heat exchanger is sub-divided into a number of cross-flow heat exchangers that are interconnected to form the overall shell-and-tube heat exchanger. For example, a 10 gas-pass, 4 water-pass heat exchanger is shown in Figure 4.5.

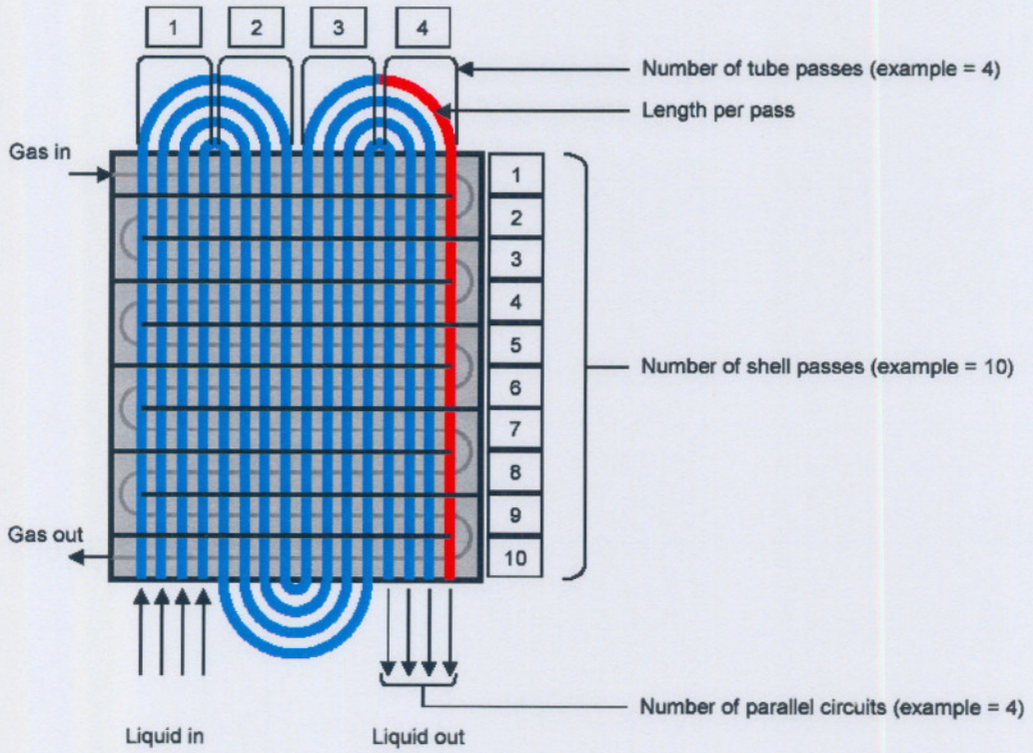

Figure 4.5 : Representation of a shell-and-tube heat exchanger in discretised elements.

This results in a matrix of 40 (4 x 10) small heat exchanger elements. Further discretisation can be done and the heat transfer in every tube row per gas pass can be analysed. The user must input the number of passes of each flow stream along with all the required dimensions needed to create a model. This includes information on the tube diameters, wall thickness, material, gas side flow areas, heat transfer area (including that attained by extended surfaces like fins) and solid masses and specific heats. In addition the point of entry of the two streams is very important for the program to do the correct discretisation. A more detailed discussion of the discretization methods used in Flownex is given by Olivier (2003).

The heat transfer and pressure drop characteristics of the heat exchanger are very dependent on the geometry involved. For example, a bare tube configuration will have much smaller pressure drops than a finned tube geometry of the same tubular pitch. However, the heat transfer per cubic meter volume of the latter is much higher due to the extra heat transfer area gained by using fins. The fin shape, pitch and thickness all affect the pressure drop and heat transfer capabilities of the geometry. These effects are modelled by means of characteristic curves. Such curves plot the *Colburn j factor* which is equal to $StPr^{2/3}$, and the friction factor against Reynolds number. Figure 4.6 shows an example of a set of characteristic curves for finned heat exchanger geometry.

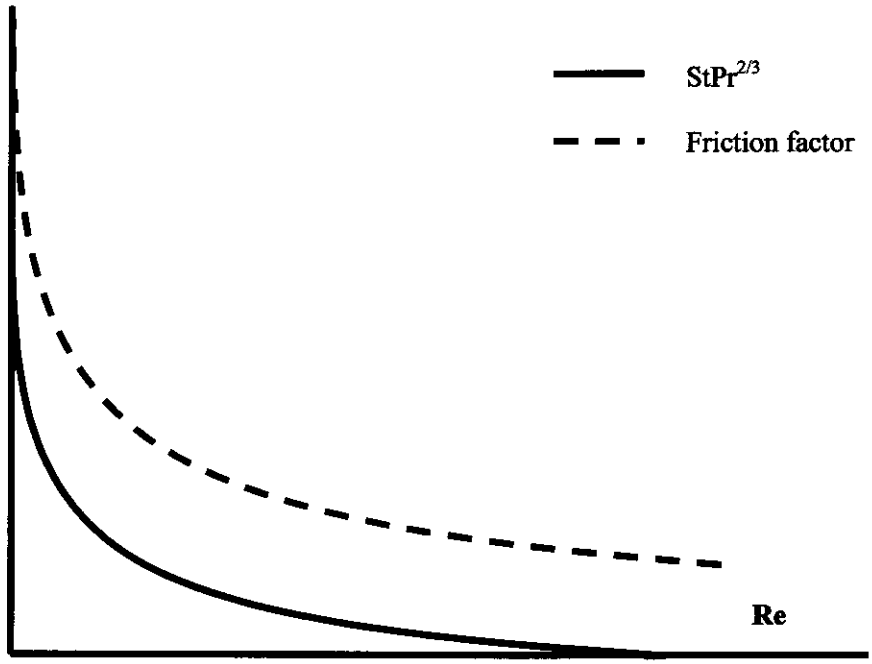

Figure 4.6 : Heat exchanger geometry characteristic curves.

The pressure drop through the pipes is calculated with the same correlations used for standard pipes, which was discussed in Section 4.6.1. On the fin side a different correlation is used:

$$\Delta p_0 = \frac{p_0}{p}\frac{4fL}{D_h}\tfrac{1}{2}\rho V^2 \qquad (4.4)$$

where p_0 = total pressure,

p = static pressure and

f = friction factor.

The velocity in Eq. (4.4) is based on the minimum flow area.

f

The heat transfer is calculated using the effectiveness-NTU approach (Incropera,1996). According to this approach the heat transfer is given by:

$$Q = \varepsilon C_{\min}(T_{hi} - T_{ci}) \tag{4.5}$$

with ε = effectiveness,

T_{hi} = inlet temperature on the hot side (tube or shell) and

T_{ci} = inlet temperature on the cold side (tube or shell) and

$C_{\min}$ = the minimum heat capacity rate of the hot and cold streams.

The heat capacity rate is the product of the streams mass flow and its constant pressure specific heat value. Each elemental heat exchanger is viewed as a cross-flow heat exchanger with the shell side mixed and the tube side unmixed. For this situation the effectiveness is given by:

$$\varepsilon = \left(\frac{1}{1 - e^{-NTU}} + \frac{C}{1 - e^{-NTU \cdot C}} - \frac{1}{NTU} \right)^{-1} \tag{4.6}$$

where

$$NTU = \frac{A_o U_o}{C_{\min}} \tag{4.7}$$

and

$$C = \frac{(\dot{m} c_p)_{\min}}{(\dot{m} c_p)_{\max}} \tag{4.8}$$

the overall heat transfer coefficient is calculated as

$$U_O = \left(\frac{1}{\lambda_o} + \frac{A_o}{A_i \lambda_m} + \frac{A_o}{A_i \lambda_i} \right)^{-1} \tag{4.9}$$

where λ_o = surface heat transfer coefficient on the shell side,

λ_i = surface heat transfer coefficient on the tube side,

λ_m = metal coefficient,

A_o = surface area on the shell side and

A_i = surface area on the tube side.

The shell-side heat transfer coefficient is determined using the Colburn j-factor ($StPr^{2/3}$) obtained from the heat exchanger characteristic curve shown in Figure 4.6. Using the definition of the Standton number (Incropera,1996) we can write that

$$\lambda_o = \frac{St \, \mathrm{Pr}^{2/3} \cdot \mathrm{Pr}^{1/3} \cdot \mathrm{Re} \cdot k_o}{D_{h_o}} \tag{4.10}$$

where $StPr^{2/3}$ = Colburn j-factor,

Pr = Prandtl number and

k_o = thermal conductivity of the fluid on the shell side.

The metal coefficient is calculated using (4.11) but usually has a small effect on the heat transfer:

$$\lambda_m = \left[\frac{r_i}{k_m}\ln\left(\frac{r_o}{r_i}\right)\right]^{-1} \tag{4.11}$$

where r_i = inner radius of tube,

r_o = outer radius of tube and

k_m = thermal conductivity of the tube material.

On the tube side the heat transfer coefficient is calculated with the *Dittus-Boelter* equation (Incropera et al., 1996:445)

$$\lambda_i = \left(0.023\,\mathrm{Re}^{0.8}\,\mathrm{Pr}^{n}\right)\frac{k_i}{D_h} \tag{4.12}$$

where k_i = thermal conductivity of the fluid inside the tubes and

D_h = the inside diameter of a tube.

The shell-and-tube model is used in the next chapter to model the various water coolers in the HTTR main and auxiliary cooling systems.

4.6.3. Recuperator model

A type of heat exchanger used to transfer heat from one part of a cycle to another part of the cycle (usually to recover heat that would otherwise have been lost) is called a *recuperator*. In the case of a direct HTR Brayton power conversion cycle the recuperator is used to transfer heat from the hot gas leaving the power turbine to the compressed gas leaving the high pressure compressor before it is heated by the main energy source (nuclear reactor, combustion chamber, etc.) Such energy recuperation greatly increases the thermal efficiency of the cycle. In the same way this element may be used to model an intermediate heat exchanger with the same counterflow configuration.

Similar to the approach followed in the shell-and-tube model, the recuperator model consists of sub-divisions of smaller heat exchangers. The reason for the sub-divisions is to better model the effect of the thermal capacitance of the heat exchanger and to better take the effect of variable physical properties such as viscosity and thermal conductivity into account. The main difference between this model and the shell-and-tube model is that here the two flows are either counter or parallel in direction. A drawback of the model is that only one length for the model can be specified, which is used in both sides' pressure drop calculations. Later in the document this drawback is emphasised in the modelling of the HTTR's intermediate heat exchanger.

In calculating the pressure loses and heat transfer through the recuperator it is firstly necessary to sub-divide the component into smaller increments or control volumes. The control volumes used in the recuperator model are shown in Figure 4.7. From the figure one

can see that each flow control volume has a centre denoted by a dark square and interfaces with its neighbouring volume on either side (denoted with a circle). The interfaces will be referred to as elements and the centres as nodes.

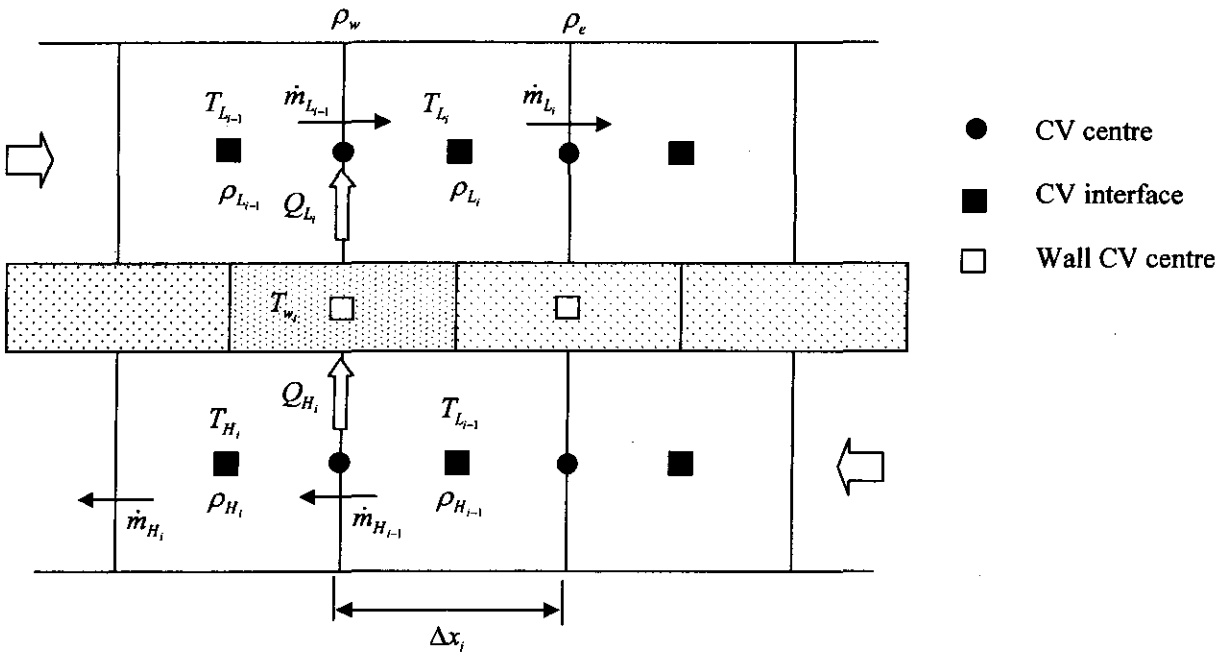

Figure 4.7 : Control volumes used in the recuperator heat transfer calculation.

The wall separating the two flows is also discretised into control volumes that are staggered in relation to the flow control volumes. This is so as to allow heat transfer to take place between adjacent flow elements and the wall node.

The pressure drop through the heat exchanger is calculated by applying mass balance to the gas control volumes:

$$A_L \Delta x_i \frac{d\rho_{L_i}}{dt} = \dot{m}_{L_i} - \dot{m}_{L_{i+1}} \tag{4.13}$$

$$A_H \Delta x_i \frac{d\rho_{H_i}}{dt} = \dot{m}_{H_i} - \dot{m}_{H_{i+1}} \tag{4.14}$$

where A is the cross-sectional area and subscripts H and L refer to the high pressure and low pressure streams respectively. Applying Newton's Second Law to the boundary velocities in the LP and HP gas streams renders the following equations:

$$\bar{\rho}_{L_i} \frac{d\bar{V}_{L_i}}{dt} = \frac{p_{L_{i-1}} - p_{L_i}}{\Delta \bar{x}_i} - \frac{\bar{f}}{2D_L} \bar{\rho}_{L_i} \bar{V}_{L_i}^{\,2} \tag{4.15}$$

$$\bar{\rho}_{H_i} \frac{d\bar{V}_{H_i}}{dt} = \frac{p_{H_{i-1}} - p_{H_i}}{\Delta \bar{x}_{i+1}} - \frac{\bar{f}}{2D_H} \bar{\rho}_{H_i} \bar{V}_{H_i}^{\,2} \tag{4.16}$$

where

$\bar{\rho}_{L_i}$ = average density between nodes i and i+1 on LPside (with subscript H for HP side),

$\bar{f}$ = average friction factor and

the over bar denoting values at the interfaces.

The heat transfer between the two sides is calculated by applying the First Law of Thermodynamics to the gas and wall control volumes renders the following equations:

$$Q_{L_i} = H_{L_i}\left(T_{w_i} - \tfrac{1}{2}\left(T_{L_i} + T_{L_{i-1}}\right)\right) \tag{4.17}$$

$$Q_{H_i} = H_{H_i}\left(\tfrac{1}{2}\left(T_{H_i} + T_{H_{i-1}}\right) - T_{w_i}\right) \tag{4.18}$$

$$A_L c_v \Delta x_i \frac{d}{dt}\left(\rho_{L_i} T_{L_i}\right) = c_p\left(\dot{m}_{L_i}\bar{T}_{L_i} - \dot{m}_{L_{i-1}}\bar{T}_{L_{i-1}}\right) + Q_{L_i} \tag{4.19}$$

$$A_H c_v \Delta x_i \frac{d}{dt}\left(\rho_{H_i} T_{H_i}\right) = c_p\left(\dot{m}_{H_i} T_{H_i} - \dot{m}_{H_{i-1}} T_{H_{i-1}}\right) - Q_{H_i} \tag{4.20}$$

$$C_{W_i}\frac{dT_{W_i}}{dt} = H_{L_i}\left(T_{L_i} - T_{W_i}\right) - H_{H_i}\left(T_{W_i} - T_{H_i}\right) \tag{4.21}$$

where

c_v = constant volume specific heat of gas,

c_p = constant pressure specific heat of gas,

C_{Wi} = product of lump mass and specific heat of wall per segment and

H_H and H_L = product of heat transfer area and heat transfer coefficient per segment.

Equations (4.13) to (4.21) may all be written in the following form:

$$\frac{dx_j}{dt} = f\left(x_1, x_2, \ldots x_n\right) \quad j = 1, 2 \ldots n \tag{4.22}$$

where x_j is the variable under consideration.

With a first-order implicit integration, the following would result:

$$\frac{x_j^{t+1} - x_j^t}{\Delta t} = f^{t+1} \tag{4.23}$$

Flownex uses a weighted time integration scheme whereby

$$\frac{x_j^{t+1} - x_j^t}{\Delta t} = \alpha f^{t+1} + (1-\alpha) f^t \tag{4.24}$$

with $0.5 < \alpha < 1$. The resulting set of equations is solved with a simultaneous Newton-Raphson method. Details of the solution algorithm may be found elsewhere (Greyvenstein 2001).

For the above equations a friction factor and a heat transfer coefficient are required. There are two options for specifying these parameters. Firstly, the model uses the laminar friction factor with a user-supplied multiplication factor to account for the specific geometry. In this case the user also has to prescribe a laminar Nusselt number for the flow path channel with a multiplication factor to account for the effect of channel shape.

The other method is to use, as with the shell-and-tube model, a user-defined characteristic curve specifying Colburn j-factor and friction factor versus Reynolds number. Sources for such data are to either use existing literature like Kays and London (1984) or to do testing on the particular geometry under investigation.

4.6.4. Compressors and turbines

An important part of any thermal-fluid system is the components that move the gas through the system and that convert fluidic energy into usable power. Such components include pumps, blowers, compressors and turbines. Flownex has the capability of simulating most of these machines. The performance of these components is specified in the form of non-dimensional performance characteristics, which gives the pressure ratio and efficiency as function of non-dimensional mass flow and rotational speed.

In using the code as a design tool, it is required that these turbo-machine curves be scaleable so as to model a machine that can fit the system resistance requirements. For example, for a given power system with piping and thermal components' geometries fixed, a compressor and turbine set must be sized to deliver adequate mass flow, pressure ratio and shaft power to the generator. In such a case Flownex allows the performance curves of the turbo-compressor to be scaled until an optimal working point is found. This scaled curve can then be returned to the turbo-machinery suppliers for changes to the turbo-machine design.

Performance curves contain all the needed parameters to describe the performance of a turbo-machine for use in the system code. These parameters are: a geometric parameter D, the shaft speed N, the mass flow $\dot{m}$, the inlet and outlet total pressures (p_{0i} and p_{0e}), the gas constant R and the inlet and outlet total temperatures T_{0i} and T_{0e}. Dimensional analysis (Shames, 1992) reduces these parameters to a set of four dimensionless parameters:

$$f\left(\frac{p_{0e}}{p_{0i}}, \frac{T_{0e}}{T_{0i}}, \frac{\dot{m}\sqrt{RT_{0i}}}{D^2 p_{0i}}, \frac{ND}{\sqrt{RT_{0i}}}\right) = 0 \tag{4.25}$$

The first term is the pressure ratio with its parameters always chosen such that its value will be greater than 1 (compressor outlet/inlet; turbine inlet/outlet). The second term can be related to isotropic efficiency by means of:

$$\eta = \frac{\left(p_{0e}/p_{0i}\right)^{\frac{\gamma-1}{\gamma}} - 1}{\left(T_{0e}/T_{0i}\right) - 1} \tag{4.26}$$

The last two terms are called the *non-dimensional mass flow rate* and the *non-dimensional speed* respectively. In Flownex the R value is specified in the fluid table and the D value is equal to one. For scaling purposes this D value can be varied to yield the required scaling. Thus equation (4.25) can be refined to the following:

$$f\left(\frac{p_{0e}}{p_{0i}}, \eta, \frac{\dot{m}\sqrt{T_{0i}}}{p_{0i}}, \frac{N}{\sqrt{T_{0i}}}\right) = 0 \tag{4.27}$$

In Flownex these parameters are represented in two types of curves, namely pressure ratio vs. non-dimensional mass flow and isentropic efficiency vs. non-dimensional mass flow. Examples of these curves for a typical gas compressor are shown in Figure 4.9 and Figure 4.9.

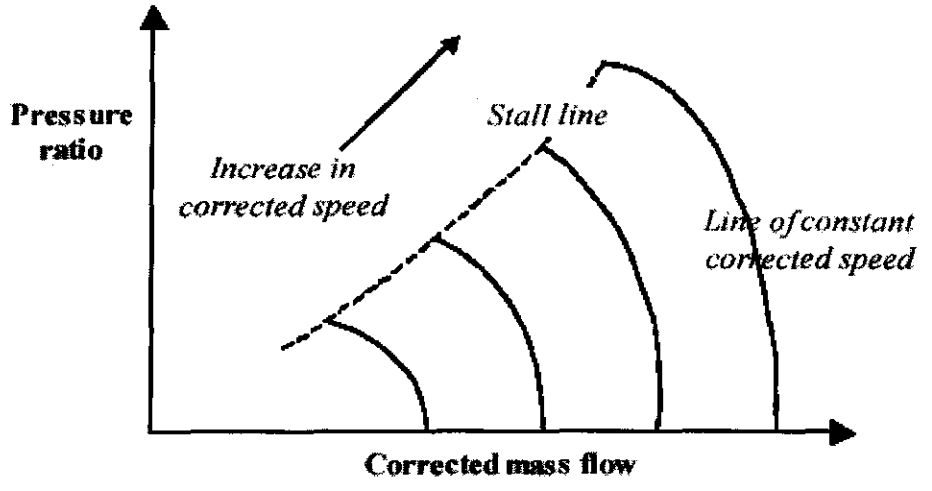

Figure 4.8 : Pressure ratio map for a typical compressor.

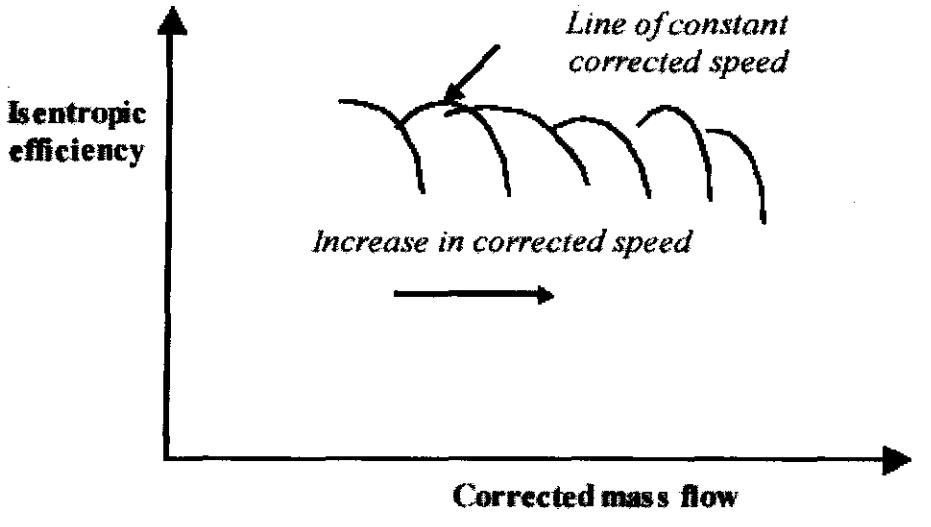

Figure 4.9 : Efficiency map for a typical compressor.

As mentioned earlier, Flownex allows the user to scale turbo-machine curves to obtain an optimal design for a specific system. There are five methods of scaling that can be categorised into two overlying groups: scaling of each of the axes of the two aforementioned

graphs or scaling all the parameters representing the machine with the same scaling factor. In the latter case a designed machine can literally be taken and all its key dimensions scaled by the particular factor to obtain a design point turbo-machine. By only scaling the individual axes it is required that the geometry of the machine be altered in an unsymmetrical way; extra stages may for example be needed, thus altering the design. Care should be taken with these factors though, as they can result in non-physical geometries, such as a turbo-machine with an efficiency greater than 1.

In the context of this document only the compressor model is further discussed, as it will be used to simulate the circulators in the HTTR main cooling circuit. A compressor's function is to increase the total pressure in a flow passing through it. A circulator, although providing a slight pressure increase, has the main function of providing volume flow through a system. Flownex is able to analyse centrifugal, axial and positive displacement compressors.

The model interpolates the pressure ratio and efficiency of the compressor from the digitised performance curves for the prescribed non-dimensional mass flow and non-dimensional speed.

The pressure increase is simple to calculate from the interpolated pressure ratio, while the energy transferred to the flow is calculated using the definition of isentropic efficiency

$$\eta_c = \frac{W_{ideal}}{W_{actual}} \tag{4.28}$$

which is rewritten as

$$W_{actual} = \frac{W_{ideal}}{\eta_c} \tag{4.29}$$

where W refers to the work done to the fluid.

These parameters are important in the simulation, as they derive the energy needed to move a certain amount of mass flow through the circuit. When designing a compressor to fit a system, care should be taken to allow a sufficient surge margin. Surge margin refers to the safety factor included in the performance curves to prevent the system from sending the compressor into surge. Surge is a destructive condition in a compressor that may cause damage to the hardware. The point at which surge occurs is difficult to pinpoint and as such a surge margin is built into the curve data. If the operating point of the compressor ever goes beyond the surge line, warnings are immediately raised to alert the user. Figure 4.10 shows a typical surge margin line and an acceptable operating point below that line.

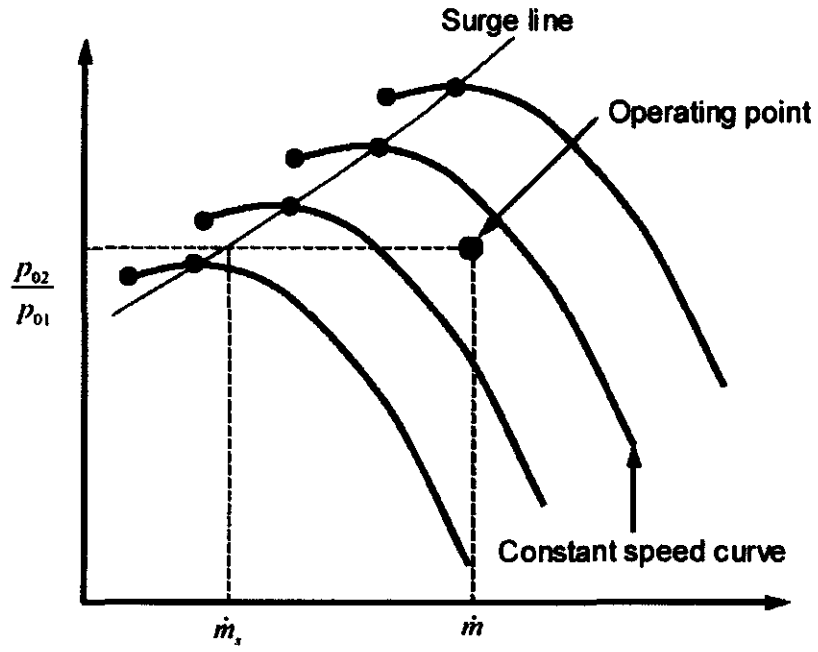

Figure 4.10 : Compressor characteristic showing surge and surge margin lines.

In transient conditions the inertia of the compressor is of cardinal importance and as such it is also one of the main input parameters.

The discussion of this section basically covers the approach used by Flownex to model a compressor. Further flexibility is provided for in the model with inputs like mechanical efficiency parameters, shaft linkage to turbines and other compressors and so on. These are not discussed here as they are not used in the HTTR modelling.

This concludes the discussion on the models used in Flownex. Only those models that are used in the following chapter were discussed. More detailed information on these and the rest of the Flownex models may be found in the user manual (Coetzee et al., 2002).

5. MODELLING OF THE HTTR IN FLOWNEX

5.1. Introduction

In the preceding two chapters a system overview of the HTTR was firstly given, followed by an overview of the system code, Flownex, used to model it. These represent the problem to be solved and the tool to be used to do this. However, aligning theoretical models with real problems is seldom a simple task. Various assumptions need to be made where information is missing or where the real problem's complexity outweighs that of the model. In this chapter the reader is sensitised to the modelling approach used and to the assumptions and problems that occurred during the process.

5.2. Overall cycle model

As discussed in Chapter 4, Flownex uses *elements* and *nodes* to represent system components. An *element* refers to components such as pipes, turbo-machines or heat exchangers. *Nodes* are junction points for elements but can also represent regions of large volume and low velocity, such as tanks and reservoirs.

Figure 5.1 is a diagram of the HTTR system as implemented in Flownex. Elements are shown as numbered circles, while the numbered squares represent nodes. The diagram shows the use of pipe elements, circulators, heat exchangers and conductive heat transfer paths. In this network both the main and auxiliary cooling systems are modelled. Cooling water flows are modelled as constant-mass flow cold-water streams.

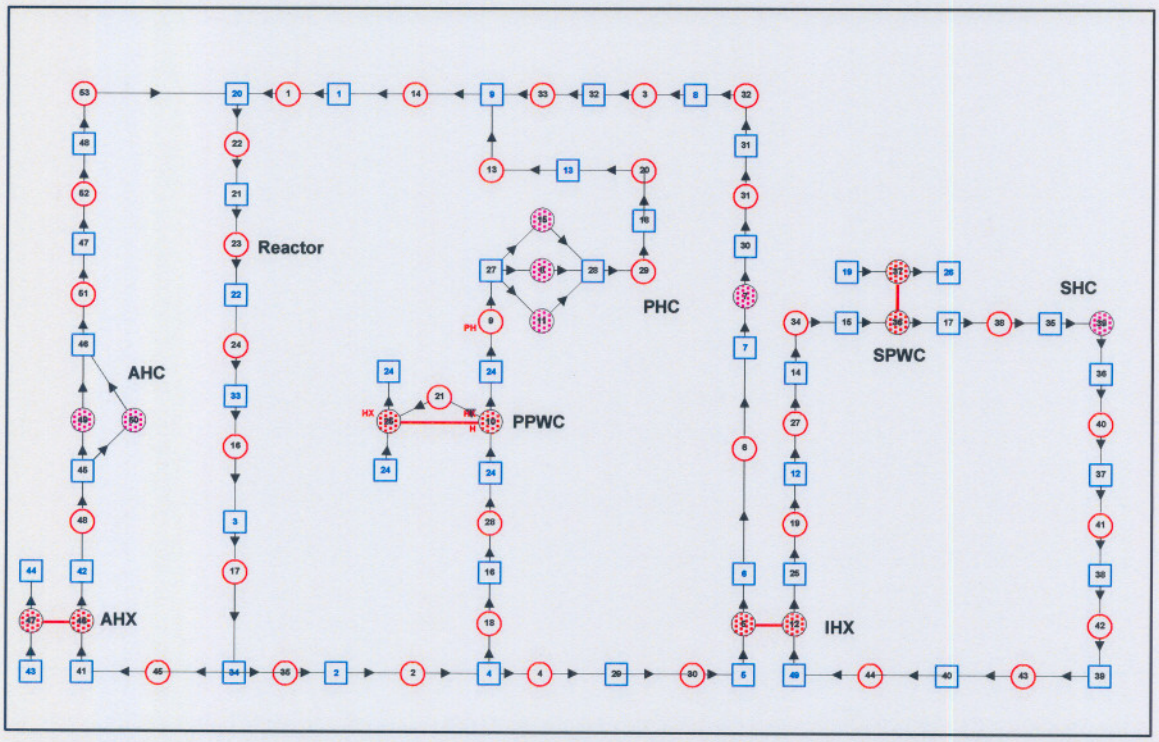

Figure 5.1 : HTTR Flownex network.

The descriptions of the elements used in the network are given in Table 5.1.

Table 5.1 : Elements used in the HTTR Flownex model.

Element	Description	Type
1	Annular duct to top of reactor	Gas duct
2	Reactor to T-junction	Gas duct
3	Contraction to gas duct	Gas duct
4	Contraction from T-junction	Gas duct
5	Intermediate heat exchanger	Heat exchanger
6	IHX to PHC	Gas duct
7	SPWC circulator	Helium circulator
8	PPWC circulator B	Helium circulator
9	PPWC to PHC	Gas duct
10	Primary Pressurised Water Cooler	Heat exchanger
11	PPWC circulator C	Helium circulator
12	IHX secondary side	Heat exchanger
13	PPWC to T-junction	Gas duct
14	T-junction to reactor	Gas duct
15	PPWC circulator A	Helium circulator
16	9th reflector layer	Gas duct
17	Hot plenum block	Gas duct
18	T-junction to PPWC	Gas duct
19	Secondary IHX to T-junction A	Gas duct
20	Annulus around PPWC	Gas duct
22	Upper reflector and shield layers	Gas duct
23	Fuel assembly (Reactor core)	HTTR
24	Lower reflector layer	Gas duct
25	PPWC water side	Heat exchanger
26	HTTR	HTTR
27	Secondary IHX to T-junction B	Gas duct
28	Distribution plate	Gas duct
29	PHC to PPWC	Gas duct
30	Contraction to IHX	Gas duct
31	PHC to IHX	Gas duct
32	Annulus around IHX	Gas duct
33	IHX to T-junction	Gas duct

Table 5.1 : Elements used in the HTTR Flownex model (continued).

Element	Description	Type
34	Distribution plate	Gas duct
35	Hot plenum outlet channel	Gas duct
36	Secondary Pressurised Water Cooler	Heat exchanger
37	SPWC water side	Heat exchanger
38	SPWC to SHC	Gas duct
39	Secondary Helium Circulator	Helium circulator
40	SHC to SPWC	Gas duct
41	Annulus around SPWC	Gas duct
42	SPWC to T-junction	Gas duct
43	T-junction to tube header feed pipes	Gas duct
44	Header feed pipes	Gas duct
45	Reactor to AHX	Gas duct
46	Auxiliary Heat Exchanger	Heat exchanger
47	AHX water side	Heat exchanger
48	AHX to AHC	Gas duct
49	Auxiliary Helium Circulator A	Helium circulator
50	Auxiliary Helium Circulator B	Helium circulator
51	AHC to AHX	Gas duct
52	Annulus around AHX	Gas duct
53	AHX to Reactor	Gas duct

5.3. Pipes and ducting

Most of the piping in the HTTR plant consists of double-walled pipes with hot flow from the reactor in the inner pipe and cooled return gas in the outer annulus of the pipe. Figure 5.2 shows a lateral cross-section through the primary cooling circuit piping. The diagram shows the double-walled piping and the lagging material surrounding the pipe for insulation. Flow from the reactor goes via the inner pipe to a T-junction where the flow is split up to a ratio of 3:1 between the PPWC and the IHX respectively. Upon returning to the reactor the helium flows through the outer annular pipe.

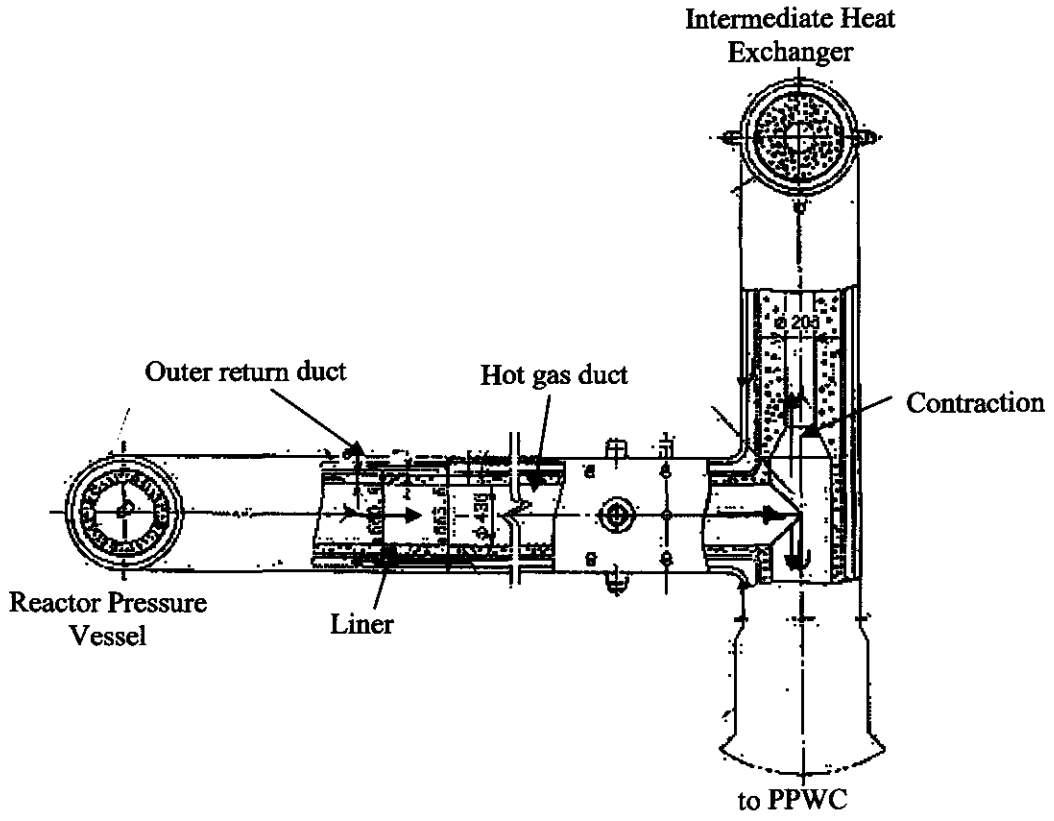

Figure 5.2 : Main cooling system primary cooling circuit duct work (Takeda et al., 2000).

In modelling the ducts, the approach was taken to let the element contain as much information on the flow path as possible. For example, a long pipe with constant diameter but with one or more bends in is modelled as a single element. All bends in the pipe length are characterised in the pipe element by means of secondary loss factors. On the other hand, any change in flow area through the length of a duct is modelled as a single element with its associated expansion or contraction loss included. Such a case is present in the contraction of the pipe leading to the intermediate heat exchanger, shown in Figure 5.2. From there on the pipe is once again of constant flow area and is modelled as a separate element.

The return gas to the reactor flows in an annulus around the hot pipes. Once again the flow path is modelled as compactly as possible, i.e. as much information as is practically possible is lumped into each element. This is to avoid having a network with lots of elements where one with fewer elements containing the same amount of information would suffice. Flownex requires both a flow area and a wetted perimeter as input for non-circular flow channels. The area is used to find flow velocity, while the perimeter is used along with area to calculate a characteristic length or hydraulic diameter used in the Reynolds number calculation.

5.4. Primary pressurised water cooler

The Primary Pressurised Water Cooler (PPWC) is essentially a shell-and-tube heat exchanger. A cutaway diagram of the PPWC is shown in Figure 5.3. The tubes used are un-finned. There are five gas passes and two tube passes in the heat exchanger. An impingement plate is placed at the inlet to spread the gas flow evenly through the first stage.

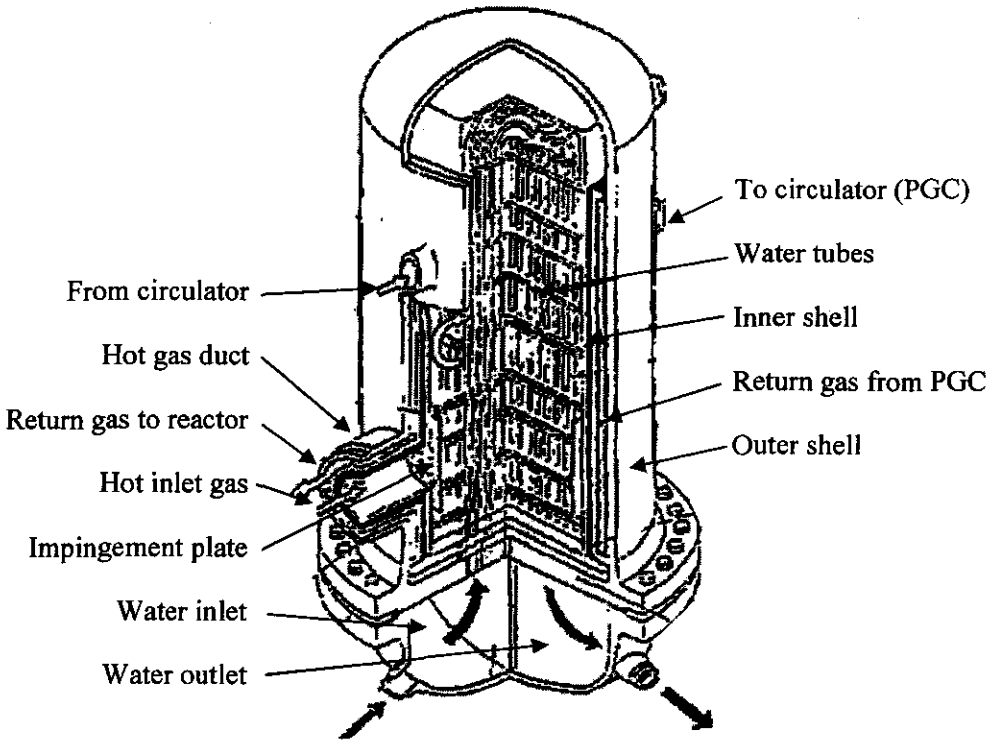

Figure 5.3 : Bird's eye view of the PPWC (Takeda et al., 2000).

In Figure 5.4 the helium flow path through the PPWC is shown. The flow channel is not of constant flow area as can be seen by the decreasing number of baffles as the hot gas moves through the heat exchanger. No explanation was given for the change in area by JAERI and it is presumed that this is due to the change in gas density as the helium is cooled in through the shell.

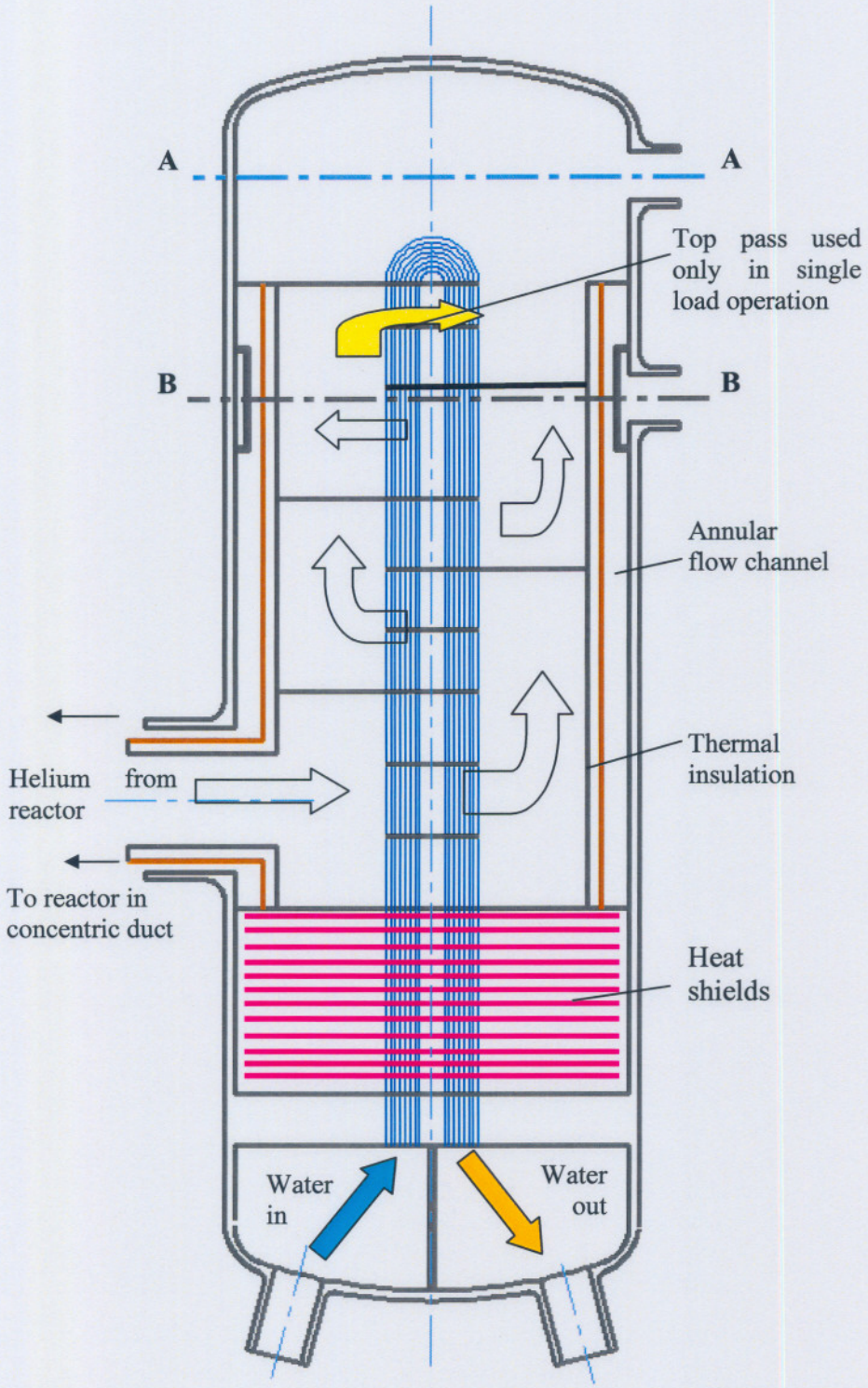

Figure 5.4 : Lateral section through PPWC.

A further complication comes in where the gas exits the cooler to the circulators. The HTTR main cooling system can be operated in two ways: single loaded operation and parallel loaded operation (Takeda et al., 2000). In single load only the PPWC is used to remove heat from the reactor whilst in parallel load mode the secondary circuit is also used. For the single load operation only the PPWC removes reactor heat and as such more heat exchanger area is required. In the figure the top pass is shown to only be used in single load operation. This extra pass provides enough cooling for the extra mass flow. In Figure 5.5 a cross-section at

position A-A is shown where one can see the three exit ducts to the primary helium circulators.

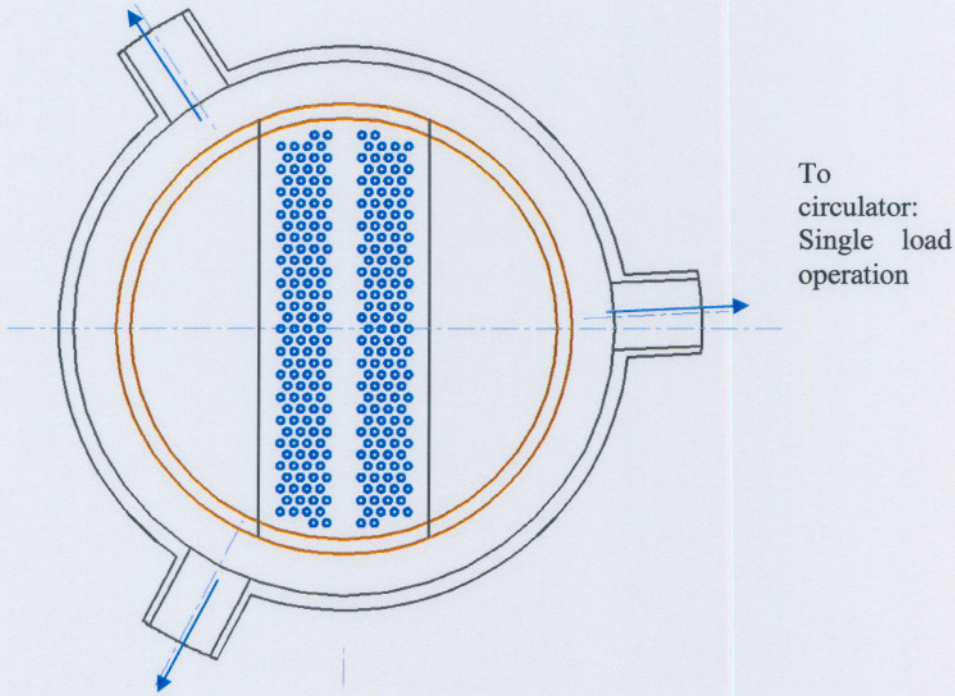

Figure 5.5 : Section A-A of PPWC.

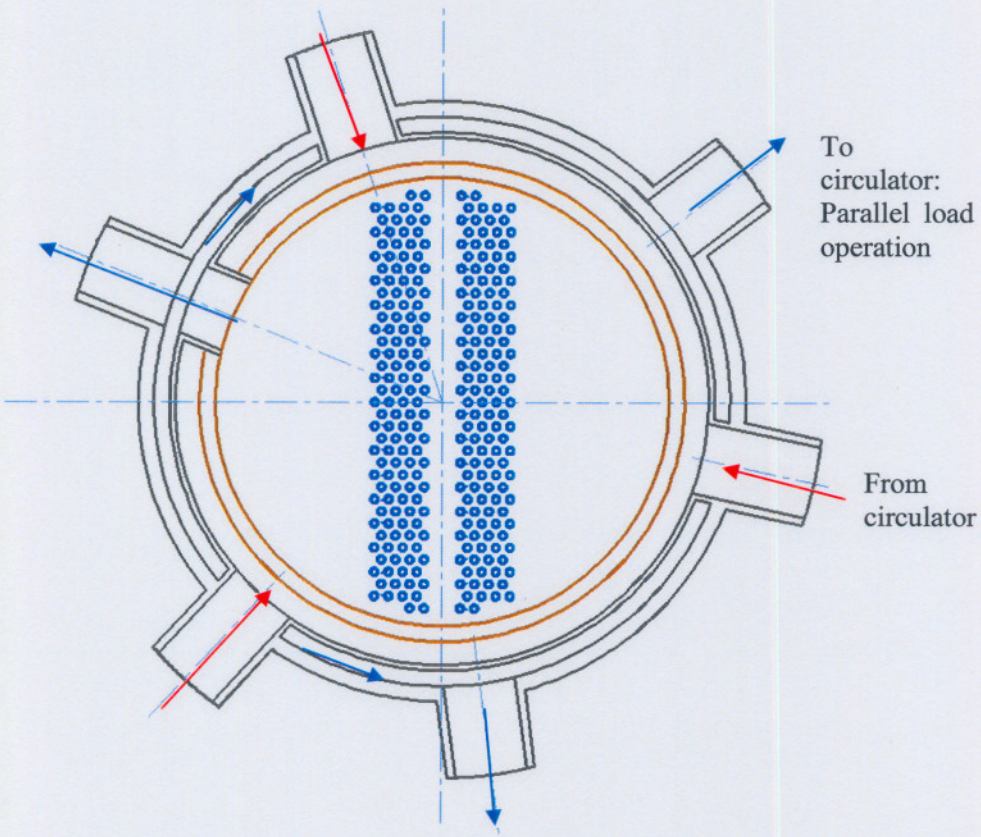

Figure 5.6 : Section B-B of PPWC.

On returning from the circulators these ducts are connected to an annular flow path inside the PPWC pressure vessel. For parallel load operation the gas bypasses the last gas pass by flowing into three outlet ducts on level B-B as shown in Figure 5.6. On the tube side water enters (as shown in Figure 5.4) at the same point at which the helium enters (i.e. at the bottom left side of the figure). It then flows into the pipes that first go through the pressure boundary tube sheet and then through a set of plates that serve to shield the hot gas from the tube sheet.

The critical parameters and dimensions are given in Table 5.2.

Table 5.2: PPWC critical parameters and dimensions (for parallel cooling).

Description	Unit	Value
Tube outer diameter	[mm]	25.4
Tube wall thickness	[mm]	2.6
Tube inner diameter	[mm]	20.2
Tube pitch perpendicular to flow	[mm]	86.6
Tube pitch parallel to flow	[mm]	50
Number of water passes	[-]	2
Number of rows per pass	[-]	8
Number of tubes per odd row	[-]	17
Number of tubes per even row[1]	[-]	16
Total number of tubes per water pass	[-]	136
Water heat exchange flow length per pass	[mm]	2490
Number of gas passes (for parallel plant operation)	[-]	4
Average gas pass cross-sectional area	[m^2]	0.7114
Shell material	[-]	2 ¼ Cr – Mo steel
Tube material	[-]	321TB stainless steel

5.4.1. PPWC model

In modelling the PPWC certain assumptions are made. These are:

- Due to the changing gas flow area an approximated flow area will be needed to make sure that the correct pressure drop and heat transfer are calculated.
- The sections of tube that are not in contact with helium are not considered in the water-side pressure drop calculations. This is because only one length input is

[1] Except row 6 and 8, which have two extra tubes per row

available in the Flownex model and the correct heat transfer length is opted for, as the water-side pressure drops do not affect the helium side markedly.

In Flownex the PPWC is modelled with a shell-and-tube heat exchanger model due to the multiple gas and water passes. If there was only one pass on either the primary on secondary side, the compact gas-liquid heat exchanger could also be used. The Flownex input parameters are given in Table 5.3 and some calculations are done here. Figure 5.7 shows what the terminology used in Flownex refers to.

Table 5.3 : PPWC *Flownex* input values for the Shell-and-Tube heat exchanger element.

Flownex input description	General description	Value
Number of parallel circuits	The number of tube rows perpendicular to the gas flow in one pass	8
Shell passes (tubes)	Tube passes through the shell	2
Tubes per pass	The total number of tubes per shell pass	136
Tube ID	Inner diameter	20.2 mm
Tube pass length	Heat exchange length per pass	2.49 m
Tube surface roughness	Used in friction calculation	40 μm
K in	Entry secondary loss – a sharp-edged entry is assumed	0.5
K out	Discharge secondary loss – a sharp-edged discharge loss is assumed	1
Shell passes	The number of times the gas passes over tube banks	4
Shell diameter	The inner diameter of the shell	1.6 m
Shell length	Heat exchange length	2.49 m
Void fraction	Ratio of volume occupied by tubes to the shell inner volume	0.956
Sigma	The ratio of free gas flow area to full frontal area	0.302
K in	The secondary inlet loss to the shell	0.5
Z1	See Figure 5.7	0.54 m
Z2	See Figure 5.7	0.095 m
Z3	See Figure 5.7	-
Z4	See Figure 5.7	-
T1	See Figure 5.7	0.21 m
T2	See Figure 5.7	0.21 m
T3	See Figure 5.7	-
T4	See Figure 5.7	-

Table 5.3 : PPWC *Flownex* input values for the Shell-and-Tube heat exchanger element (continued).

Flownex input description	General description	Value
Configuration	Assuming the water inlet is always on the bottom left, this parameter specifies where the helium enters the cooler	Bottom left
Heat transfer area	On the shell side	54 m^2
Heat transfer area ratio	Ratio of shell side to tube side areas	1.256
Wall HT coefficient	The metal coefficient of the wall, see (11)	10130 $W/m^2/K$
Heat capacity	Product of the metal mass and its specific heat	604.345 kJ/K

The heat transfer and friction factors through the tube bundles are characterised in curves of Colburn j-factor and friction factor versus Reynolds number. Kays and London (1984) was used to find suitable data to represent the tube geometry used. In the reference no exact geometrical match could be found for the PPWC tube geometry given in Table 5.2. It is assumed that using the data that closest matches the dimensions will yield results that are good enough for use in the model. However, another source of analytical data was found in Incropera (1996) in the form of a global Nusselt number and friction factors for flow over banks of tubes.

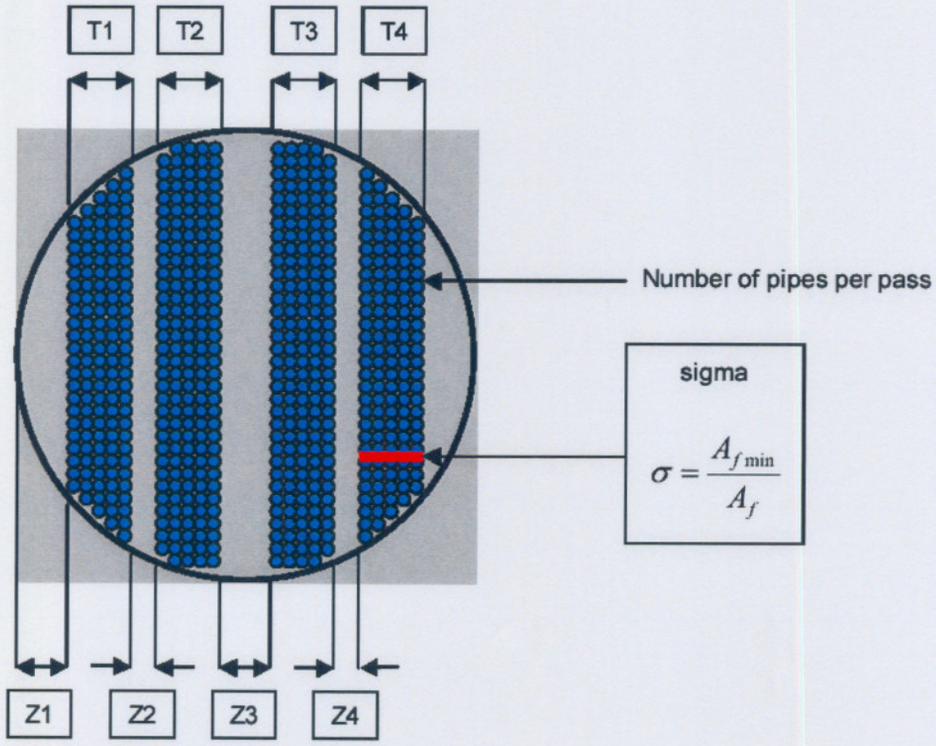

Figure 5.7 : Terminology used in Flownex model (Flownex User Manual).

In the text of Incropera, Grimison's correlation is used to find the Nusselt number for banks of tubes of 10 or more rows deep:

$$Nu_D = 1.13 C_1 \, \mathrm{Re}_{D,\max}^{m} \, \mathrm{Pr}^{1/3} \qquad (5.1)$$

where: $2000 < Re_{D,max} <= 40000$

$Pr >= 0.7$

and

$$\mathrm{Re} = \frac{\rho V_{\max} D}{\mu} \qquad (5.2)$$

where V_{max} is the maximum velocity through the tube bank (either at A_1 or A_2).

In the correlation C_1 and m are obtained from tables. For rows of tubes less than 10 correction factors are applied. For 8 tube rows the correction factor is 0.98. In addition, distinction is made between aligned and staggered tube banks. In Figure 5.8 the required parameters are given to characterise a staggered tube bank as is found in the PPWC.

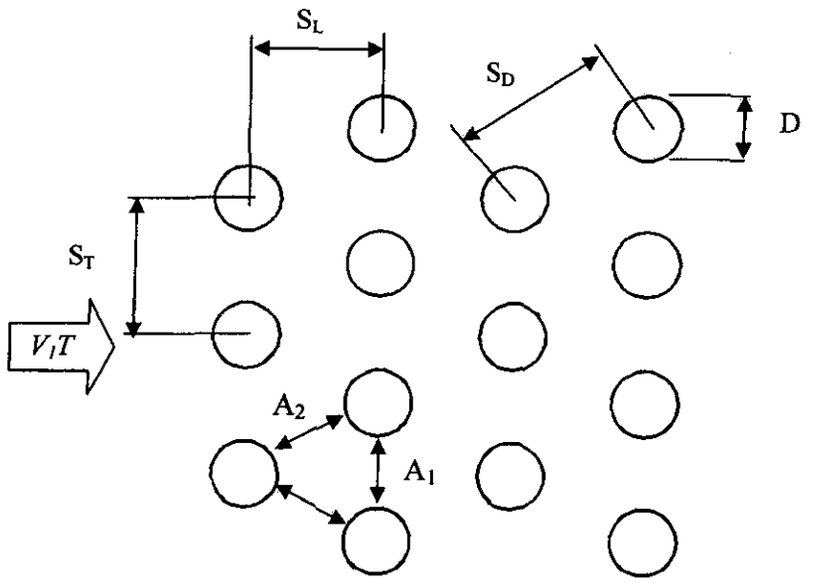

Figure 5.8 : Tube arrangement parameters in a staggered tube bank.

From the PPWC geometry the following parameters were calculated:

$S_L = 0.05\ m$

$S_T = 0.0866\ m$

$S_D = 0.066\ m$

$D = 0.0254\ m$

$S_L/D = 1.97 \sim 2$

$S_T/D = 3.41$

The available data only goes up to a S_T/D of 3 and thus extrapolation is required and shown in the next table..

Table 5.4: Staggered tube bank parameters for the PPWC.

S_T/D	2	3	3.41
C_1	0.482	0.449	0.435
m	0.556	0.57	0.576

This coefficient and exponent are used along with the correction factor of 0.98 to calculate Nusselt numbers for a Reynolds number range from 0 to 26000. It is noted that the correlation is not valid for Re less than 2000 but it is assumed that the variance will be small and the operating point of the fluid will be in a region higher than Re = 2000. The Nusselt number is converted to a Colburn j-factor ($StPr^{2/3}$) using:

$$St\,\mathrm{Pr}^{2/3} = \left(\frac{Nu}{\mathrm{Re}\,\mathrm{Pr}}\right)\mathrm{Pr}^{2/3} \qquad (5.3)$$

The resulting curve is shown below.

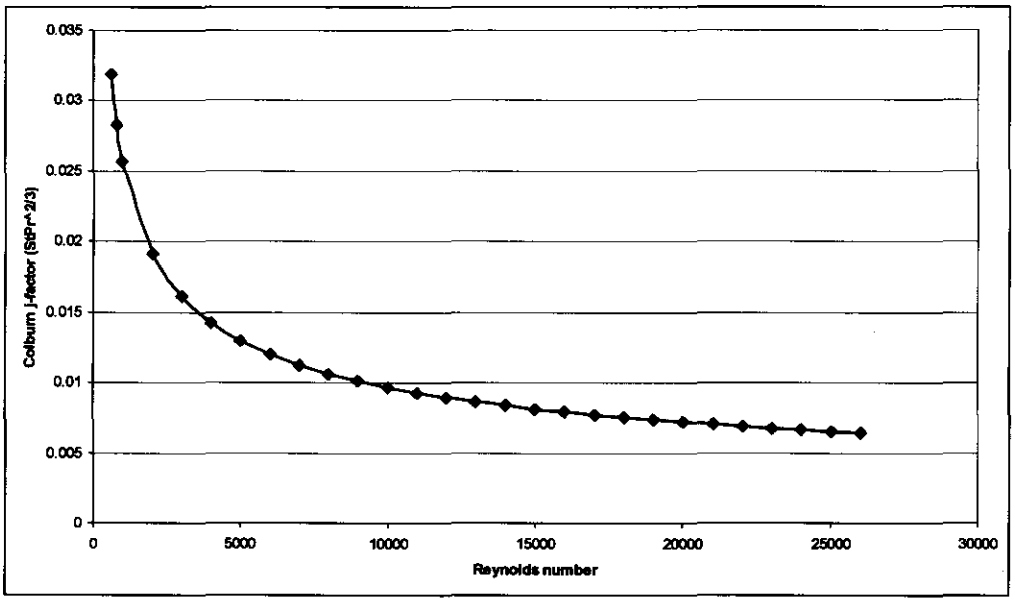

Figure 5.9 : Colburn j-factor vs. Reynolds number for PPWC tubes.

The friction factors at varying Reynolds numbers are calculated from curves found in Incropera (1996). The resultant friction factors versus Reynolds number are shown in Figure 5.10.

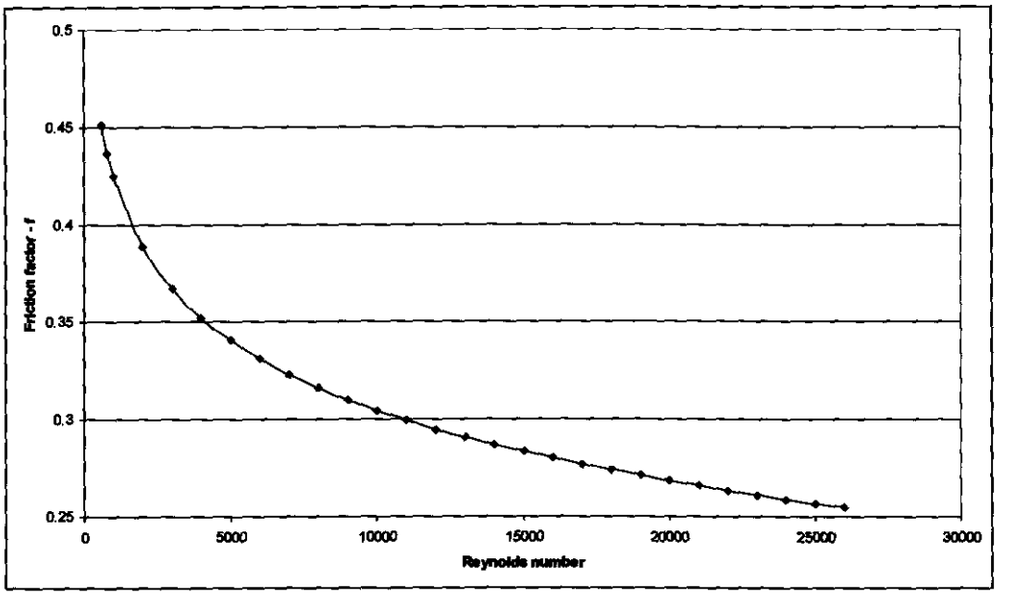

Figure 5.10 : PPWC gas-side friction factor.

5.5. Intermediate Heat Exchanger

The intermediate heat exchanger or IHX functions as an energy interface between the primary and secondary cooling circuits. The IHX is composed of helically coiled tubes on the inside of a double walled shell. A cut-away and cross-sectional view of the IHX is shown in Figure 5.11 and Figure 5.12 respectively.

Hot gas from the reactor enters from below and flows up over the helical tube bundles to a manifold volume at the top of the heat exchanger. From there it goes to a circulator and back again through the outer annulus of the heat exchanger pressure vessel. Inside the tubes cool gas flows from the secondary cooling circuit. This gas flows down from the top of the heat exchanger, making the configuration counterflow.

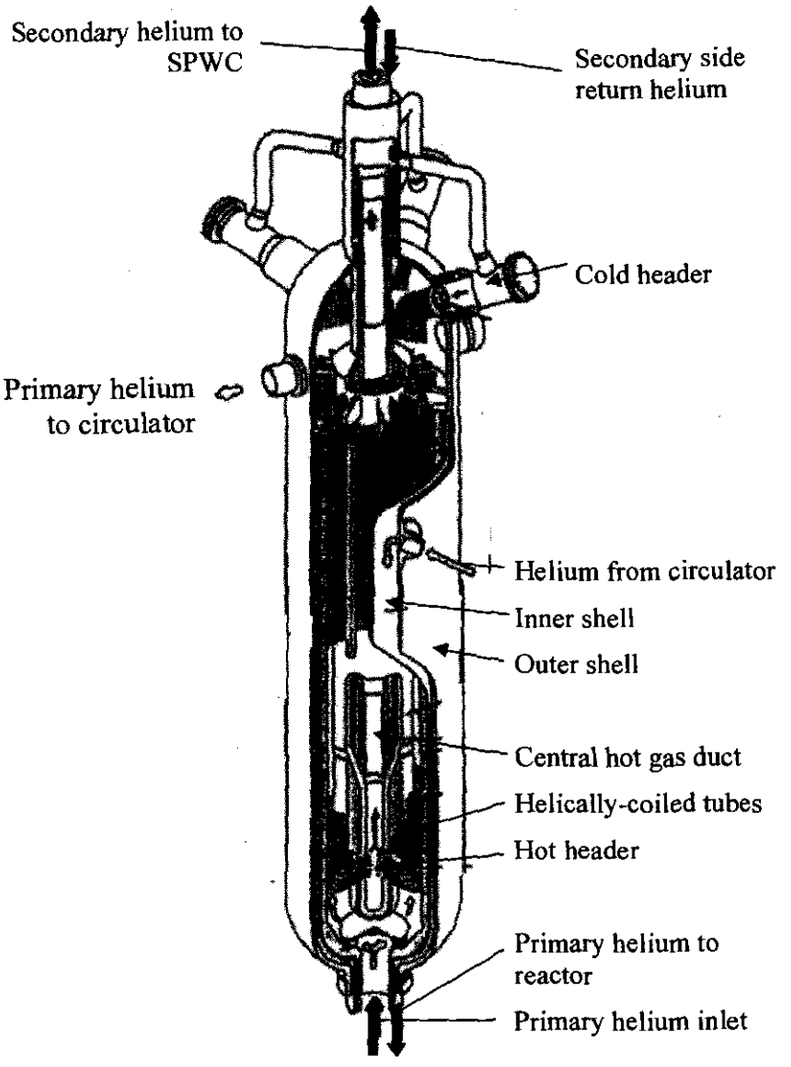

Figure 5.11 : Cutaway view of IHX (Takeda et al., 2000).

This type of heat exchanger is known as a helical configuration. Such geometry is not specifically catered for in Flownex and one of the available models must thus be modified to try and capture the behaviour of this configuration. For this the recuperator model is best suited, as both the thermal and hydraulic characteristics of the primary and secondary sides can be modelled individually. From the onset of the modelling it was evident that care must be taken to verify each assumption made in modelling the helical configuration with a simplified model.

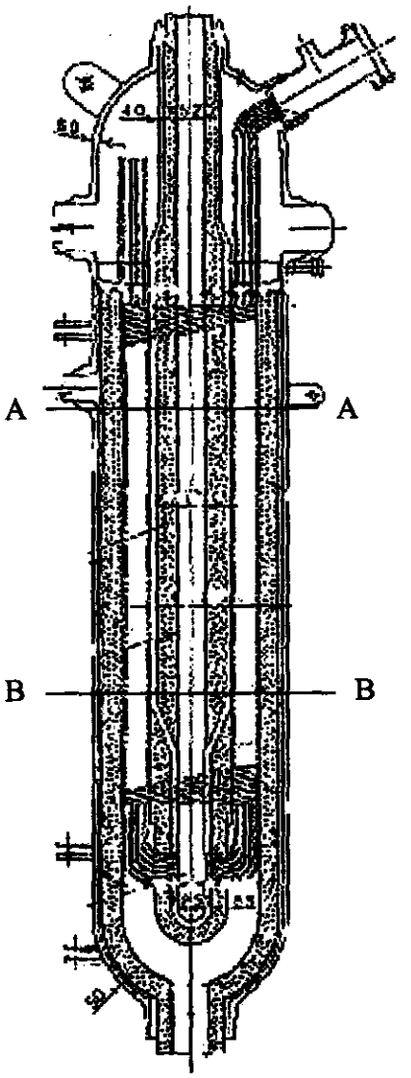

Figure 5.12 : Longitudinal section of the Intermediate Heat Exchanger (Takeda et al., 2000).

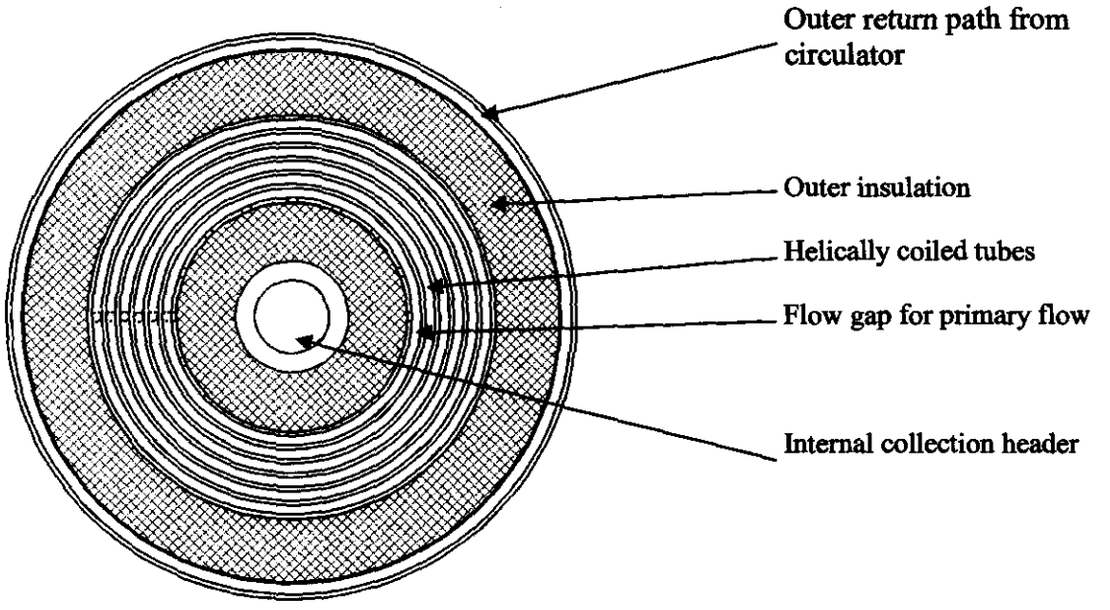

Figure 5.13 : Cross-section A-A through IHX showing primary side heat exchange flow section.

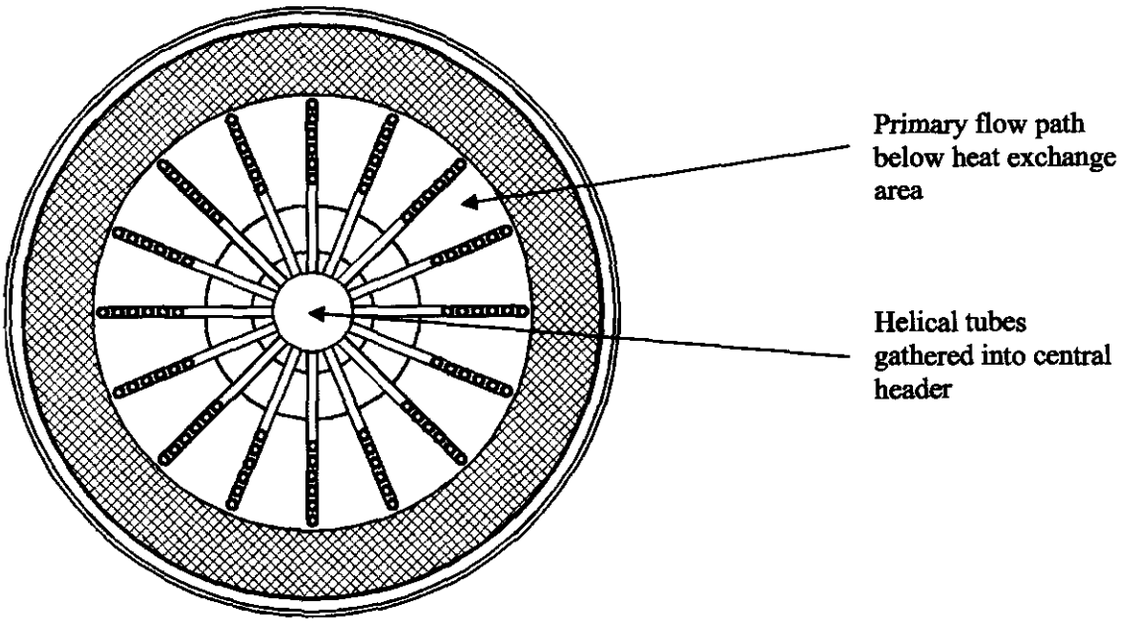

Figure 5.14 : Cross-section B-B through IHX showing tube routing below heat exchange section.

A careful look at the configuration reveals that the secondary gas side is nothing other than a set of parallel pipes all coiled into a helix. The advantage of using a helical tube is that heat transfer is enhanced by secondary flows induced by the centrifugal force acting on the gas in the tube. To model this flow, a standard hydraulic pipe model may be used incorporating a secondary pressure loss factor and altered Nusselt number to account for the helical bend. The pressure losses at the inlets and outlets to the tube bundle are modelled in the preceding and succeeding elements respectively.

On the primary side it can be assumed that the flow over concentric pipes of the helix (see Figure 5.13) can be modelled similarly to flow over a conventional staggered tube bank. The heat transfer is a more difficult issue to contend with due to lack of detail in empirical results or pre-test estimates. The estimates do not allow one to set up a detail model of the heat exchanger and benchmark it. Only inlet and outlet temperatures are given. Thus the Nusselt factors used in the model need to be adjusted until steady-state predictions of heat transfer are matched.

The helical coil consists of 16 sets of 6 pipe rows arranged axi-symmetrically around the centreline, totalling 96 pipes on the secondary side. As not much geometrical information is given about the system it is assumed that each coil rises with a pitch of 200mm per revolution. This results in each coil consisting of 12 revolutions over the heat transfer length of 2,49m (Takeda et al., 2000). The length of a coil is found in Miller as:

$$L = \pi \cdot D \cdot n\left[1 + \frac{P^2}{4D^2}\right]^{0.5} \tag{5.4}$$

where L = Length of the coiled tube,

D = The coil diameter,

P = the tube pitch and

n = number of revolutions per coil.

Thus for the pitch and number of revolutions described above the approximate diameters and lengths of each row are:

- Row 1 (inner): $D = 0.84$ m & $L = 31.9$ m
- Row 2: $D = 0.934$ m & $L = 35.2$ m
- Row 3: $D = 1.028$ m & $L = 38.8$ m
- Row 4: $D = 1.122$ m & $L = 42.3$ m
- Row 5: $D = 1.216$ m & $L = 45.8$ m
- Row 6 (outer): $D = 1.31$ m & $L = 49.4$ m

The pipes all have an inner diameter of 24.8 mm with a wall thickness of 3.5mm. The material used for the tubes is Hastelloy XR of which properties are given in Takeda (2000). These properties are used along with the metal volume to find the mass capacitance of the heat exchanger. As with the PPWC the mass capacitance is very important in the accurate transient simulation of the heat exchanger. Furthermore the pipe lengths and diameters are used in the heat transfer area and area ratio calculations.

The effective heat transfer length parameter in Table 5.5 (*Length*) is a limitation in the program in that it expects the heat transfer length for both sides to be the same. In this case the secondary gas flow through the helical coils involves a much longer heat transfer length than the primary side. To solve this problem the real primary side heat transfer length is used while the secondary side's loss of heat transfer length is compensated for in the Nusselt factor.

Concerning the parameters on primary and secondary sides, both require hydraulic diameters. On the primary side it is assumed that the helix radii are large enough to approximate the pipe bundle as a bank of tubes. For such a case the hydraulic diameter is simply the outer diameter of the tube. The hydraulic diameter on the secondary side is the inner diameter of the tube. The flow area input in Table 5.5 is simply the free flow cross-sectional area that the fluid sees. The remaining parameters influence the frictional and heat transfer properties of the flow path. These were fixed on a stand-alone model of the IHX where the overall performance was matched to the predicted values from Takeda et al. (2000). All the Flownex input values are shown in the next table.

Table 5.5 : IHX *Flownex* input values (as usedin a Flownex recuperator element).

Flownex input description	**General description**	**Value**
Number of increments	Discretisation in the flow path direction	10
Mass capacitance	Product of metal mass and metal specific heat	*3054.47 kJ/kg*
Conduction	Conduction coefficient of interface material	*18.239 W/m/K*
Wall thickness	Average conduction length through interface material	0.0035 m
Heat area	Primary side heat exchange area	*214.8 m^2*
Area ratio	Ratio of primary to secondary heat areas	1.282
Length	The flow length (the same for both primary and secondary sides)	4.87 m

Table 5.5 : IHX *Flownex* input values (as usedin a Flownex recuperator element - continued).

Flownex input description	General description	Value
Heat exchanger configuration	Counter or parallel flow	Counterflow
Hydraulic diameter (in and out) – Primary side	The characteristic length on the primary side. Used for Reynolds number calculation. The flow path is of constant cross-section throughout.	0.0605 m
Flow area (in and out) – Primary side	Cross-sectional free-flow area.	1.495
Laminar friction factor – primary side	Factor used in pressure drop calculation	1
Turbulent friction factor – primary side	Multiplication factor to account for turbulence.	1
Laminar Nusselt number – primary side	Nusselt number for flow path sectional profile.	1
Turbulent Nusselt factor – primary side	Multiplication factor to account for turbulence.	6.5
Roughness – primary and secondary sides	Surface roughness	30 μm
Hydraulic diameter (in and out) – secondary side	The characteristic length on the primary side. Used for Reynolds number calculation. The flow path is of constant cross-section throughout.	0.0248 m
Flow area (in and out) – secondary side	Cross-sectional free-flow area.	0.0468 m^2
Laminar friction factor – secondary side	Factor used in pressure drop calculation	1
Turbulent friction factor – secondary side	Multiplication factor to account for flow path cross sectional profile.	1
Laminar Nusselt number – secondary side	Nusselt number for flow path cross sectional profile.	1
Turbulent Nusselt factor – secondary side	Multiplication factor to account for flow path cross sectional profile.	1.8

These input parameters were first used in a stand-alone model of the IHX to verify the steady-state performance of the model.

5.6. Helium circulators

The helium circulators used in the gas circuits are single-stage centrifugal compressors. Helium from the associated cooler enters the circulator inlet and goes through a filter before

being compressed. A variable- speed motor is used to control the helium flow rate delivered by the circulator.

In Flownex turbines, blowers and compressors are modelled by means of characteristic curves. The pressure ratio versus non-dimensional mass flow $\left(\dot{m}\sqrt{T_0}/P_0\right)$ and efficiency versus corrected mass flow characteristic curves for different non-dimensional shaft speeds $\left(N/\sqrt{T_0}\right)$ are used. The shaft speed is used along with the inlet gas conditions to find the operating point on the curves.

The graphs of pressure ratio versus invariant mass flow rate and invariant power versus invariant mass flow rate were supplied by JAERI. Graphs were supplied for the primary, secondary and auxiliary circuit machines. These graphs had to be converted into the Flownex compressor curve file format before it could be used in the circuit.

Conversion of invariant mass flow to non-dimensional mass flow:

$$\dot{m}_{cor} = \dot{m}_{inv} / 3600 \tag{5.4}$$

$$\dot{m} = \frac{\dot{m}_{cor} p_{01}}{\sqrt{T_{01}}} \tag{5.5}$$

Since Flownex requires a graph of efficiency versus non-dimensional mass flow rate, the invariant power data had to be modified to obtain efficiency. This was done as follows:

$$P = P_{Inv} p_{01} \sqrt{T_{01}} \tag{5.6}$$

$$P_{fluidic} = (PR^{(\gamma-1)/\gamma} - 1) c_p T_{01} \dot{m} / 1000 \tag{5.7}$$

$$\eta = P_{fluidic} / P \tag{5.8}$$

where P = power input to the compressor,

$P_{fluidic}$ =Power delivered to fluid

PR = pressure ratio (JAERI),

η = compressor efficiency,

T_{01} = inlet temperature and

p_{01} = inlet pressure.

The characteristic maps for the primary and secondary circulators are the same and are shown in Figure 5.15 and Figure 5.16. The primary circulator runs at a speed of 9400rpm, while the secondary machine is slightly faster at 9900rpm at 30MW. For 15MW they operate at 8900rpm and 9500rpm respectively.

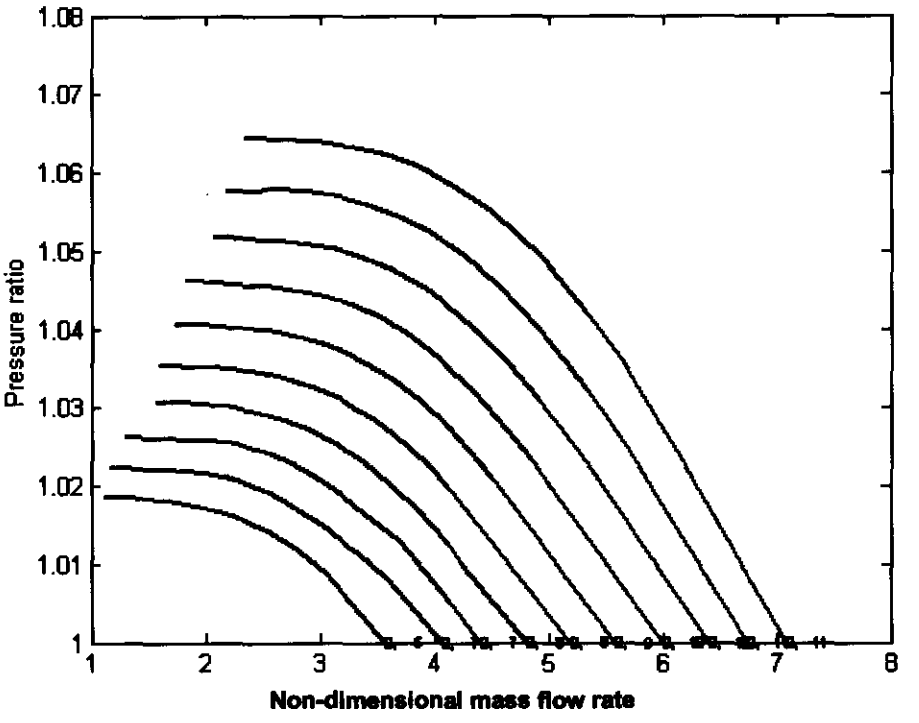

Figure 5.15 : Primary and Secondary circuit pressure ratio curves for different shaft speeds.

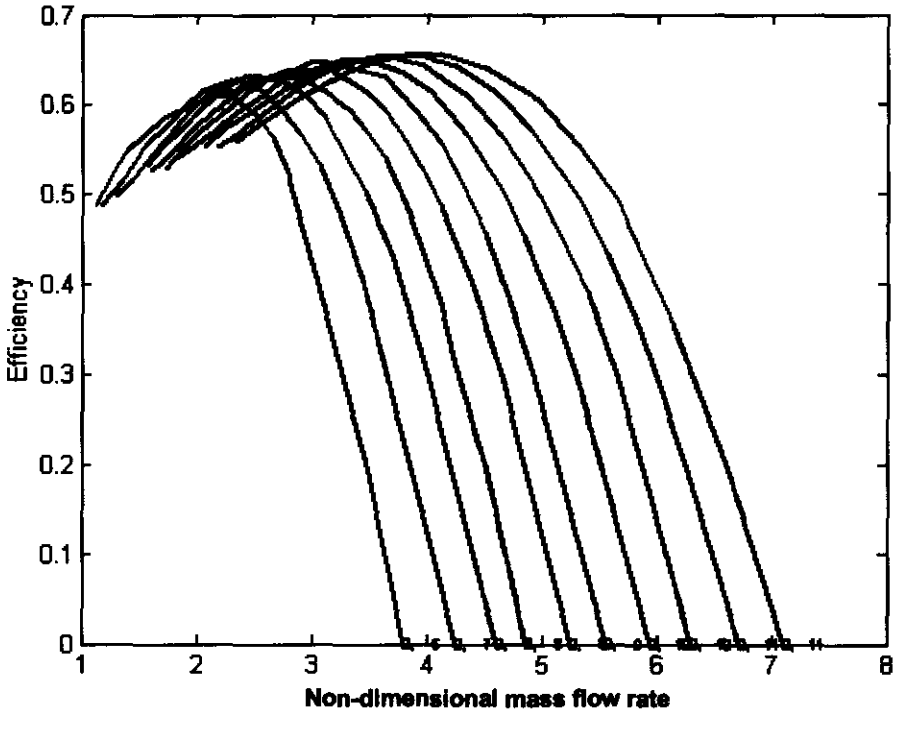

Figure 5.16 : Primary and secondary circuit circulator efficiency curves for various shaft speeds.

5.7. Reactor core model

The HTTR reactor is shown in Figure 5.17. Due to the high pressure of the system the reactor is contained in a large pressure vessel. The very high temperature forced the designers to use

ceramic compounds in the core, as the cost of high temperature alloys was exorbitant. The core itself consists of many graphite blocks or bricks that have been packed to form the core. These graphite blocks serve both a structural function and as a neutron reflector. The blocks are mostly hexagonal in shape, as is shown in Figure 5.18 and have various holes drilled through them fulfilling various functions. Such functions include conduits for instruments, control rods, absorber material and as containment for fuel rods.

The fuel rods consist of metallic sleeves containing cylindrical pellets made out of uranium oxide fuel kernels in a compacted form. Each fuel rod has spacers that position it in the middle of the boring in the graphite block. The gap between the rod and the block is the flow path for helium flowing through the reactor. More than one fuel rod is required to heat the gas in as short a distance as possible.

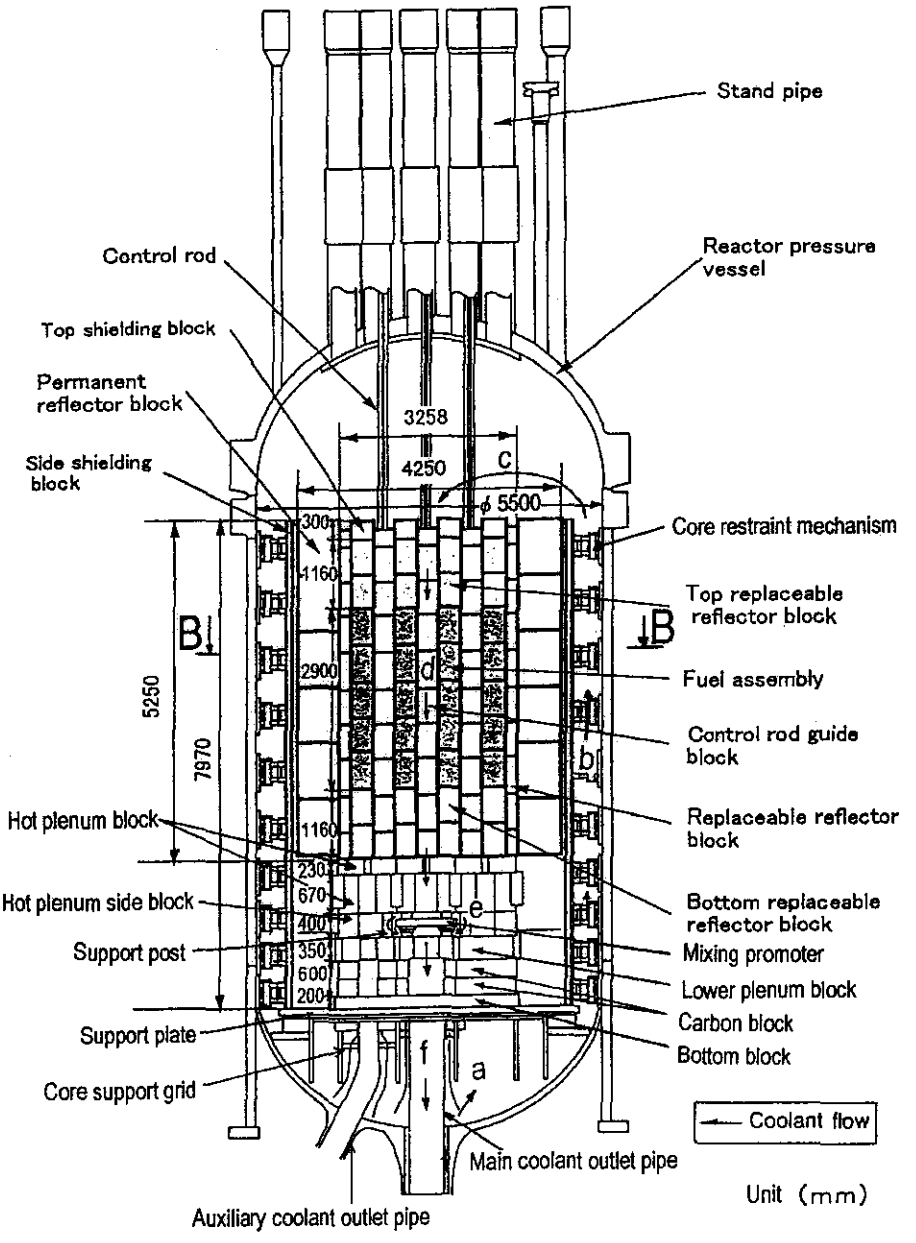

Figure 5.17 : Sectional view through the HTTR reactor (Takeda et al., 2000).

Helium enters the pressure vessel at the bottom and flows vertically upward outside of the core in a flow passage formed between the reactor core and the pressure vessel. The flow

then enters the core from the top plenum. The gas flows downward through the borings in the reflector and then over the fuel rods. At the bottom of the core the hot gas is gathered into a volume called the *hot plenum*, from which it exits into the cooling system duct work.

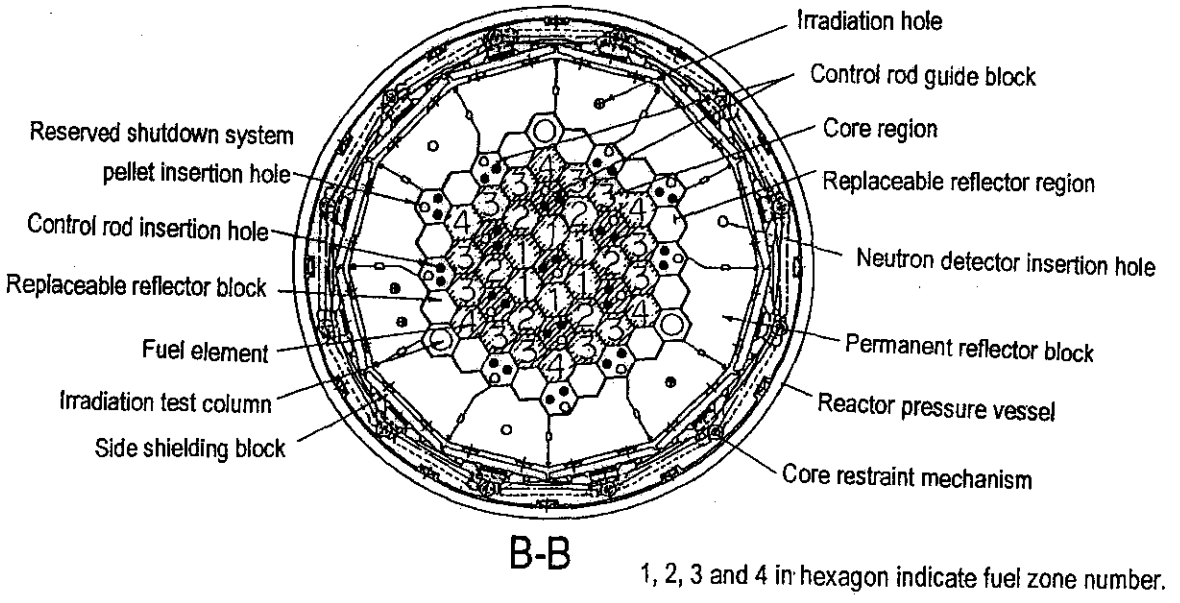

Figure 5.18 : Horizontal section through the reactor core (Takeda et al., 2000).

The HTTR reactor is modelled with a specially developed HTTR element in Flownex. Rousseau and Greyvenstein (2002) discuss the important aspects of the development of this model. The model is validated by Van der Merwe (2003) by means of an explicit code known as Xnet. Xnet is a thermal fluid code developed by MTech Industrial in association with the School of Mechanical and Materials Engineering at the Potchefstroom University. The code uses a Runge Kutta time integration process to solve the discretised equations.

Due to Xnet being a validation code, it has a limited number of elements and is more focused on basic or so called primitive elements that can be used to represent more complex components. These include pipe elements, conductive heat transfer (CHT) elements, convective elements and radiation elements. On closer inspection of the HTTR it is seen that it is merely a collection of pipe elements; conduction, convection and radiation paths and heat sources (where the fuel is situated). For Xnet to be used as a validation code it first needed to be validated itself. For this purpose various tests were done, such as pressure step-up behaviour in a long pipe, temperature changes in a conductive heat transfer scenario and equalisation of tank pressures in Xnet. These were all verified against their equivalent Flownex models, which have in turn been validated against analytical results. In the validation of Xnet very good comparison was found with the Flownex results.

In modelling such a complex structure as the HTTR various assumptions had to be made. Rousseau and Greyvenstein (2002) simplify the complicated geometry of Figure 5.18 by means of annular regions, as shown in Figure 5.19. The outer ring represents the permanent reflector blocks, while the ring just inside of that represents the replaceable reflector blocks. The ring numbered 3 represents the fuel assembly blocks numbered 3 and 4 in Figure 5.18, i.e 18 fuel assembly blocks in total. The ring numbered 2 represents the fuel assembly blocks numbered 2 as well as the reflector blocks in-between the fuel blocks, i.e. a total of 12 blocks.

The composition of ring 2 is assumed to be homogeneous, with an average of only 16.5 fuel rods per block to account for the reflector blocks in-between. The ring numbered 1 represents the six fuel blocks also numbered 1 and the central cylinder represents the single reflector block at the centre of the original core geometry.

When viewed from the top, the surface area of each of the representative axi-symmetric rings is exactly the same as the total surface area of all the hexagon-shaped blocks represented by that ring. The rings each have the same height as that of the layer of blocks that it represents. This emphasis is placed on having the correct solid volume so that the total thermal mass of the core will be exactly equal to that of the original core, which is important during transient events. Each of the rings can be discretised into a number of control volumes in the axial direction to improve accuracy. A uniform temperature distribution is assumed within each of the control volumes at any time step. Therefore, each control volume can be represented by a single thermal mass node connected via a thermal resistance to the adjacent thermal mass nodes at the top, bottom, inside and outside. The thermal resistances are adjusted to account for the porosity of the blocks containing the flow passages.

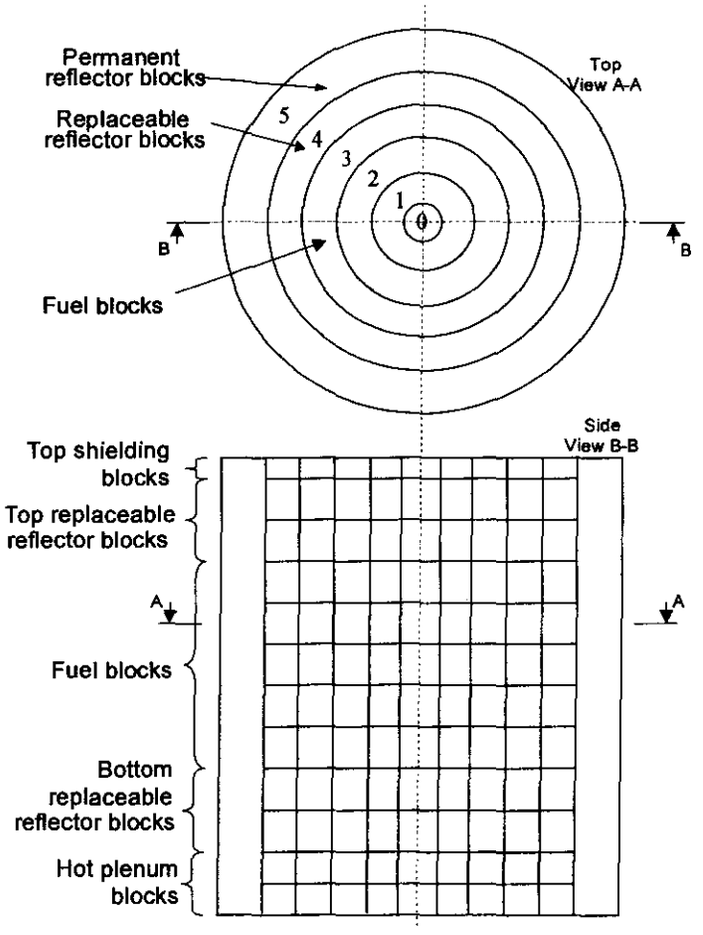

Figure 5.19 : Schematic layout of the axi-symmetric core geometry approximation.

Each of the nodes representing the fuel assembly blocks also represents the surface temperature of the flow passages inside the fuel assembly block containing the fuel rods. This surface temperature is coupled via a forced convection heat transfer resistance to the gas flow passing through the flow passages. The gas flow in the fuel assembly blocks is in turn connected via a forced convection heat transfer resistance to the outside surface of the graphite reflector that forms part of the fuel rod. The graphite shield and fuel compact can in

turn be discretised into a number of layers each represented by a single thermal mass node and connected to the adjacent nodes via conduction heat transfer resistances. The innermost surface of the fuel compact can be assumed to be an adiabatic surface, since the heat capacity of the gas contained within the inner cylinder is negligible. As a first approximation the effect of radiation between the fuel rod surface and the fuel assembly block surface as well as heat losses on the outside surfaces of the core were neglected. The reactor power is distributed within the fuel compact layers only.

The gas flow path through the core from the plenum at the top to the plenum at the bottom is formed by a combination of cylindrical and annular flow passages. A section through the geometry of a typical flow path is shown schematically in Figure 5.20. The flow path is discretised, as indicated by the node-element-node configuration shown on the right-hand side of the diagram. Although only one flow channel is shown in the schematic representation, each block can be discretised into any number of smaller flow elements in order to improve accuracy.

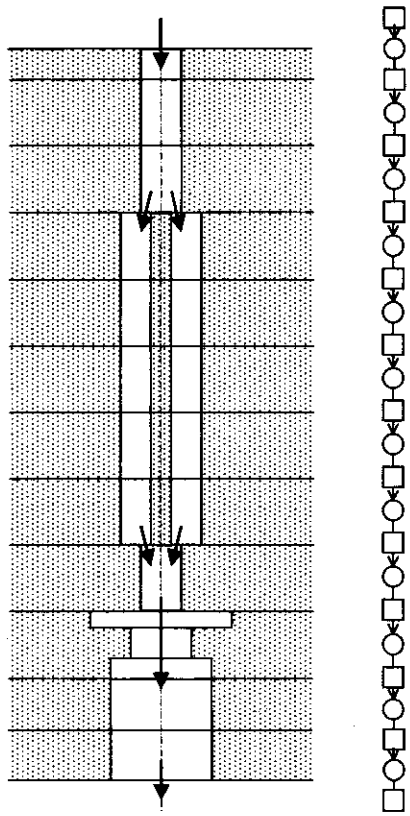

Figure 5.20 : Schematic of a typical flow path network.

The network topology of the complete reactor model is shown in Figure 5.21, showing the flow path elements and thermal capacitance elements. Based on the neutronic power generated within the fuel elements, a fixed axial power distribution profile is specified along the height of the reactor. The normalised power distribution profile as a function of the normalised position along the height of the fuel block section in the reactor. For steady-state conditions a fixed value of the total power can be specified and for reactor scram transients a suitable time-dependent decay heat power curve is specified.

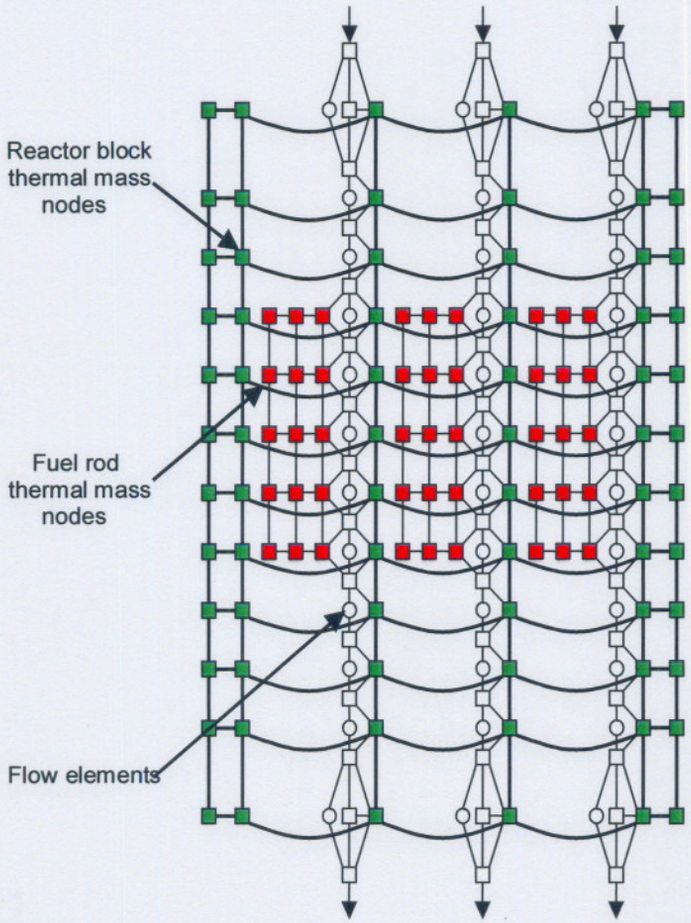

Figure 5.21 : Complete flow element and path layout.

To validate this model Van der Merwe (2003) created a primitive element network of the reactor in Xnet. In the beginning of the investigation some discrepancies were found with regard to heat transfer coefficients. These were due to a difference in correlations used in Flownex and those used by JAERI. Other factors, such as the effect of the element grid, were investigated and it was found that the chosen grid resolution was adequate. In conclusion the 30MW and 15MW steady-state power levels were tested and differences were judged to be negligible. The Flownex and Xnet models also responded well to fast transients, with very small discrepancy in their results.

5.8. Conclusion

In this chapter the important part of modelling the HTTR system in Flownex was discussed. This is such an important aspect of the study because the code is very sensitive to the type of inputs that are given to it. If the models are not set up correctly to fairly represent the physical component, the entire system simulation is flawed. However, the amount of detailed work that went into developing the models is not fully described, as it is not within the scope of this study. The next chapter tests the system model by comparing analysis results with empirical data.

6. STEADY-STATE RESULTS

6.1. Introduction

This chapter presents the steady-state results of the simulation of the HTTR system with Flownex. The first section discusses the 15MW power level of the HTTR. Distinction is made between the Flownex results, the experimental values and the original design values provided by JAERI (Takeda et al., 2000).

6.2. Steady-state results comparison – 15MW operation

This section discusses the results for the 15MW loss-of-power benchmark. The results tables contain four columns: the first column tabulates the predicted HTTR data as sent out in JAERI's first document on the benchmark (Takeda et al., 2000), the second column contains the test data as obtained in the 15MW loss-of-power experiment, the third column gives the Flownex data and the last one gives a percentage difference between the HTTR experimental data and the Flownex results.

Table 6.1 : Reactor core results comparison for 15 MW power operation.

Parameter	HTTR Estimate	HTTR Experimental	Flownex	Percent difference
Thermal power [MW]	15	15	15	0
Helium inlet temp. [°C]	241 (About)	242	240.5	0.62
Helium outlet temp. [°C]	470 (About)	468	472.7	1
Helium pressure [kPa]	3000 (About)	2900	2795	3.62
Helium mass flow rate [kg/s]	12.4	12.4	12.44	0.32
Hot plenum block temp. [°C]	490 (About)	391	-	-

Table 6.2 : Intermediate heat echanger results comparison for 15 MW power operation.

Parameter	HTTR Estimate	HTTR Experimental	Flownex	Percentage difference
Primary helium inlet temp. [°C]	468 (About)	468	472.7	1
Primary helium outlet temp. [°C]	238 (About)	235	240.77	2.39
Primary helium pressure [kPa]	3000 (About)	2800	2784	0.57
Primary helium mass flow rate [kg/s]	4.1	4.1	4.078	0.53
Secondary helium inlet temp. [°C]	154 (About)	158	160.6	1.61
Secondary helium outlet temp. [°C]	431 (About)	420	423.7	0.87
Circulator speed [rpm]	9500	8770	8770	0
Secondary helium pressure [kPa]	3100 (About)	2900	2900	0
Secondary helium mass flow rate [kg/s]	3.6	3.6	3.59	0.28

Table 6.3 : Primary pressurised water cooler results comparison for 15 MW power operation.

Parameter	HTTR Estimate	HTTR Experimental	Flownex	Percentage difference
Helium inlet temp. [°C]	468 (About)	468	472.7	1
Helium outlet temp. [°C]	242 (About)	235	240.77	2.4
Helium pressure [kPa]	3000 (About)	2800	2784	0.57
Helium mass flow rate [kg/s]	8.3	8.2	8.308	1.3
Circulator Speed [rpm]	8900	8000	8000	0
Water inlet temp. [°C]	89 (About)	79	79	0
Water outlet temp. [°C]	110 (About)	100	101.29	1.27
Water pressure [kPa]	2600 (About)	2300	2300	0
Water mass flow rate [kg/s]	115	111	111	0

Table 6.4 : Secondary pressurised water cooler results comparison for 15 MW power operation.

Parameter	HTTR Estimate	HTTR Experimental	Flownex	Percentage difference
Helium inlet temp. [°C]	430 (About)	420	423.6	0.85
Helium outlet temp. [°C]	154 (About)	152	155.86	2.47
Helium pressure [kPa]	3100 (About)	2900	2861	1.34
Helium mass flow rate [kg/s]	3.6	3.6	3.59	0.27
Circulator speed [rpm]	8100	8130	8130	0
Water inlet temp. [°C]	89 (About)	79	79	0
Water outlet temp. [°C]	110 (About)	100	99.9	0.1
Water pressure [kPa]	2500 (About)	2300	2300	0
Water mass flow rate [kg/s]	60	57	57	0

The data shows that the Flownex results are closer to the experiment than to the predicted values. This is possibly because, for the experiment, the speeds of the circulators were greatly reduced from predicted values. It was found that if the predicted speeds are used in the simulation, the mass flow becomes much higher than what is needed for 15MW power delivery in the reactor. It is assumed that JAERI was conservative in their calculation of the system resistance and hence the circulators were oversized.

There are small differences in pressure and temperatures, but until more detailed data becomes available on pressure drops through the HTTR these differences are within acceptable limits of 5 percent. The tables below provide a comparison of the Flownex results against the computed results supplied by JAERI for the various parts of the HTTR system.

6.3. Steady-state results comparison – 30MW operation

This section gives the steady-state results for the 30MW simulations. The tables below each contain five columns: the first for the HTTR predicted results, the next for Flownex results using the prescribed shaft speeds for 30MW, then results obtained when the shaft speeds are kept as for the case of the 15MW results, then the HTTR experimental results and lastly a comparison between columns three and four. The reason for using the 15MW shaft speeds is because of the large difference between the Flownex data with 30MW speeds and the test data. No confirmation of shaft speeds for the 30MW test was given and thus it is assumed that the 15MW speeds were used. It is assumed that the system resistance was incorrectly estimated prior to the test and thus changes to shaft speed were made during the test to keep key parameters, like pressure and temperature, as close to the input values as possible. When the 15MW speeds are used the resulting differences are not that large. As with the 15MW case, a percentage difference less than 5 percent is considered acceptable.

Table 6.5 : Reactor core results comparison for 30MW operation.

Parameter	HTTR Estimate	Flownex – Pre-scribed Shaft speeds	Flownex – 15 MW Shaft speeds	HTTR – test	Percentage difference.
Thermal power [MW]	30	30	30	30	0
Helium inlet temp. [°C]	395	412	402.7	392	2.65
Helium outlet temp. [°C]	850	789.2	858.9	828	3.6
Helium pressure [kPa]	4000	3993	3995.7	4000	0.1
Helium mass flow rate [kg/s]	12.4	15.31	12.66	12.4	2.05

Table 6.6 : Intermediate heat exchanger results comparison for 30MW operation.

Parameter	HTTR Estimate	Flownex – Pre-scribed Shaft speeds	Flownex – 15 MW Shaft speeds	HTTR – test	Percentage difference
Circulator speed [rpm]	9900	9900	8770	-	-
Primary helium inlet temp. [°C]	850	789.2	858.9	828	3.59
Primary helium outlet temp. [°C]	395	419.53	421	383	9.02
Primary helium pressure [kPa]	4000	3977.4	3983.67	4000	0.4
Primary helium mass flow rate [kg/s]	4.1	4.8	4.08	4.1	0.48
Secondary helium inlet temp. [°C]	241	260.7	262.74	248	5.6
Secondary helium outlet temp. [°C]	783	724.4	721.1	751	3.98
Secondary helium pressure [kPa]	4100	4092.5	4092	4000	2.25
Secondary helium mass flow rate [kg/s]	3.6	3.87	3.86	3.6	6.73

Table 6.7: Primary pressurised water cooler results comparison for 30MW operation.

Parameter	HTTR Estimate	Flownex – Prescribed Shaft speeds	Flownex – 15 MW Shaft speeds	HTTR - test	Percent difference
Circulator speed [rpm]	9400	9400	8000	-	-
Helium inlet temp. [°C]	850	789.2	856.8	828	3.36
Helium outlet T [°C]	395	401	388.4	390	0.41
Helium pressure [kPa]	4000	3977	3984	4000	0.4
Helium mass flow rate [kg/s]	8.3	10.45	8.54	8.2	3.98
Water inlet temp. [°C]	135	135	135	120	11.11
Water outlet temp. [°C]	175	177	177	160	9.6
Water pressure [kPa]	3500	3500	3500	3500	0
Water mass flow [kg/s]	115	115	115	113	1.73

Table 6.8 : Secondary pressurised water cooler results comparison for 30MW operation.

Parameter	HTTR Estimate	Flownex – Prescribed Shaft speeds	Flownex – 15 MW Shaft speeds	HTTR - test	Percentage difference
Circulator speed [rpm]	8100	8100	8130	-	-
Helium inlet temp. [°C]	782	719.9	723.4	751	3.671
Helium outlet T [°C]	240	256	256	243	5.08
Helium pressure [kPa]	4100	4054.7	4054	4000	1.33
Helium mass flow rate [kg/s]	3.6	3.87	3.88	3.6	7.22
Water inlet temp. [°C]	135	135	135	120	11.11
Water outlet temp. [°C]	175	171	171	158	7.6
Water pressure [kPa]	3400	3400	3400	3500	2.85
Water mass flow [kg/s]	60	60	60	59	1.67

For the 30MW case the mass flow required is the same as for 15MW; the difference in power is due to differences in inlet and outlet temperatures of the core. However, the mass flow requirement is dominant in sizing the circulators' rotational speeds and since the mass flow is the same as for 15MW, the rotational speeds should be roughly the same. The percentage differences are slightly higher than the predetermined allowable value of 5 percent. A possible cause of this is the discrepancy in water inlet temperature that is 11 percent less than the prescribed value.

6.4. Conclusion

From the above discussion it is evident that the Flownex results are reasonably close to the test and estimate values. The discrepancies can possibly be attributed to instrumentation resolution in the plant. A further cause of differences is possibly due to certain key process conditions in the test differing from those estimated by JAERI and used as Flownex input. It is assumed that JAERI had difficulty in reaching the prescribed values in the actual test. Such differences can be expected in a newly commissioned plant. The next chapter discusses the transient results for the loss-of-power benchmark.

7. TRANSIENT RESULTS

7.1. Introduction

This section presents the transient results of the loss-of-power benchmark for both the 15MW and 30MW cases. Firstly the setup of the transient analysis is described and then the results are presented.

7.2. Simulation setup

This transient involves a coasting down of the main loop circulators of the HTTR. A reactor SCRAM and loss of heat exchanger cooling mass flow are also included in the transient. Later in the analysis the auxiliary circulators are started and the cooling of the reactor's decay heat, via the auxiliary cooling system is commenced.

In Flownex, transient events, such as the loss of power test presented in this study, are put into the program in the form of specific changes in the systems input parameters at different times of the event. In Flownex a transient event editor allows the user to change alter parameters such as the time step during the simulation.

For the first part of the transient in question (time 0 to time 15 seconds) a time step of 0.1 seconds is used; from then to where the auxiliary cooling system starts up a time step of one second is used; and then 0.1s is again used for the auxiliary cooling. This is to allow better resolution during the time periods where rapid changes take place. The event inputs into Flownex are tabulated below.

Table 7.1 Transient events as modelled in Flownex

Simulated event	Time [s]	
	15 MW	30 MW
Coast down of the five main loop circulators commences. The speed of the circulators is hard-coded to be the same as the speed decrease prescribed by JAERI.	0	0
Water flows in the PPWC and SPWC is stepped down to 5 kg/s.	0	0
The circulator models become unstable in Flownex due to operation far outside of the circulator map's range. The circulators are replaced by mass flow sources that decrease at the same rate as the circulator mass flows did before 3.4 seconds.	3.4	3.4
Reactor SCRAM is initiated. The decay heat curve is read as input into the reactor model.	8.2	8.2
The IHX circulator flow has reached 0 kg/s.	12	10.8
The PPWC circulators have reached 0 kg/s.	13.4	14.5
The SPWC mass flow has reached 0 kg/s.	15	18
The auxiliary cooling system is activated.	52	52

7.3. 15 MW Loss-of-power transient results

As stated in Section 4.6.4, Flownex models circulators and other turbo-machinery by means of their characteristic curves or "maps". Hence, in a situation such as the loss-of-power benchmark, where the performance of the circulators determines the behaviour of the rest of the system, it is very important that accurate maps are used. In this case the speeds of the circulators are specified as input to the circulator models from which an operating point is found on the maps. The need for a moment of inertia in the model, important in predicting the deceleration of the circulator, is thus taken away by specifying the speed decrease over time.

Figure 7.1 shows the rotational speed of the PPWC, SPWC and IHX circulators over the first part of the transient. The curves for the decrease in speed were specified by JAERI as an input to the study (Takeda,2001). Figure 7.2 shows a locus plot of the movement of the operating point of the PPWC circulator on its map. It is clear that during normal operation at 15MW power the operating point is already off the map. As speed is reduced, the operating point moves toward the origin and so further away from the mapped region.

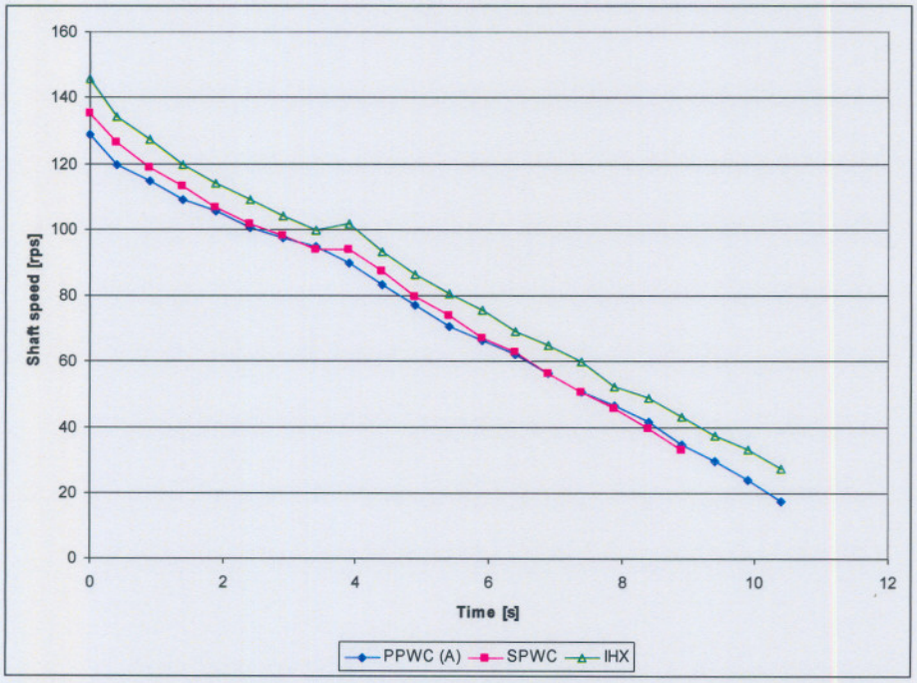

Figure 7.1 : Circulator shaft rotational speed – Flownex input data from JAERI (Takeda, 2000).

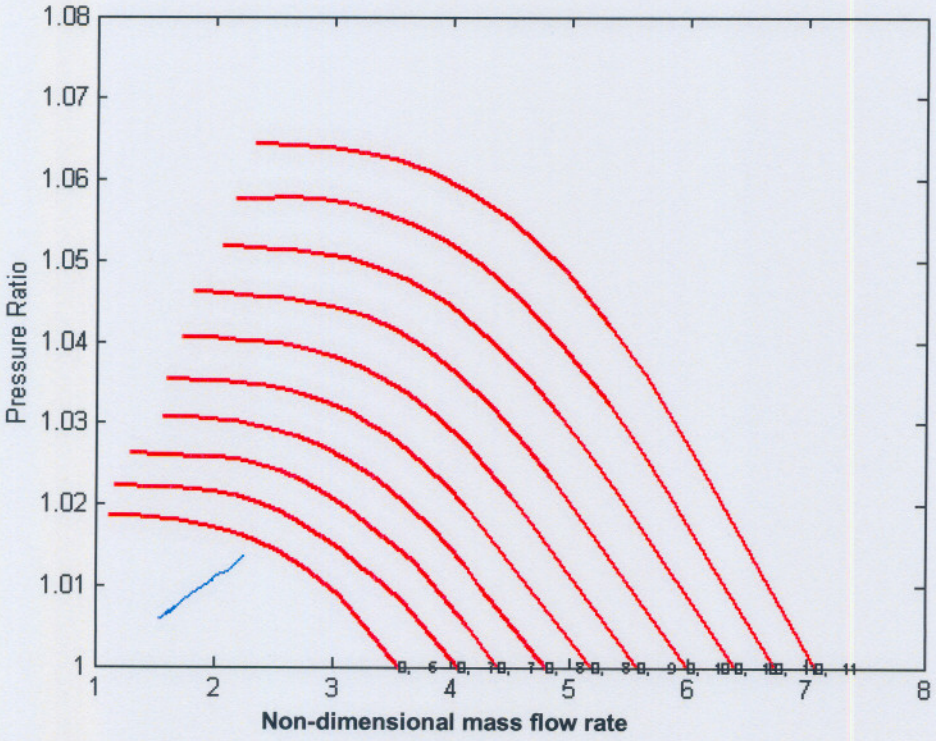

Figure 7.2 : Locus plot of circulator coast down (blue line) on a Pressure ratio vs. corrected mass flow rate map.

Figure 7.3 shows the simulation mass flows plotted against the test results for the 15 MW case. The figure shows that the simulation predicts a much faster decline in mass flow rate than that of the test data. To check the Flownex results further study had to be performed on the circulator maps to ensure that Flownex gives the correct results.

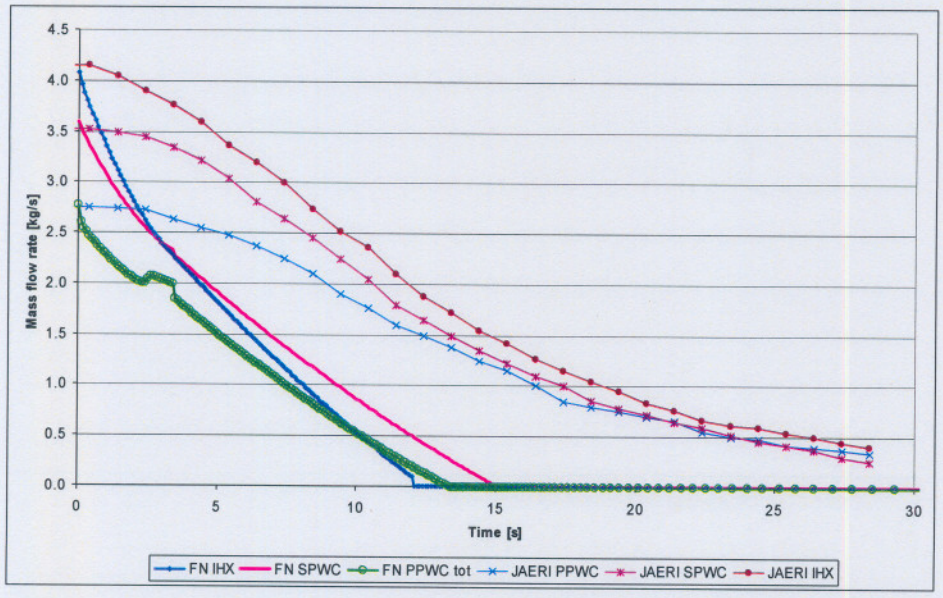

Figure 7.3 : Circulator mass flow rates of Flownex compared to JAERI test results

To verify this it was first necessary to find a way of mapping the region in which the circulator is operating for this transient. The method of Song, Kim, Kim and Ro (Song et al.,2001) was used to further non-dimensionalize the curves by expressing the characteristic

data in a speed- independent form. This is done by plotting the pressure ratio data in terms of flow coefficient,

$$\phi = \frac{C_x}{N} \tag{7.1}$$

and pressure coefficient,

$$\psi = \frac{C_p T_{01}(PR^{(\gamma-1)/\gamma} - 1)}{N^2} \tag{7.2}$$

where C_x = axial flow velocity,

N = rotational speed,

C_p = specific heat,

T_{01} = inlet temperature,

PR = pressure ratio and

γ = specific heat ratio.

The axial flow velocity (C_x) is obtained from the non-dimensional mass flow using a flow area of one. This area can be used because the coefficients calculated in this exercise are all relative and the flow is virtually incompressible. For a given non-dimensional mass flow, non-dimensional speed and pressure ratio the flow area and inlet conditions have no effect on the resulting flow and pressure coefficient. When these parameters are plotted against each other the graph shown in Figure 7.4 is produced. The data can then be matched to a correlation by using regression analysis. The figure shows the regression line through the data which is in the form of a third order polynomial.

From this polynomial the process can be reversed to obtain data for any constant speed line, thereby populating the lower left part of the map where the operating point will be found. The new mapped region is shown in Figure 7.5.

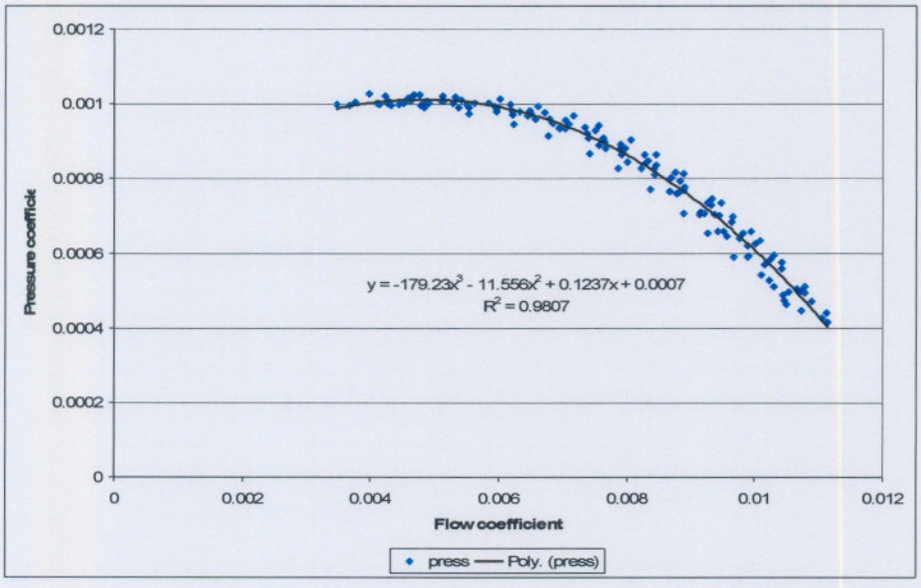

Figure 7.4 : The pressure coefficient versus the flow coefficient for the JAERI PPWC circulator data.

As an extra check on the new data it was once again non-dimensionalised into flow and pressure coefficients and a correlated third order polynomial was once again generated. The polynomial obtained was exactly the same as the original shown in Figure 7.5 which indicates that the transformation of the data was done correctly. The new map was then used in the transient with the results shown in Figure 7.6. The new locus of the operating point on the map is shown in Figure 7.5 with the old one indicated with markers. It is evident from this that the extrapolated data of the old map matches very closely to the new data.

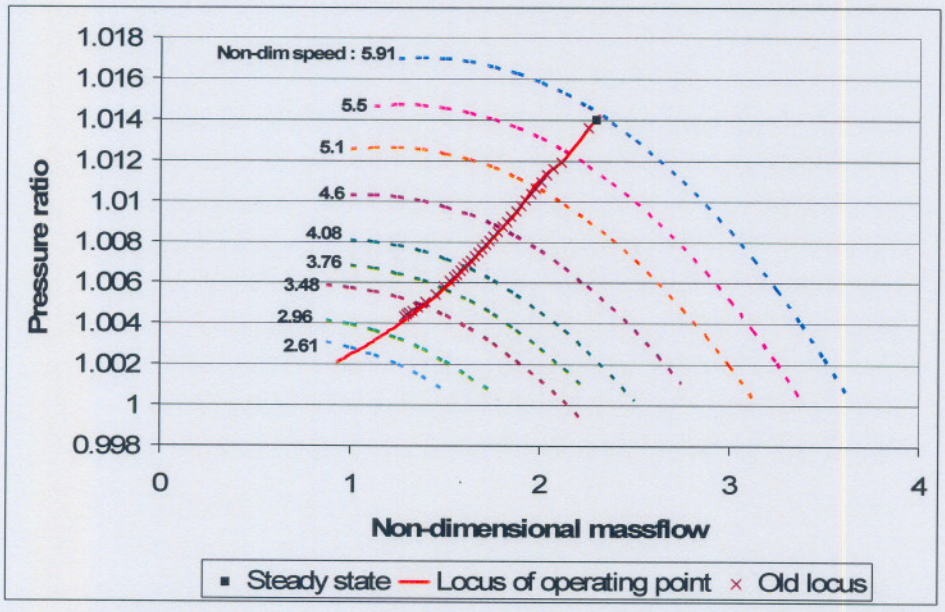

Figure 7.5 : PPWC circulator map with newly developed speed curves and operating point locus.

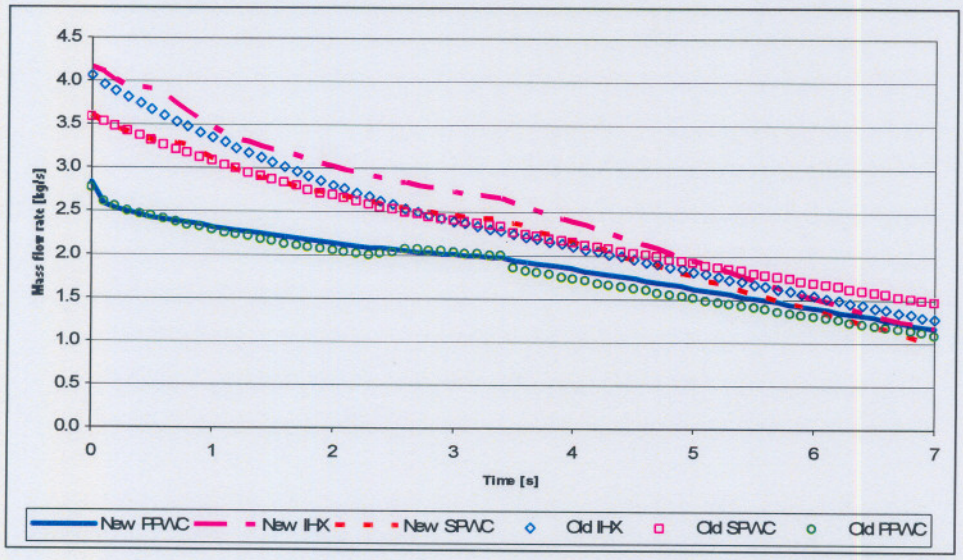

Figure 7.6 : Mass flow results obtained with the new map versus the old results.

As can be seen in the above results the new map yields essentially the same data as before. This can be expected due to the locus plots being so similar. The only explanation for the large discrepancy between the Flownex data and the test data of Figure 7.3 must be that either the test data is incorrect or that there were some additional events in the transient that was not passed on by JAERI.

As a further check the system resistance curve is plotted on the circulator map. This curve is calculated on the basis that the pressure rise over the circulator (same as the system resistance the circulator must overcome) is directly proportional to the square of the volumetric flow rate. This is true for flows where the gas density is constant which is true in this case where the pressure ratio is far less than 1.3.

From the steady state operating point a proportionality constant can be found for the pressure rise - volumetric flow rate relationship. This quadratic function is then converted into pressure ratio versus non-dimensional mass flow data and plotted on the circulator map, shown in Figure 7.7. The system resistance was calculated correctly as the locus of the circulator's operating point is on this system resistance curve.

With this curve the test speed data is used to find the mass flow at that speed based on the intersection of system resistance and circulator speed. At times 2 and 6 seconds the speeds are 105 rps and 77 rps respectively. For circulator inlet conditions of 235°C and 2735 kPa the equivalent non-dimensional speeds are 4.65 and 3.42, which yields non-dimensional mass flows of 1.95 and 1.1. These are converted using the inlet conditions to mass flows of 2.33 kg/s and 1.35 kg/s respectively. In comparison, Figure 7.3 gives test data mass flows of 2.75 kg/s and 2.4 kg/s. This is a difference of up to 77 percent.

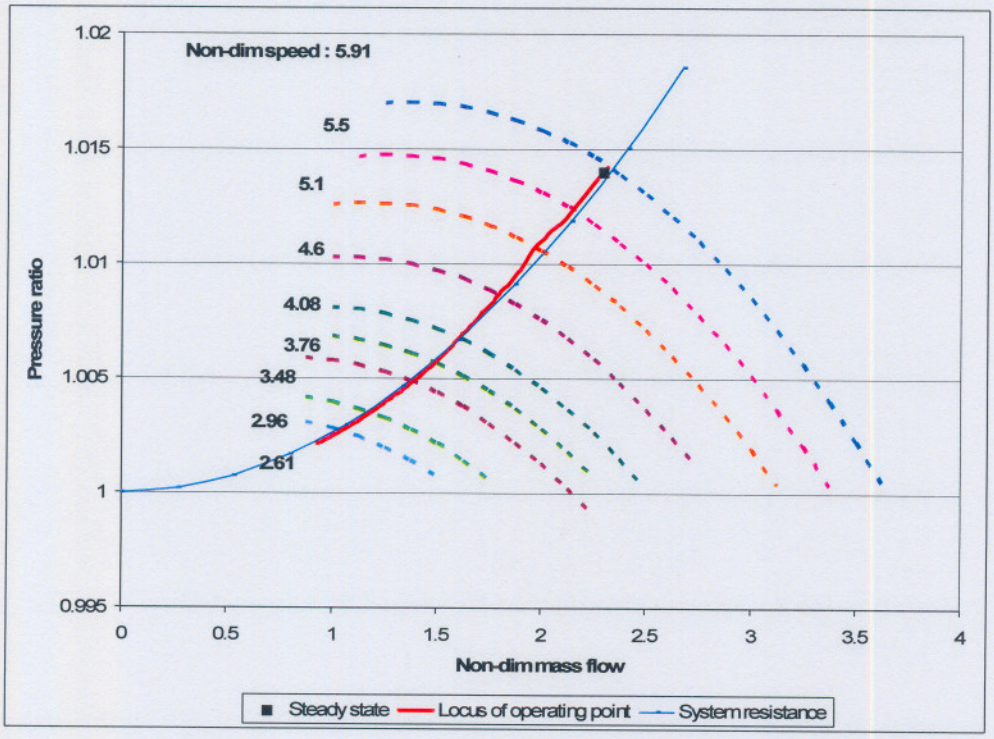

Figure 7.7 : PPWC circulator map with system resistance curve and locus of the circulator operating point.

In the rest of this section the Flownex results are given for some other key parameters in the system. No experimental data was available for these parameters and thus no conclusions could be made with regard to the code's accuracy.

The Flownex results for the transient performance of the reactor are shown in Figure 7.8. Note the sudden drop in reactor power at 8 seconds due to the SCRAM. The remaining decay heat curve is as prescribed by JAERI. Figure 7.9 shows the transient fluctuation in system pressure. It is expected that once the system is not running, the pressure will be close to the

operating pressure due to the lack of a high system pressure ratio and large volumes of helium.

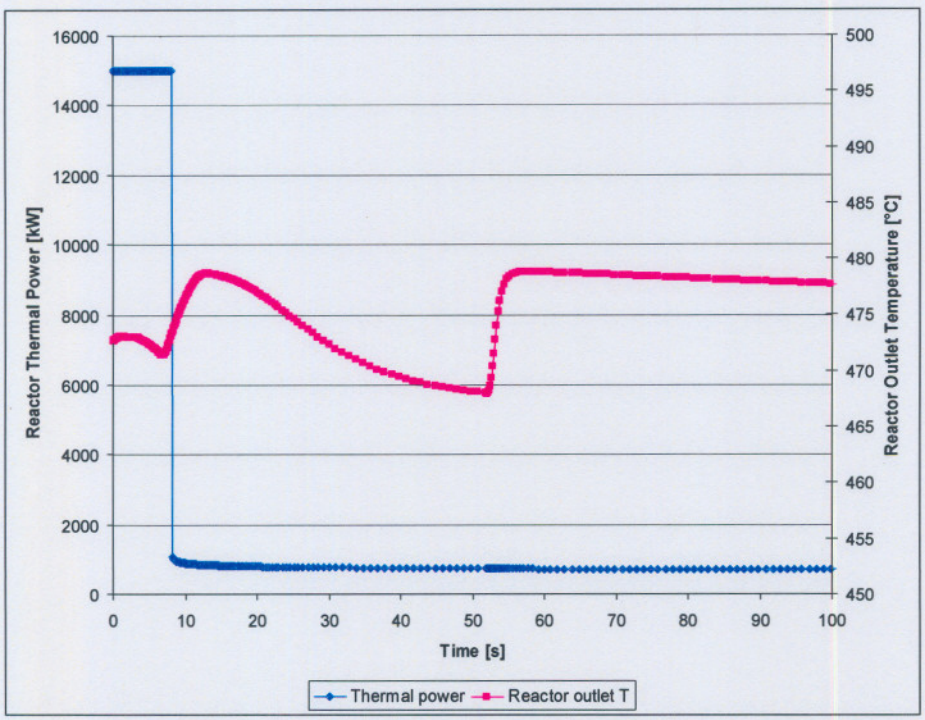

Figure 7.8 : Flownex results of HTTR Reactor thermal power and outlet temperature.

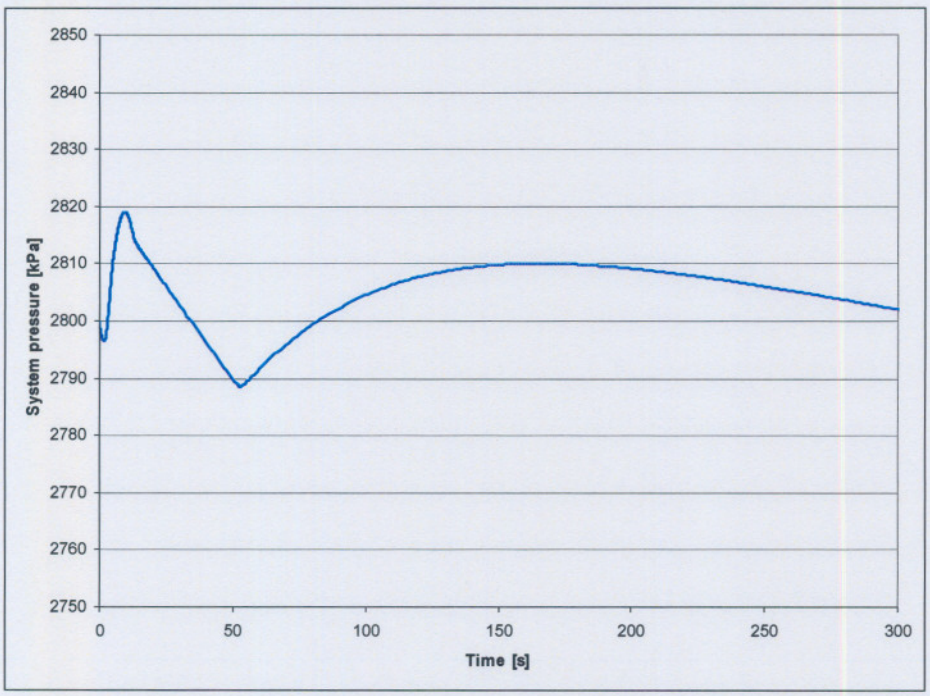

Figure 7.9 : Flownex results of HTTR system pressure (at PPWC circulator outlet).

Finally, in Figure 7.10 the mass flow rates are plotted for the whole transient from the coast down to when the auxiliary cooling system is activated.

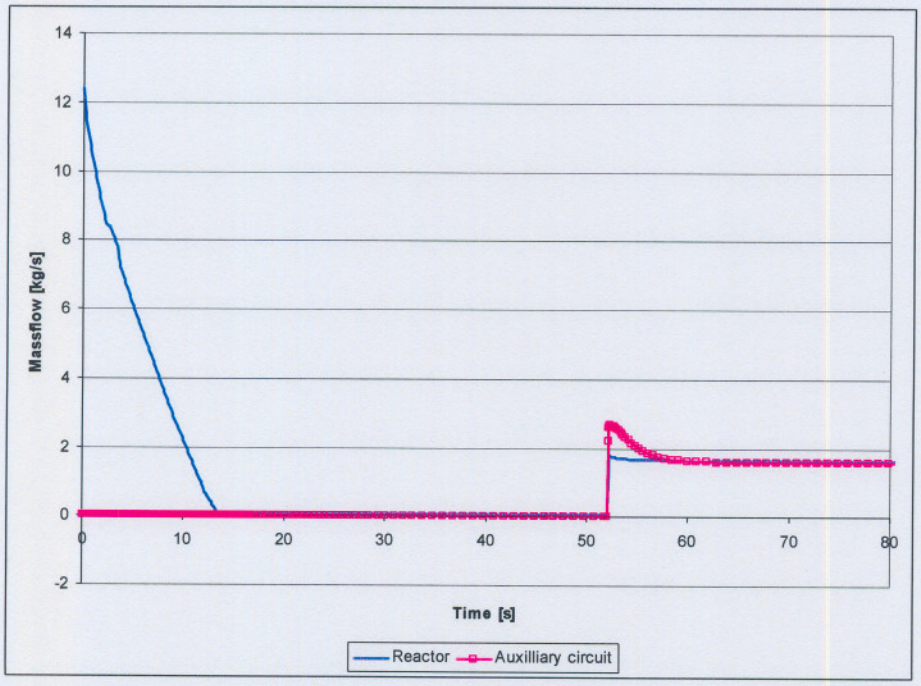

Figure 7.10 : Flownex results of reactor and auxiliary mass flow rates.

It is evident from the figure that the system coasts down to a zero mass flow, where it stays for approximately 35 seconds before the auxiliary cooling system is activated.

The only way to really verify these assumptions is to get more experimental data from JAERI, specifically temperatures and pressures through the system as measured during the experiment. The little data that was made available had very poor resolution probably due to instrumentation inaccuracies and could not be used for comparison.

7.4. 30 MW Loss-of-power transient results

At the time of documenting these results, the 30MW experimental data was not available from JAERI. Therefore the 30MW simulation results are unverified but are still presented in this section. Figure 7.11 and Figure 7.12 show the system mass flows during the coast-down and entire periods of the transient respectively. As with 15MW it is expected that the actual mass flow rate decrease will be slower than in the simulation.

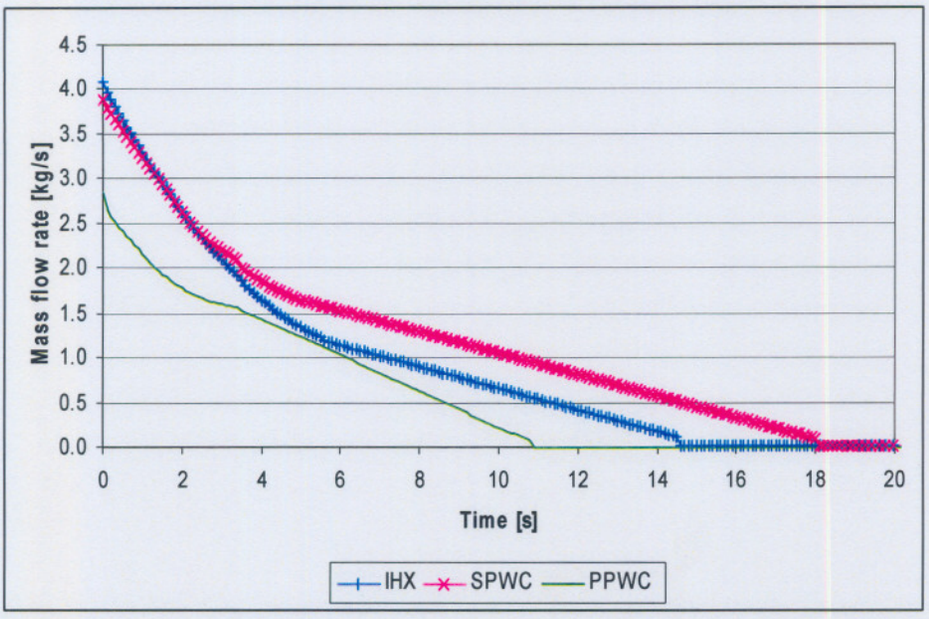

Figure 7.11 : Flownex results of circulator mass flow rates in coast-down phase.

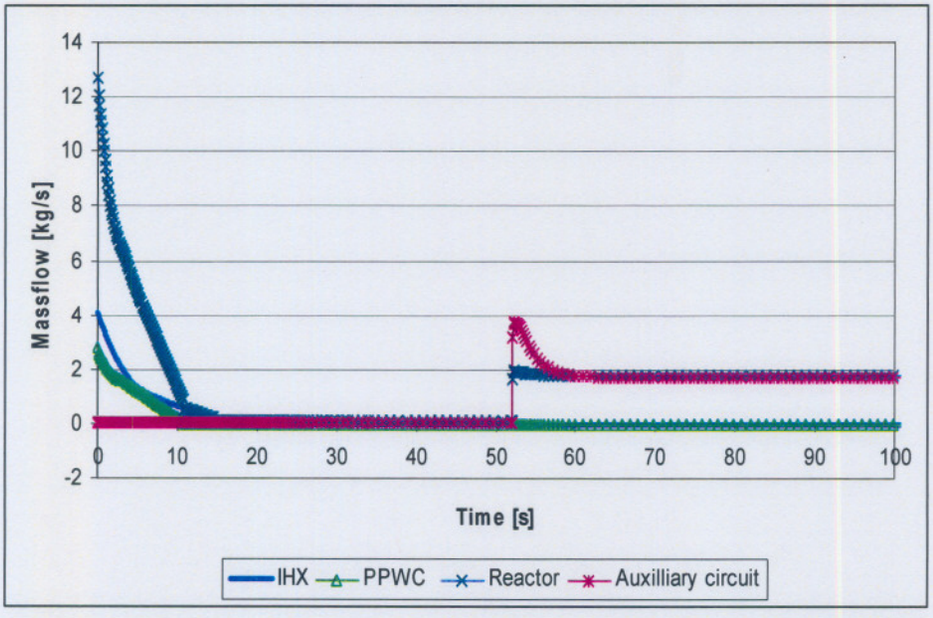

Figure 7.12 : Flownex results of reactor and auxiliary mass flow rates

The general form of these trends is similar to the 15 MW results and it is expected that the same conclusions would be reached had the experimental data been available.

The reactor performance is shown in Figure 7.12. It is shown that the system mass flow declines to zero and stays there until the auxiliary cooling system is activated.

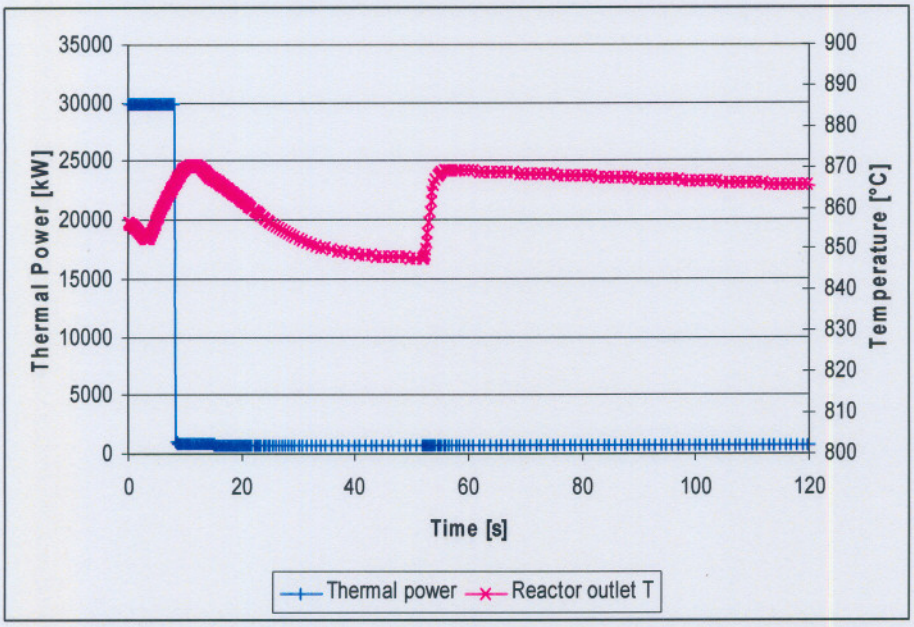

Figure 7.13 : HTTR Reactor thermal power and outlet temperature.

From Figure 7.13 it is seen that the reactor power drops away rapidly at about 8 seconds. This is due to the reactor being "SCRAMed". The temperature steadily increases due to the decline in mass flow. Once the reactor has been shutdown the temperature declines. The sudden rise in temperature close to 55 seconds is possible due to the sudden influx of auxiliary cooling which causes the nuclear reaction to increase, resulting in higher temperatures.

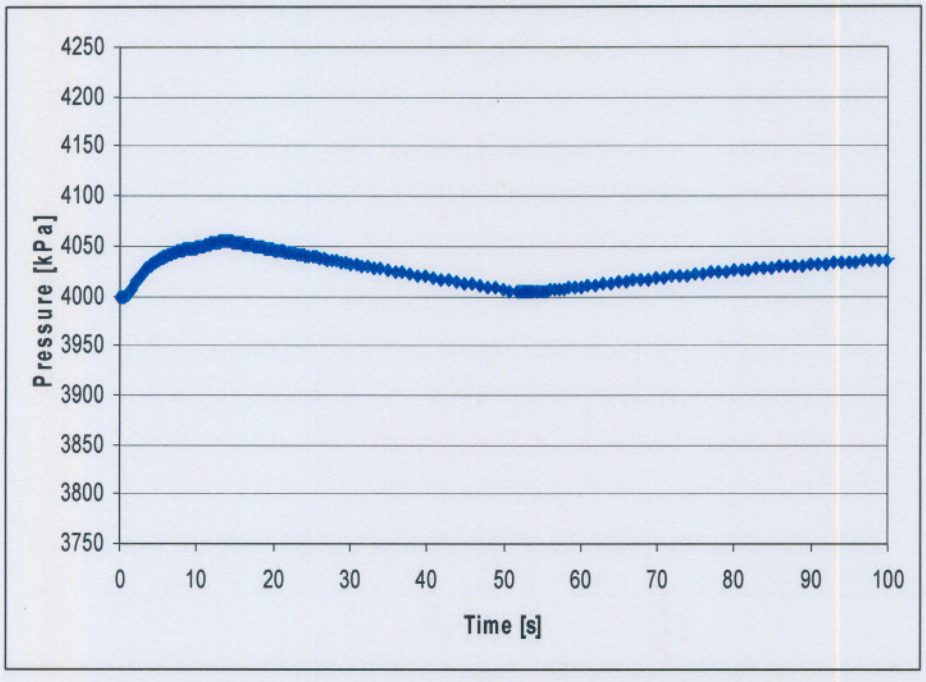

Figure 7.14 : HTTR system pressure (at PPWC circulator outlet).

The fluctuation of pressure in the system is due to the changes in mass flow rates. The changes are not markedly high, due to the low pressure ratio in the system. Figure 7.15 shows a locus plot of the PPWC circulators' operating point movement on the map.

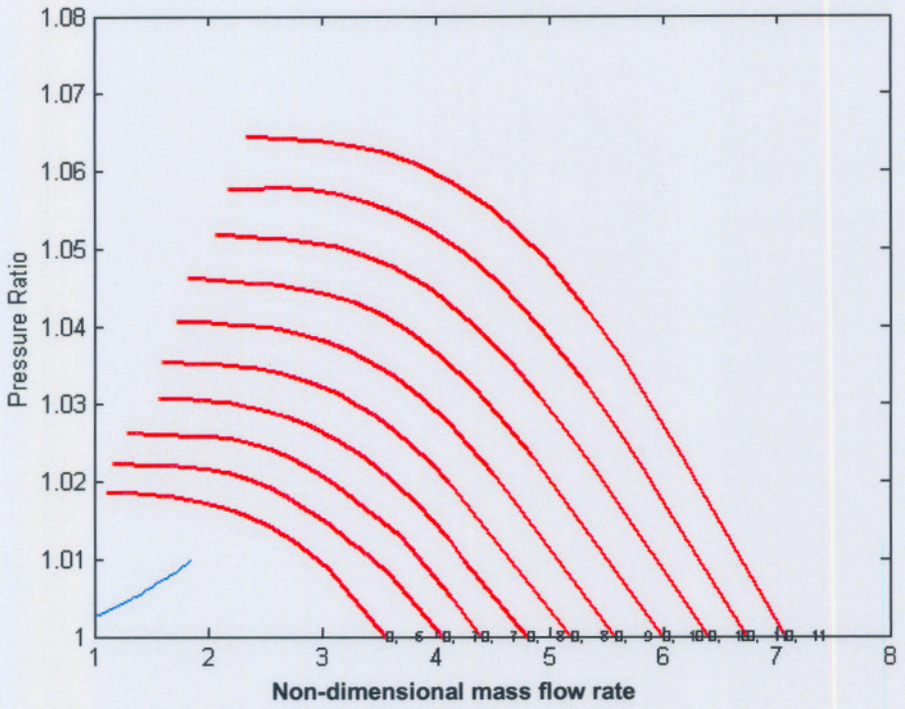

Figure 7.15 : Locus plot of circulator coast down on a pressure ratio vs. corrected mass flow rate map

The figure clearly shows the over-sizing of the circulators, since if they were sized correctly, the start of the locus plot would at least have been inside the map domain.

7.5. Conclusion

The transient data for the 15MW and 30MW loss-of-electrical-power transients are discussed in this chapter. Though no experimental data was obtainable from JAERI, the trends of the Flownex data appear to be correct. Problems were encountered due to the circulators running off the original maps. However, the circulator maps were enlarged to the cover the working area of the circulator. The cause of the low running points can be attributed to the HTTR designers over predicting the system resistance and thus over-sizing the circulators for the work they had to do. Such a mistake is not uncommon in system design, as design methods used to predict system resistance are not always that accurate: on paper the design may be apt but in practice assumptions made in the design are sometimes not correct or too conservative. The final conclusion is that Flownex is capable of analysing HTGR systems, provided the input data is as close to the real system behaviour as possible.

8. SUMMARY, CONCLUSION AND RECOMMENDATION FOR FURTHER WORK

8.1. Summary

This study discussed the need for benchmarking of thermo-hydraulic system codes used for the modelling of HTRs. Strict guidelines and requirements have been formulated and implemented by regulating authorities to enforce a high standard of quality for these codes. Hence, the developers of Flownex have a rigid Verification and Validation process in place to ensure that the guidelines are followed.

Furthermore, the system codes used in power system design, especially HTR nuclear power plants, were discussed. This was done in order to investigate the other commercial codes available in the market, highlighting their features and shortfalls. The outcome of the investigation showed that there are many customisable programs on the market, like Aspen Custom Modeller, that can simulate a wide range of problems but require the user to put in a lot of effort in developing a model. On the other hand, some of the codes are not at all flexible and the user is restricted to using specific component models. Flownex is such a program, although it does allow the user to alter model inputs to account for different geometries. Where a special model was needed in the study, the developers assisted in creating new models.

Following the literature survey, the HTTR was discussed to introduce it as the benchmark HTR plant for this study. Despite the system being small in the number of components present, it still has very complex components. These include the reactor and the IHX, which required many assumptions in obtaining a workable model. Thereafter the system code Flownex was presented to show its functionality and the mathematics behind the solver. The modelling in Chapter 5 highlighted the assumptions needed to get to a workable model. A great deal of effort went into the modelling of the heat exchangers and the reactor, which were quite different to the standard models in Flownex.

The steady-state results obtained from Flownex for the 15MW case showed good correlation to the experimental data when the circulator speeds were lowered to the actual values. The 30MW results showed a larger difference between the test results and the Flownex results. When 15MW shaft speeds were used on the helium circulators, much better correlation was achieved. The transient test results are shown in Chapter 7 and although no data was made available regarding the actual test, the trends of the simulation data appear to be correct.

8.2. Conclusion

It appears that original speed estimates provided by JAERI were based on over-conservative system resistance predictions. This resulted in the circulators being oversized for the required operating point. The working points are just off the range of the circulator curves and as such the accuracy of the analysed working point is dependent on the extrapolation routines in the simulation code. This issue of accuracy becomes more evident in the loss-of-power event, where the working point moves further away from the map. The effect can be seen in the mass flow plots, where the experimental flow rates take longer to decrease than the simulated results.

However, other factors cannot be ruled out, as temperature and pressure effects can also play

a role in the discrepancies. The only way to verify that this is not the cause, is to get more detailed system data for the tests from JAERI. This was, however, not possible, as much of the detailed information is proprietary and could not be obtained.

The steady-state simulation results and those obtained from the actual plant are in fair agreement. Only the transient results for the 15 MW power level could be compared as the other data was not made available by JAERI. The Flownex results showed a much faster drop in system mass flow for decreasing circulator speed than the test results indicated. Initially it was thought that because the operating point locus was outside the mapped region of the circulator maps that the Flownex extrapolation method was inaccurate. This was checked by non-dimensionalising the maps in terms of speed and finding a regression polynomial to describe the data. This third order polynomial was then used to developed speed lines in the working point region. Then the simulation was repeated but found to yield essentially the same working point locus as before. This indicated that the locus does run on the system resistance line that traverses the map as it should. The conclusion was that either the JAERI data was incorrect or there were changes in the system design not passed on from JAERI. In general, though, Flownex did not have any difficulty in simulating the transient events.

The biggest contribution of the study is that it demonstrated Flownex's ability to accurately predict the steady-state operation of the HTTR. It also demonstrated that it can model the loss-of-off-site transient. As for the CRP, it is difficult to comment on its success due to the long periods involved with research programmes. Until the date of this publication no official conclusions were available with regard to the CRP. Discussions with other participant countries have shown, however, that the participant results were in reasonable agreement and as such the CRP appears to have been a success.

8.3. Recommendations for future work

It is firstly recommended that the 30MW transient data be obtained and that a comparison be drawn between it and the results in this study. This will confirm any of conclusions drawn with regard to the differences in transient results. Furthermore, it is recommended that future studies focus on the individual component models and not on system-wide simulation. For example, there is still much work to be done on the helically coiled type of heat exchanger as used for the IHX. This work would include developing a helical coil heat exchanger model in Flownex to account for the special conditions encountered in such a component. Where system-wide integrals tests are still required, it is recommended that the detail of test data be increased and that more instruments be made available for the benchmarking.

9. REFERENCES

BOTHA, F. 2000. An explicit method for the analysis of transient flow in pipe networks. Potchefstroom. (Thesis - M.Eng.) 120 p.

COETZEE, R.V., VAN DER MERWE, J. & VAN RAAVENSWAAY, J, 2002. Flownex 6.4 User Manual. Potchefstroom. MTech Industrial. 428p.

DUDERSTADT, J.J. & HAMILTON, L.J., 1942. Nuclear Reactor Analysis. New York : Wiley. 637p.

EMSLIE,F.N. & GREYVENSTEIN, G.P., Modelling of the PBMR using a pipe network approach. *Proceedings of the IFAC Conference on Technology Transfer in Developing Countries – Automation in Infrastructure*, Pretoria 2000.

GREYVENSTEIN, G.P. & LAURIE, D.P., 1994. A segregated CFD approach to pipe network analysis. *International Journal for Numerical Methods in Engineering*, 37: 3685 – 3705, February.

GREYVENSTEIN, G.P., 2001, An implicit method for the analysis of transient flows in pipe networks. *Journal for numerical methods in engineering*, (53):1127-1143, Jan. 29.

GREYVENSTEIN, G.P., VAN RAVENSWAAY, J.P. and ROUSSEAU, P.G.," Dynamic modelling of heat, mass and momentum transfer in the Pebble Bed Modular Reactor", *1st International Conference on Heat Transfer, Fluid Mechanics, and Thermodynamics*, 2002.

IDELCHIK, I.E. & Fried,E, 1989. Flow Resistance: a design guide for engineers. Hemisphere.

IEEE Std 1059 – 1993, "IEEE Guide for Software Verification and Validation Plans"

INCROPERA, F.P and DE WITT, D.P. Fundamentals of heat and mass transfer". 4th edition, 1996, Wiley.

KAYS, W.M. & LONDON, A.L. 1984. Compact Heat Exchangers. 3rd Edn., McGraw Hill.

KENDALL, J. Overview of IAEA Co-ordinated Research Project on Evaluation of HTGR Performance. IAEA, 2001.

LEVY, S. 1999. Two-phase flow in complex systems. New York : Wiley.

MACROFLOW. 2003. General Flow systems website. [Web:] www.macroflow.com [Date of access: 10 July 2003].

MELESE, G. and KATZ, R., 1984. Thermal and Flow Design of Helium-cooler Reactors. Illinois : American Nuclear Society.

MILLER, D.S. Internal Flow Systems. *BHRA Fluid engineering series, Volume 5.*

OLIVIER, J.C., 2003. Network modelling of transient heat exchanger performance. Potchefstroom. (Thesis – M.Eng.) 134p.

PATANKAR, S.V. & SPALDING, D.B., 1970. A calculation procedure for heat, mass and momentum transfer in three dimensional parabolic flows. *International Journal on Heat and Mass transfer*, 15 : 1787 – 1806.

ROUSSEAU, P.G., GREYVENSTEIN, G.P. 2002. Modelling of the HTTR in Flownet. Potchefstroom. Department of Mechanical Engineering: Potchefstroom University for Christian Higher Education. 5 p.

SAAD, M.A., 1985. Compressible fluid flow. New Jersey : Prentice Hall, Inc. 560p

SAITO, S. et al, 1994. Design of High Temperature Engineering Test Reactor (HTTR). JAERI.

SHAMES, I.H., 1992. Mechanics of Fluids. Singapore : McGraw-Hill. 857p.

SONG, T.W., et al., 2001. Performance prediction of axial flow compressors using stage characteristics and simultaneous calculation of interstage parameters. *Proceedings of the Institution of Mechanical Engineers*, 215, Part A.

TAKEDA,T, et al., 2000. Analytical Evaluation on loss of off-site electric power simulation of the High Temperature Engineering Test Reactor. JAERI 2000-016.

TAKEDA, T. 2000. Correspondence by facsimile from Takeshi Takeda, Research engineer at JAERI, 15 March 2000.

TAKEDA, T. 2000. Correspondence by facsimile from Takeshi Takeda, Research engineer at JAERI, 24 August 2000.

TAKEDA, T. 2001. Results on loss of off-site electric power test from 15MWoperation of the high temperature engineering test reactor. Correspondence by facsimile from Takeshi Takeda, Research engineer at JAERI, 26 May 2001.

VERKERK, E.C., KIKSTRA, J.F.,2003. Comparison of two models for a high temperature reactor coupled to a gas turbine. *Nuclear engineering and design* 220, Elsevier.

WYLIE, E.B. and STREETER, V.L., 1993. Fluid transients in systems. Englewood Cliffs,NJ : Prentice Hall, Inc.